CNWRA *A center of excellence in earth sciences and engineering*

A Division of Southwest Research Institute™
6220 Culebra Road • San Antonio, Texas, U.S.A. 78228-5166
(210) 522-5160 • Fax (210) 522-5155

August 24, 2000
Contract No. NRC–02–97–009
Account No. 20.01402.661

U.S. Nuclear Regulatory Commission
ATTN: Mr. Jeffrey Pohle
Division of Waste Management
TWFN Mail Stop 7-D13
Washington, DC 20555

Subject: Thermal Effects on Flow KTI Intermediate Milestone 01402.661.010: Mountain-Scale Thermal-Hydrologic Analyses—Status Report

Dear Mr. Pohle:

Enclosed please find the report titled "Evaluation of the Drift-Scale Heater Test Thermal-Hydrological Conceptual Model Data, and U.S. Department of Energy Thermal Test Results—Status Report." This technical document fulfills the requirements for the subject milestone, which is due August 25, 2000.

The subject report summarizes an analysis of the U.S. Department of Energy (DOE) Drift-Scale Heater Test (DST) using numerical model simulations performed using the MULTIFLO code. The analysis was conducted to review the appropriateness of the DOE conceptual model used to simulate heat and mass transfer at the DST. In addition, DOE data describing the physical and hydrologic character of the DST host rock were evaluated. Analysis results identified fracture permeability, infiltration rate, block size, and thermal conductivity as the most important parameters to the thermal-hydrological simulations. Lastly, the effect of mass loss through the DST thermal bulkhead was evaluated and found to have a measurable effect on temperature predictions during the heating phase of the DST.

If you have any questions, please contact Dr. Ronald Green at 210.522.5305 or me at 210.522.5151.

Sincerely yours,

Asadul H. Chowdhury, Manager
Mining, Geotechnical, and
Facility Engineering

AHC/jw
Enclosure

cc: J. Linehan (w/o enclosure)
D. DeMarco
B. Meehan
E. Whitt
J. Holonich
W. Reamer
K. Stablein
D. Brooks
T. McCartin
P. Justus
J. Greeves
R. Codell
B. Leslie
M. Nataraja
J. Trapp
T. Essig
W. Patrick
CNWRA Dirs
CNWRA EMs
T. Nagy (SwRI Contracts)
R. Green
D. Hughson
G. Ofoegbu
S. Hsiung
S. Mohanty

Washington Office • Twinbrook Metro Plaza #210
12300 Twinbrook Parkway • Rockville, Maryland 20852-1606

EVALUATION OF THE DRIFT-SCALE HEATER TEST THERMAL-HYDROLOGICAL CONCEPTUAL MODEL DATA, AND U.S. DEPARTMENT OF ENERGY THERMAL TEST RESULTS—STATUS REPORT

Prepared for

Nuclear Regulatory Commission
Contract NRC–02–97–009

Prepared by

Ronald T. Green
Debra L. Hughson
Scott L. Painter
Melissa E. Hill

Center for Nuclear Waste Regulatory Analyses
San Antonio, Texas

August 2000

ABSTRACT

This report evaluates the status of the U.S. Department of Energy's (DOE's) Drift-Scale Heater Test (DST). Preliminary modeling results of the DST conducted at the Center for Nuclear Waste Regulatory Analyses are presented in this report as part of the evaluation. A series of simulations were conducted to evaluate the importance of various input parameter values on the ambient matrix saturation. Results from these sensitivity analyses indicated that infiltration rate and block size had a significant effect on predicted ambient matrix saturations. Evaluation of thermohydrological simulations identified fracture permeability and thermal conductivity as significant factors in the prediction heat and mass transfer in response to heating at the Exploratory Studies Facility DST. Thermohydrological simulations were also performed to evaluate the importance of mass loss through the thermal bulkhead. Our results suggest that removing water mass from the bulkhead results in reduction of condensate buildup and refluxing above the heated drift. Results from modeling the DST are used to provide a basis for evaluating if the DOE thermal testing program is achieving their testing objectives.

CONTENTS

FIGURES

FIGURES (cont'd)

FIGURES (cont'd)

FIGURES (cont'd)

TABLES

ACKNOWLEDGMENTS

This report documents work performed by the Center for Nuclear Waste Regulatory Analyses (CNWRA) for the U.S. Nuclear Regulatory Commission (NRC) under Contract No. NRC–02–97–009. The activities reported here were performed on behalf of the NRC Office of Nuclear Material Safety and Safeguards, Division of Waste Management. The report is an independent product of the CNWRA and does not necessarily reflect the views or regulatory position of the NRC.

The authors thank J. Winterle and B. Sagar for technical and programmatic reviews of this document. The authors are thankful to P. Houston and J. Wike for skillful typing of the report and to A. Woods and C. Cudd for providing a full range of editorial services in preparation of the final document. The authors also thank D. Coffin for assistance with performing MULTIFLO simulations and to M. Seth for assistance in assessing applications of the MULTIFLO code.

QUALITY OF DATA, ANALYSES, AND COMPUTER CODES

DATA: No CNWRA-generated original data are contained in this report.

ANALYSES AND CODES: Used MULTIFLO Version 1.2 software developed under CNWRA Quality Assurance procedures.

1 INTRODUCTION

The thermal effects on flow key technical issue is relevant to the performance of the proposed repository for two reasons. The first reason is that thermal loading from the decay of spent nuclear fuel, and its resultant effects on unsaturated zone hydrology at Yucca Mountain (YM), Nevada, govern the distribution of temperature, pressure, and relative humidity (RH) in the unsaturated zone. These variables are fundamental to the long-term stability of the engineered barrier system (EBS). Related to this stability is the possibility that moisture mobilized by heat may contact waste packages (WPs) through mechanisms such as vapor transport and condensation or focusing of condensate drainage in fractures. The background in chapter 2 is presented as a basis for conceptualizing characteristics of thermal hydrology (TH) and evaluating various conceptual models for representing TH processes. The ability of TH models to represent important mechanisms of thermally driven moisture transport is considered crucial in evaluating the potential for water to contact WPs during and following the thermal period of the repository. The second reason is the adequacy of data obtained by the U.S. Department of Energy (DOE) site characterization activities, through its thermal testing program. Numerous simulations were run to identify the properties whose values have a prominent effect on ambient matrix saturation. These simulations were important because variations in the pretest matrix saturation proved to have a prominent effect on thermal-hydrologic simulations of the heating phase of the Exploratory Studies Facility (ESF) Drift-Scale Heater Test (DST). Additional simulations were performed to evaluate the effect of property value assignment on predicted heat and mass transfer in response to heating at the DST. Parameters whose changes affected the modeling results were selected for the sensitivity analyses. The potential importance of heat and mass loss through the thermal bulkhead was evaluated. Modeling results indicate that mass loss, caused by ventilation, may significantly affect the development of water reflux in fractures.

1 INTRODUCTION

The thermal effects on flow key technical issue is relevant to the performance of the proposed repository for two reasons. The first reason is that thermal loading from the decay of spent nuclear fuel, and its resultant effects on unsaturated zone hydrology at Yucca Mountain (YM), Nevada, govern the distribution of temperature, pressure, and relative humidity (RH) in the unsaturated zone. These variables are fundamental to the long-term stability of the engineered barrier system (EBS). Related to this stability is the possibility that moisture mobilized by heat may contact waste packages (WPs) through mechanisms such as vapor transport and condensation or focusing of condensate drainage in fractures. The background in chapter 2 is presented as a basis for conceptualizing characteristics of thermal hydrology (TH) and evaluating various conceptual models for representing TH processes. The ability of TH models to represent important mechanisms of thermally driven moisture transport is considered crucial in evaluating the potential for water to contact WPs during and following the thermal period of the repository. The second reason is the adequacy of data obtained by the U.S. Department of Energy (DOE) site characterization activities, through its thermal testing program. Numerous simulations were run to identify the properties whose values have a prominent effect on ambient matrix saturation. These simulations were important because variations in the pretest matrix saturation proved to have a prominent effect on thermal-hydrologic simulations of the heating phase of the Exploratory Studies Facility (ESF) Drift-Scale Heater Test (DST). Additional simulations were performed to evaluate the effect of property value assignment on predicted heat and mass transfer in response to heating at the DST. Parameters whose changes affected the modeling results were selected for the sensitivity analyses. The potential importance of heat and mass loss through the thermal bulkhead was evaluated. Modeling results indicate that mass loss, caused by ventilation, may significantly affect the development of water reflux in fractures.

2 THE U.S. DEPARTMENT OF ENERGY THERMAL TESTING PROGRAM

2.1 BACKGROUND AND OBJECTIVES

The DOE is conducting a thermal testing program in support of their high-level nuclear waste (HLW) repository program. Tests conducted in the ESF Thermal Test Facility (Alcove 5) are an integral component of the site investigation to characterize YM in Nye County, Nevada, for the permanent disposal of HLW. The thermal testing program will acquire an in-depth understanding of the coupled thermal, mechanical, hydrological, and chemical (TMHC) processes expected to occur in the rock mass surrounding the proposed geologic repository at YM (TRW Environmental Safety Systems, Inc., 1997a). This objective is consistent with the objectives originally stated in the Site Characterization Plan (U.S. Department of Energy, 1988), which noted that *in situ* thermal tests are to provide TMHC information on the near-field environment. Stated further, the ESF *in situ* thermal tests are to provide a major portion of the experimental basis supporting the validation of coupled TMHC process models used in total system performance assessments of the proposed repository (Buscheck and Nitao, 1996). In addition, results from the thermal tests are expected to supply data, information, and model refinement to support any license application.

The ESF Thermal Test Facility is the location of two *in situ* heater tests, the single heater test (SHT) and the DST. The DST is evaluated in this status report relative to: (i) the original objectives of the test, (ii) subsequent modifications to the DST, (iii) other DST evaluations, and (iv) available DST results. The specific pretest objectives for the DST, reported below, were taken from analyses by Buscheck and Nitao (1996) and the DST design and forecast results report by TRW Environmental Safety Systems, Inc. (1997a). The latter report identifies several TMHC parameters and processes to be monitored during the test and states that an overall objective of the DST is to evaluate conceptual models that calculate the coupled TMHC behavior so realistic bounds can be developed for the expected near-field environment. The report states, however, that the primary emphasis of the DST is the measurement and prediction of TH behavior. The forecast report also notes that developing a better understanding of TH behavior on a scale comparable to waste emplacement drifts is important because of the potential consequences to repository performance (TRW Environmental Safety Systems, Inc., 1997a).

The Buscheck and Nitao (1996) analysis report predated the final design of the DST, but the report includes a description of the DST objectives key to achieving the goals of the thermal testing program. Additionally, their report contains thermal test calculations that proved instrumental in developing the final DST design and elaborates on technical considerations important for achieving the objectives of the thermal testing program. Their report concludes that *in situ* tests should be designed to provide sufficient information to determine the following:

- The dominant mode(s) of heat flow
- The major TH regime(s) and TMHC processes that govern the magnitude and direction of vapor and condensate flow
- The major TH regimes, TMHC processes, and site conditions that govern dryout and rewetting of the dryout zone

- The influence of heterogeneous properties and conditions on the flow of heat, vapor, and condensate, with particular emphasis on rock dryout and rewetting

Buscheck and Nitao (1996) stated that the primary goal of the ESF thermal tests is to understand modes by which water may contact WPs, including liquid-phase flow, condensation of water vapor, and the related temperature and aqueous geochemistry. Another important goal is to understand how TMHC processes influence radionuclide mobilization, release from the WP, and transport. Buscheck and Nitao (1996) note that the thermal tests must provide critical information about decay heat-driven TH behavior and related coupled TMHC processes in the near-field altered zone and how coupled TMHC processes influence radionuclide transport through the EBS and near-field altered environment.

The consensus of the preliminary modeling report by Buscheck and Nitao (1996) and the forecast report by TRW Environmental Safety Systems Inc. (1997a) is that the primary objective of the ESF thermal tests, in general, and the DST, in particular, is to investigate and understand coupled TMHC processes potentially important in the near-field environment of the proposed geologic repository at YM. Both reports note, however, that an understanding of the coupled TH process is fundamental to understanding the more complex TMHC couplings that may affect the total system performance of the proposed repository. Adequate understanding of the coupled TH processes active at the DST, therefore, is prerequisite to understanding the fully coupled TMHC processes. Buscheck and Nitao (1996) provided additional descriptions of the objectives for the *in situ* thermal tests and noted that tests conducted under thermal loading conditions reasonably representative of repository conditions are required to provide an understanding of coupled processes, such as

- TH behavior, with emphasis on the dominant mode(s) of heat flow and the dominant TH regime(s)

- Geochemical behavior (with emphasis on coupling with TH behavior), alteration of flow and transport properties, and the resulting chemistry of water that may affect the EBS

- Geomechanical behavior, with emphasis on heat-driven opening and closing of fractures and the initiation of new fractures and on the effect those events may have on flow and transport properties (e.g., permeability and porosity), TH behavior, and the geomechanical stability of the emplacement drifts

- The influence of introduced materials on coupled TMHC processes, with emphasis on the modes of flow and chemistry of water potentially affecting the EBS

Buscheck and Nitao (1996) noted that the single most important purpose of the ESF thermal tests could be to determine the major TH flow regime(s) that will govern the magnitude and direction of vapor flow (and the resulting condensate flow) in the unsaturated zone at YM. They identified three distinct TH flow regimes:

- **Throttled, nonbuoyant advective rock dryout.** In this regime, the bulk permeability of the rock, k_b (a bulk average of the matrix and fracture permeabilities), is sufficiently low (i.e., $k_b < 1$ mD) to throttle (or impede) the rate of boiling-driven advective rock dryout. Vertically symmetric temperature and saturation profiles, gas pressures substantially above 1 atm, and minimal RH reduction are experienced.

- **Unthrottled, nonbuoyant advective rock dryout.** In this regime, k_b is sufficient (i.e., $k_b > 1$ mD) to slightly throttle the rate of boiling-driven advective rock dryout, but not high enough (i.e., $k_b < 5$ D) to allow buoyant gas-phase flow. The saturation and temperature profiles for this regime are vertically symmetric unless focused liquid flow depresses the upper boiling isotherm. Gas pressures remain near 1 atm, thus RH reduction can be significant.

- **Unthrottled, buoyant advective rock dryout.** In this regime, k_b is sufficient to avoid throttling the rate of boiling-driven advective rock dryout and also high enough ($k_b > 5$ D) to allow buoyant gas-phase convection. The vertical saturation and temperature profiles for this flow regime are asymmetrical, and RH reduction would be significant.

With reference to this categorization, significant objectives of the DST would be successfully achieved if the data permitted identification of the dominant TH regime in the DST and, by extension, at least a portion of the proposed repository. The TH flow regime will determine where vaporized water condenses relative to the location of the WPs (e.g., water vapor that condenses above the WPs will be available to flow downward, potentially penetrating the boiling isotherm and entering the emplacement drifts; whereas, vapor condensation in nonbuoyant TH regimes would occur both above and below the WPs, potentially limiting the amount of available liquid water above the emplacement drift). The TH regime will also dictate the ambient RH in the WP environment—a parameter important to the corrosion rate of WPs. In addition, Buscheck and Nitao (1996) examined temporal and spatial limitations associated with *in situ* thermal tests. If the dryout zone is small compared to the scale of heterogeneity, the TH processes may be dominated by local heterogeneity. Buscheck and Nitao (1996) recommended the following be considered as criteria in determining the desired size and duration of the DST: volume of the dryout zone, rate of change of temperature, maximum rock temperatures, spatial temperature gradients, extent and duration of condensate buildup above the dryout zone, and velocity of the advancing dryout front.

In particular, the tests require a minimum size and duration to accomplish the following:

- Incorporate a representative network of fractures that is sufficiently connected to allow examination of important decay-heat-driven processes, such as boiling, vapor diffusion, buoyant gas-phase convection, and nonequilibrium, liquid-phase fracture flow

- Permit the possible development of condensate buildup above the dryout zone

- Examine whether heterogeneity in the gas- and liquid-phase pathways results in focusing of condensate drainage sufficient to cause water to drip onto WPs

- Prevent boundary effects such as edge-cooling effects from dominating TH behavior in the vicinity of the test

- Diagnose the significance of buoyant gas-phase convection on moisture movement and heat flow

2.2 DRIFT-SCALE HEATER TEST SITE DESCRIPTION

The ESF Thermal Test Facility (Alcove 5) is located in the Topopah Spring middle nonlithophysal (Tptpmn) unit, within the horizon of the proposed YM repository (TRW Environmental Safety Systems, Inc., 1997b). The Tptpmn unit is approximately 30–40 m thick at the location of the DST, overlain by the Topopah Spring upper lithophysal (Tptpul) and underlain by the Topopah Spring lower lithophysal (Tptpll) units. Alcove 5 is at Construction Station 28 + 27 (a coordinate system in meters following the axis of the ESF and originating at the North Portal) just past the bend from the North Ramp to the Main Drift (as shown in figure 2-1) (taken from TRW Environmental Safety Systems, Inc., 1997b). The DST test block was characterized prior to the onset of heating. On-site characterization of the local geology, *in situ* hydrology, and local rock mass quality was supplemented with laboratory tests of TMHC properties. Characterization data collected from the SHT block (TRW Environmental Safety Systems, Inc., 1997b) were also incorporated. The ensemble of these data provides the characterization of the DST block and model parameters. These data are consistent with results from previous nonthermal test studies by Brechtel et al. (1995) and TRW Environmental Safety Systems, Inc. (1997b). The data are also consistent with parameter values cited in the Total System Performance Assessment-Viability Assessment (TSPA-VA) (TRW Environmental Safety Systems, Inc., 1998a).

The primary components of Alcove 5 indicated in figure 2-2 [taken from TRW Environmental Safety Systems, Inc. (1997b)] are the site of the SHT (known as the thermomechanical alcove), the observation drift, connecting drift, and heated drift. A plan-view schematic of the relative placement of the heated drift to the observation drift is shown in figure 2-1. The 5-m-diameter, 47.5-m-long heated drift is terminated at the east end by a thermal bulkhead. Approximately 12 m of the west end of the heated drift are lined with cast-in-place concrete ground support. Concrete inverts were placed along the entire floor of the heated drift. Heat sources for the heated drift consists of nine canister heaters, placed end to end on the floor of the heated drift, and a total of 50 wing heaters (25 on either side) emplaced in horizontal boreholes drilled into the sidewalls of the heated drift about 0.25 m below the springline. The wing heaters are spaced 1.83 m apart. Each wing heater has two segments, both 5 m long, with a larger power output from the outer segment. The inner wing heater segment is separated from the heated drift by a space of 1.5 m.

The DST is instrumented with a variety of sensors to monitor the progress of the test. A summary of the installed sensors is presented in table 2-1 (TRW Environmental Safety Systems, Inc., 1998b).

In addition, the DST is actively monitored on a periodic basis with air permeability borehole testing and with geophysical measurements over three scales [borehole neutron probe, cross-hole ground penetrating radar (GPR) tomography, and cross-hole electrical resistivity tomography (ERT)] to provide information on changes in saturation associated with TH-coupled processes. Acoustic emissions are continuously monitored in anticipation of detecting microfracturing related to thermal-mechanical-coupled processes. Limited additional instrumentation was installed after heating was started in the DST. Heat dissipation probes and time domain reflectometers were installed in the ceiling on the cool side of the thermal bulkhead approximately 5 months after the onset of heating to track the movement of heat and moisture in the rock mass near the thermal bulkhead of the heated drift. These instruments were installed after water condensation on the drift walls immediately outside of the bulkhead was observed after about 40 days of heating.

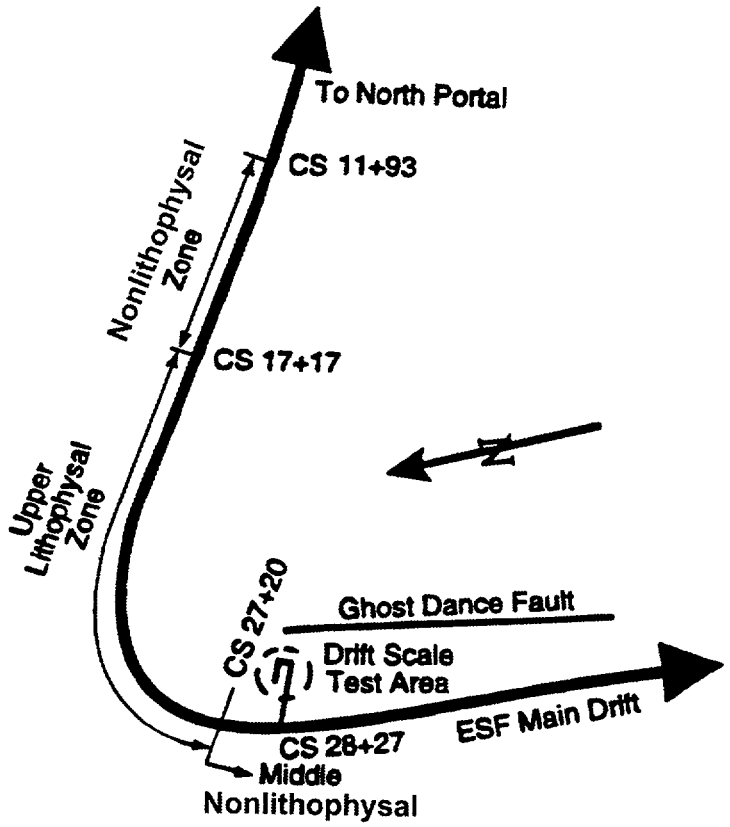

(a) Plan View

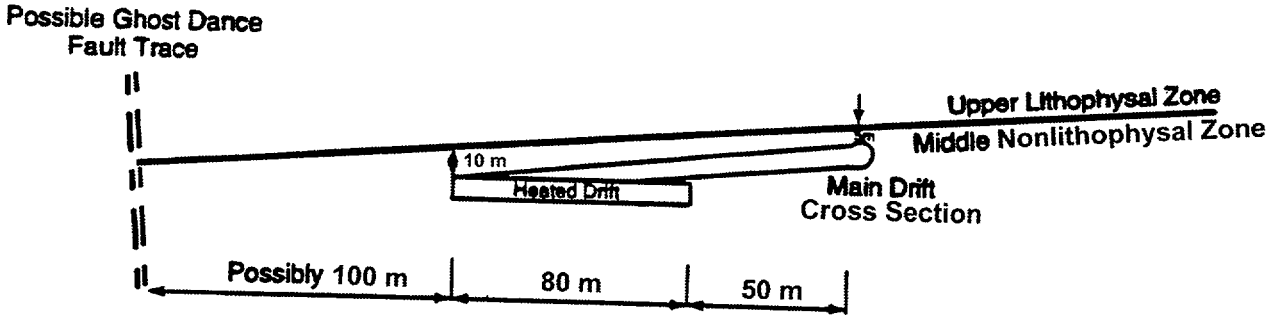

Reference Only
(SCALE APPROXIMATE)

(b) Profile View

Figure 2-1. (a) Plan view at the North Ramp of the Exploratory Studies Facility and Drift-Scale Test area, (b) cross section of the Drift-Scale Test area showing the heated drift in relation to the main drift and contact between geological units (TRW Environmental Safety Systems, Inc., 1997a)

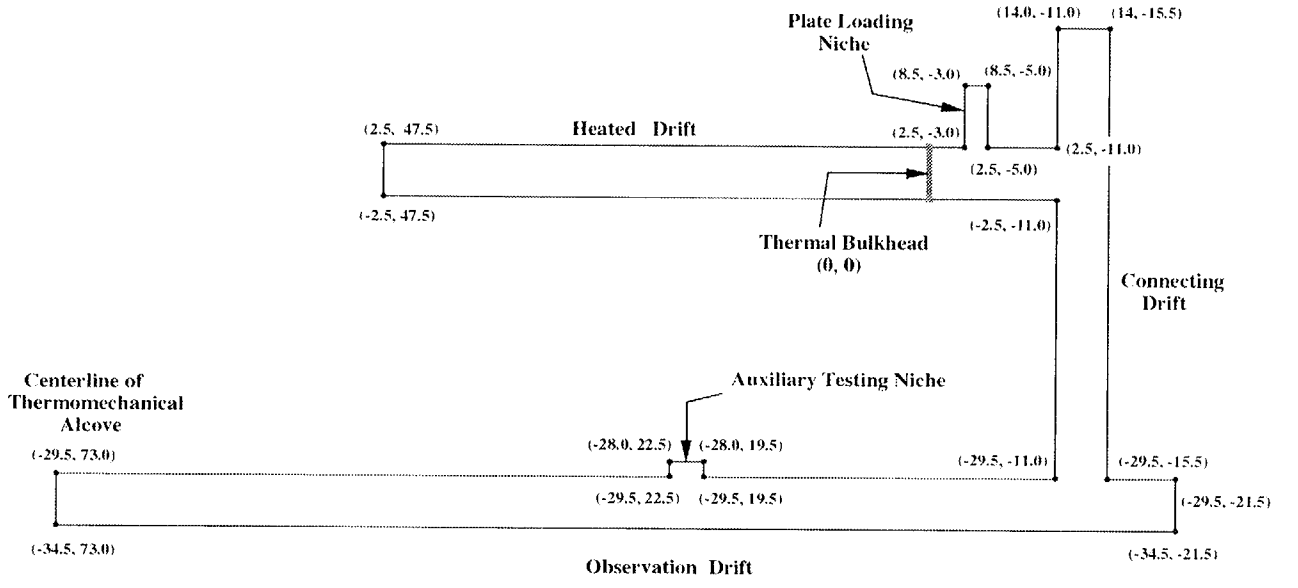

Notes:
1. X and Y coordinates are given in meters.
2. Z coordinates (vertical) are not included.
3. Only key locations are provided.
4. Coordinates are based on design with the following as-builts tolerances:
   Horizontal alignment = - 0 to + 0.5m
   All other = - 0 to + 0.3m

Figure 2-2. Plan view schematic of the primary components of Alcove 5 and the Drift-Scale Heater Test region (TRW Environmental Safety Systems, Inc., 1997b)

Table 2-1. Instrumentation for data collection in the Drift-Scale Heater Test (TRW Environmental Safety Systems, Inc., 1998b)

Number of Instruments	Instrument Type	Number of Channels	Data Collected
784	Thermocouples	784	Borehole and instrument temperature
1,936	Resistive temperature devices	3,872	Borehole and instrument temperature
19	Multi-point borehole extensometers	110	Rock displacement
10	Cross-drift wire extensometers	10	Rock displacement
19	Resistive strain gages	76	Deformation
48	Humidity sensors	48	Borehole humidity
48	Pressure sensors	48	Borehole pressure
195	Other temperature sensors	195	Borehole temperature
130	SEAMIST sensors	130	Rock chemistry
640	Heater monitors	640	Heater performance
30	Miscellaneous monitors	30	Heater adjustments

2.3 THERMAL BULKHEAD

Loss of energy and mass through the bulkhead at the east end of the heated drift, which separates the heated drift from the connecting drift, has been a subject of concern since the planning and design phases of the DST. From a pretest TH analysis, Buscheck and Nitao (1996) concluded that "the single-drift, winged thermal test can clearly discriminate between the throttled and unthrottled, nonbuoyant TH regimes" but cautioned about "the importance of isolating the heater drift from direct pneumatic interference with the rest of the tunnel system in the ESF." They suggest that it may "be necessary to bleed off some of the gas pressure (P_g) buildup and monitor the flux of water vapor leaving the heater drift through such a pressure relief system." Air permeability tests conducted in Alcove 5 prior to heating indicated a bulk average permeability for the fracture network on the order of 1×10^{-13} m^2 (Tsang and Cook, 1997) or approximately 0.1 D. Clearly this permeability is high enough to avoid throttled advective rock dryout and to allow dissipation of gas-pressure buildup. Subsequent pretest TH modeling (Birkholzer and Tsang, 1997) treated the bulkhead as a perfect thermal insulator and presumably also as impervious to gas flow although this was not explicitly stated in their report. Additional pretest modeling analyses (TRW Environmental Safety Systems, Inc., 1997a) showed a maximum pressure increase during heating of 0.07 atm for no gas allowed to escape through the bulkhead compared to a maximum increase of 0.05 atm with pressure relief through the bulkhead. The maximum vertical extent of the dryout zone was slightly greater (17.8 m versus 17.6 m) when venting through the bulkhead was allowed. Consequently, the bulkhead was designed as a thermal insulator and not to restrict gas flow between the heated drift and the ESF tunnel system.

Approximately 40 days after initiation of heating in the heated drift, condensation was noticed dripping from the ceiling outside the heated drift near the thermal bulkhead (TRW Environmental Safety Systems, Inc., 1998c). RH inside the heated drift was also noticed to fluctuate inversely with the barometric pressure in the access drift. Temperatures inside the heated drift appeared to respond almost immediately to changes in the ventilation system in the access drift (TRW Environmental Safety Systems, Inc., 1998d). These observations of condensation and temperature fluctuations led to the installation of heat dissipation probes in the drift ceiling on the cool side of the thermal bulkhead, sealing of leaks in the bulkhead such as the camera door and cable outlets, and redirection of the ventilation duct outlets near the bulkhead. Following discussions at several of the DOE Quarterly Thermal Testing Workshops, it was decided to investigate heat loss through the thermal bulkhead. Conductive heat loss was measured with heat flux meters placed on the thermal bulkhead at seven locations. These results indicated conductive heat loss of 5 kW through the thermal bulkhead (TRW Environmental Safety Systems, Inc., 1998d). Estimates of convective heat loss, based on water vapor collected from a small-diameter pipe in the bulkhead over a 60-min period, ranged from 2 to 20 kW. These estimates were later updated to 5–7 kW of conductive heat loss and from 4 to 30 kW of convective heat loss (TRW Environmental Safety Systems, Inc., 1999a).

Heat and mass losses through the thermal bulkhead were the central topics of a U.S. Nuclear Regulatory Commission (NRC)/DOE Appendix 7 meeting held on April 28, 1999, at the DOE offices in Las Vegas, Nevada. At this meeting, the NRC/Center for Nuclear Waste Regulatory Analyses (CNWRA) expressed concern that unmonitored heat and mass loss through the thermal bulkhead increased uncertainty in interpreting DST results and decreased the utility of the DST for determining if water would reflux into the heated drift or enter the drift during cooldown. The DOE responded that continuous monitoring of heat and mass loss through the bulkhead was problematic, prone to its own uncertainties, and was unnecessary since losses through the bulkhead could be estimated by matching model results with temperature data from the heated drift. Subsequently, an acceptance criterion was included in the Thermal Effects on Flow Issue Resolution Status Report (U.S. Nuclear Regulatory Commission, 1999) stating that thermohydrologic tests should be conducted "to account for all mass and energy losses/gains in the thermal test system."[1]

Buscheck presented results at the 8th Quarterly Thermal Testing Workshop on April 27, 1999, in Las Vegas, Nevada, from modeling studies conducted by Lawrence Livermore National Laboratory regarding the leaky thermal bulkhead boundary condition. These results indicated that loss of heat from the system through the bulkhead reduced potential dryout but may have caused more dryout early on because of the effects of ventilation. Reiterating his previous conclusions from Buscheck and Nitao (1996), he stated that unrestricted gas flux through the thermal bulkhead precludes the possibility of observing throttled advective dryout behavior. Buscheck also noted that effects of heat loss from the system might be important at the end of the heated drift farthest away from the thermal bulkhead because of heat deposition near the bulkhead from condensation.[2]

---

[1]An Interoffice Correspondence memo (footnote TRW Environmental Safety Systems, Inc.) dated October 21, 1999, summarized the April 28, 1999, Appendix 7 meeting and concluded that no modifications would be made to the DST and that heat and mass loss through the thermal bulkhead would not be continuously monitored.

[2]Hughson, D.L., and R. Green. 8th Thermal Workshop, Las Vegas, Nevada, April 27: Trip Report. 1999.

3 MODELING ANALYSES OF THE DRIFT-SCALE HEATER TEST BY THE CENTER FOR NUCLEAR WASTE REGULATORY ANALYSES STAFF

3.1 CENTER FOR NUCLEAR WASTE REGULATORY ANALYSES MODELING RESULTS PRESENTED AT THE APRIL 28, 1999, APPENDIX 7 MEETING

Preliminary modeling results presented by CNWRA staff at the NRC/DOE Appendix 7 Meeting, April 28, 1999, were similar to those presented by Buscheck at the 8th Quarterly Thermal Testing Workshop on April 27, 1999. A portion of those CNWRA modeling results, obtained using the code MULTIFLO 1.2 β (Lichtner and Seth, 1997), are presented here for completeness and to document part of the motivation for conducting further analyses on the effects of mass and energy losses from the DST system. Modeling analyses prior to the April 28, 1999, Appendix 7 Meeting used a structured two-dimensional (2D) grid, in an 80 m vertical and 120 m horizontal domain. Only one-half of this domain (60 m) was actually simulated because of the vertical symmetry resulting as a consequence of uniform properties and a symmetrical heat load. The 2D domain represented a vertical slice through the center of the heated drift, perpendicular to the long axis of the drift. Possible mass losses through the bulkhead were simulated as mass sink terms of magnitudes 2.2×10^{-6}, 4.4×10^{-6}, 8.8×10^{-6}, and 1.8×10^{-5} kg/m^2/s. These losses are equivalent to about 0.8, 1.6, 3.2, and 4.8 kg/hr of total mass from the total length of the drift, (approximated as 50 m long). Mass loss was distributed over elements in the upper half of the heated drift, which may have introduced some vertical asymmetry in the results. Figure 3-1 shows the temperatures above and below the heated drift after a heating time of 1.5 yr. The center of the heated drift is located at 42.5 m in the vertical coordinates. Constant temperatures of just below 100 °C in the vertical coordinate above 40 m and below 45 m for the case with no mass loss is the heat pipe signature of the zone of refluxing. The heat pipe is identified as the region with close-to-boiling temperature, which experiences a counter current of water vapor flowing away from the heat source and a liquid return flow by capillary or gravity forces. This heat pipe signature corresponds to the higher saturations in the fractures (shown in figure 3-2 for zero mass loss above the heated drift) from condensate drainage in the reflux zone. Figures 3-1 and 3-2 show that the reflux zones above and below the heated drift are slightly affected by 0.8 kg/hr of water loss over the length of the drift. Loss of 1.6 and 3.2 kg/hr from the model system through a mass sink within the heated drift causes collapse of the reflux zone above the heated drift so that there is no longer any noticeable heat pipe signature. DOE measurements of water vapor condensing from vapor flow through a small pipe in the bulkhead and a comparison of DOE models and temperature data were reported as being approximately 35 L/hr of water vapor loss through the bulkhead. To convert this estimate to mass flux, a specific volume of 2.9 m^3/kg was used representing saturated steam at the boiling point of water.[1] A loss of 35 L/hr was estimated to correspond to about 0.02 kg/hr, or a mass loss magnitude about 40 times smaller than the 0.8 kg/hr sensitivity shown in figures 3-1 and 3-2. It is likely that water vapor lost through the thermal bulkhead may have a noticeable effect on the development of refluxing above the heated drift during the heating phase if the DOE estimates of mass loss through the bulkhead match or exceed actual losses. The effect of gas flux through the thermal bulkhead on rewetting of the dryout zone and the potential for liquid water to enter the heated drift during the cooldown phase remain to be evaluated.

[1]TRW Environmental Safety Systems, Inc., Interoffice Correspondence memo dated October 21, 1999.

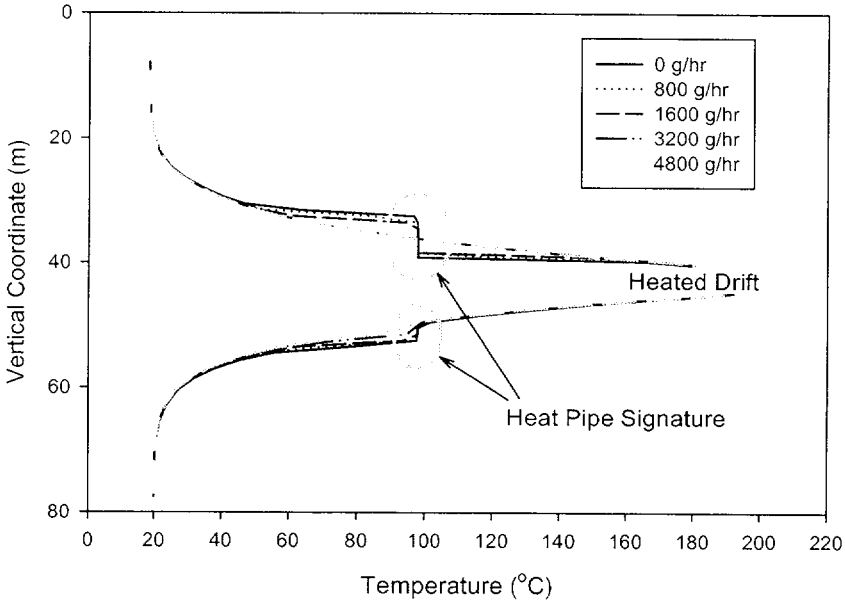

Figure 3.1 Temperatures above and below the heated drift after heating of 1.5 yr. The center of the heated drift is at 42.5 m in the vertical coordinate.

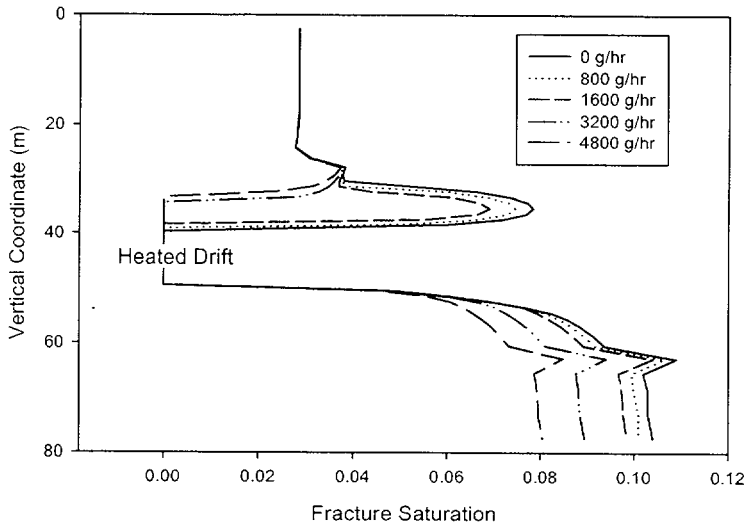

Figure 3-2. Saturation of liquid water in the fractures above and below the heated drift after heating for 1.5 yr. The center of the heated drift is at 42.5 m in the vertical coordinate.

3.2 OBJECTIVES OF THE CURRENT DRIFT-SCALE HEATER TEST THERMAL-HYDROLOGICAL ANALYSES

TH analyses of the DST reported in this document were performed to evaluate whether data collected from the DST are sufficient to achieve the goals outlined by Buscheck and Nitao (1996) and TRW Environmental Safety Systems, Inc. (1997a). Specific DOE objectives of the DST evaluated in these analyses are

- Do results from the DST permit identification of the dominant mode(s) of heat flow and the dominant TH flow regime?
- Is it possible to determine if a sufficiently large network of fractures has been incorporated by the DST to assess important decay-heat-driven processes such as boiling, vapor diffusion, buoyant gas-phase convection, and nonequilibrium, liquid-phase fracture flow?
- Is the DST sufficient
  - to allow for potential condensate buildup above the boiling zone?
  - to assess whether or not spatial variability in the gas- and liquid-phase pathways could focus enough condensate drainage to cause water to drip onto WPs?
  - to prevent edge-cooling effects from dominating TH behavior?
  - to allow evaluation of the significance of buoyant gas-phase convection on moisture movement and heat flow?

3.3 DRIFT-SCALE HEATER TEST MODEL DESCRIPTION

3.3.1 Numerical Model

Numerical analyses were performed using the flow component module, METRA, of the two-phase, multidimensional, nonisothermal heat and mass transfer simulator, MULTIFLO Version 1.2 (Lichtner et al., 2000). A dual-continuum conceptual model (DCM) was used to represent the fractured, welded Topopah Spring Tuff (TSw). The DCM formulation is consistent with the dual permeability continuum (DKM) formulation used in recent DOE numerical simulations (TRW Environmental Safety Systems, Inc., 2000). The DCM and DKM conceptualizations provide separate continua for the matrix and the fractures. These dual continua are coupled throughout the model domain by transfer functions for heat and mass transfer between the fractures and matrix. Use of a DCM increases the complexity of the numerical model used in the simulations. The relative importance of the parameters required for the DCM and their assigned values are evaluated in this analysis. Following is a description of key components to the DCM used in the numerical analyses of the DST.

The size of block designated in the DCM has a profound effect on the simulation of heat and mass transport. This effect is manifested in the ambient saturation, predicted by running the simulation to steady state in the absence of an internal heat source and in the temperatures and saturations predicted in response to a heat source. Block size directly affects two model properties: (i) the interfacial area between the matrix

and fracture continua in a DCM and (ii) the gradients that drive heat and mass between the two continua. In particular, increasing the block size reduces the area available for heat and mass transfer between the matrix and fracture continua and increases the distance over which changes in pressure and temperature occur, thereby reducing their respective gradients.

The interfacial area between the two continua, A_{fm}, is defined in terms of block dimensions, l_i, where $i = x$, y, and z. For two dimensions, the interfacial area per unit volume is defined

$$A_{fm} = 2\left(1-\varepsilon_f\right)\left[\frac{1}{l_x}+\frac{1}{l_z}\right] \tag{3-1}$$

which, for a cubic block geometry (i.e., $l_x = l_z$), becomes

$$A_{fm} = 4\left(\frac{1-\varepsilon_f}{l}\right) \tag{3-2}$$

where ε_f is fracture porosity.

Mass flow per unit volume across the matrix/fracture interface is directionally dependent. Liquid flow from the matrix to the fracture continuum is defined

$$Q_{l-\text{mass}}^{\text{m}\rightarrow\text{F}} = \frac{A_{fm}A_{\text{mod}}}{\mu_l} k_{\text{harmonic}} k_r \frac{P_{lm}-P_{lf}}{d} \tag{3-3}$$

and liquid flow per unit volume from the fracture to the matrix is defined

$$Q_{l-\text{mass}}^{\text{F}\rightarrow\text{m}} = \frac{A_{fm}A_{\text{mod}}A_{\text{mod}}^{*}}{\mu_l} k_{\text{harmonic}} k_r \frac{P_{lf}-P_{lm}}{d} \tag{3-4}$$

where k is liquid permeability, μ is viscosity, P_l is liquid pressure, and the m, f, l, and r subscripts denote matrix, fracture, liquid, and relative. The term d is the distance between the center of matrix block and the center of the fracture defining the edge of the block. The fracture-matrix distance is related, but not equivalent, to block size. For the case where the element is a cube, $d = l/2 + \delta/2$, where δ is fracture aperture. Fracture aperture is calculated in terms of block size, element size, and fracture porosity.

A_{mod} is a modifier term included to allow a reduction, but not an increase, in the interfacial area between the matrix and fracture continua. An additional area modifier term, A_{mod}^{*} is included in Eq. (3-4) to permit additional reduction in interfacial area experienced with flow from the fracture to the matrix continuum when fractures are less than fully saturated. For a tuff with low matrix permeability and partially saturated fractures, a value of 1.0 is typically assigned to A_{mod}, and a significantly smaller value

(i.e., 5.0×10^{-4}) is assigned to A^{*}_{mod}. A value of 1.0 assigned to A_{mod} keeps matrix gas pressures from increasing unrealistically. A value of less that 1.0 can be assigned to A_{mod} to account for interfacial permeability reductions caused by fracture coatings or other related physical mechanisms.

Relative liquid permeability, k_{rl}, is calculated as the upstream weighted average of the fracture and matrix permeabilities. Relative liquid permeability is calculated using the Mualem (1976) relationship

$$k_{rl} = \sqrt{s_l^{\text{eff}}}\left\{1-\left[1-\left(s_l^{\text{eff}}\right)^{1/\lambda}\right]^{\lambda}\right\}^2 \tag{3-5}$$

where capillary pressure is related to saturation by the van Genuchten (1980) relationship

$$s_l^{\text{eff}} = \left[1+\left(\alpha\left|P_c\right|\right)^{\text{m}}\right]^{-\lambda} \tag{3-6}$$

and effective liquid saturation, s_l^{eff}, is defined

$$s_l^{\text{eff}} = \frac{s_l - s_l^{\text{res}}}{s_l^{o} - s_l^{r}} \tag{3-7}$$

where res and o denote residual and maximum saturations; λ is related to m in Eqs. (3-5) and (3-6) by $\lambda = 1 - 1/\text{m}$. The harmonic mean for liquid permeability is expressed

$$k_{\text{harmonic}} = \frac{k_f\ k_m}{k_l + k_m} \tag{3-8}$$

An analogous form of Eq. (3-3) defines mass flow of gas from the matrix to the fracture continua.

$$Q_{g-\text{mass}}^{\text{m}\rightarrow\text{F}} = \frac{A_{fm}A_{\text{mod}}}{m_g}k_{\text{harmonic}}k_r\frac{P_{gm}-P_{gf}}{d} \tag{3-9}$$

where P_g is gas pressure. Note that mass flow of gas between the matrix and fracture continua is not directional. The A_{mod} for matrix to fracture gas flow is equal to the A_{mod} for fracture to matrix gas flow. The relative gas permeability is specified as the complement to relative liquid permeability

$$\text{k}_{rg} = 1 - \text{k}_{rl} \tag{3-10}$$

Analogous to mass flow are expressions and relationships for heat flow. Heat flow across the matrix fracture interface is defined

$$Q_{heat} = A_{fm} A_{mod} \kappa_{arithmetic} \frac{T_f - T_m}{d} \tag{3-11}$$

where T is temperature and thermal conductivity is defined by the arithmetic mean. Thermal conductivity is also defined as a function of saturation (Somerton et al., 1974).

$$\kappa = \kappa(sat) + \sqrt{s_l^{eff}} \left\{ \kappa(sat) - \kappa(dry) \right\} \tag{3-12}$$

where $\kappa(sat)$ and $\kappa(dry)$ are the thermal conductivities under fully saturated and dry conditions.

Note that heat transfer and mass transfer across the matrix/fracture interface are coupled processes, but each responds to its respective driving forces calculated over the same distance, d. Gradients that drive mass and heat transfer are decreased when the block dimensions are increased

3.3.2 Drift-Scale Heater Test Model Domain

A vertically oriented 2D cross section of the DST was assembled for these analyses. The cross section intersects the axis of the heater drift middistance between the bulkhead and the terminus of the heated drift. The modeled area extends 200 m in the vertical direction and 160 m in the horizontal direction with the center of the heated drift placed at the center of the numerical model. The model is represented using an unstructured grid loosely patterned after the grid of Birkholzer and Tsang (1997). The full grid, consisting of 1,744 nodes, is illustrated in figure 3-3, and a close-up view of the grid in the vicinity of the heated drift is shown in figure 3-4, which illustrates the finer mesh resolution in areas expected to experience large temperature, saturation, and pressure gradients. Three hydrostratigraphic units were included in the model: the Tptpul (TSw33), Tptpmn (TSw34), and the Tptpll (TSw35) units of the Topopah Spring welded unit. The thickness of the Tptpmn in the vicinity of Alcove 5 is approximately 35 m, with the centerline of the heated drift approximately 24 m below the base of the Tptpul (TRW Environmental Safety Systems, Inc., 1997a).

3.3.3 Model Property Assignments

Property values for the three hydrostratigraphic units of the DST model, the TSw33, TSw34, and TSw35 were taken from the TSPA-VA (TRW Environmental Safety Systems, Inc., 1998a). The particular values from the TSPA-VA used in this study were taken from the TH parameter set that was calibrated against the SHT. These values are summarized in tables 3-1 through 3-3.

3.3.4 Model Initial and Boundary Conditions

The vertical boundaries of the model were specified as adiabatic with no fluid flow. The top boundary for the basecase was specified as either a Neumann boundary with a constant flux or a mixed boundary with specified flux, and the bottom boundary was a prescribed pressure, temperature, and saturation. The difference between the two upper boundary conditions is the Neumann boundary condition

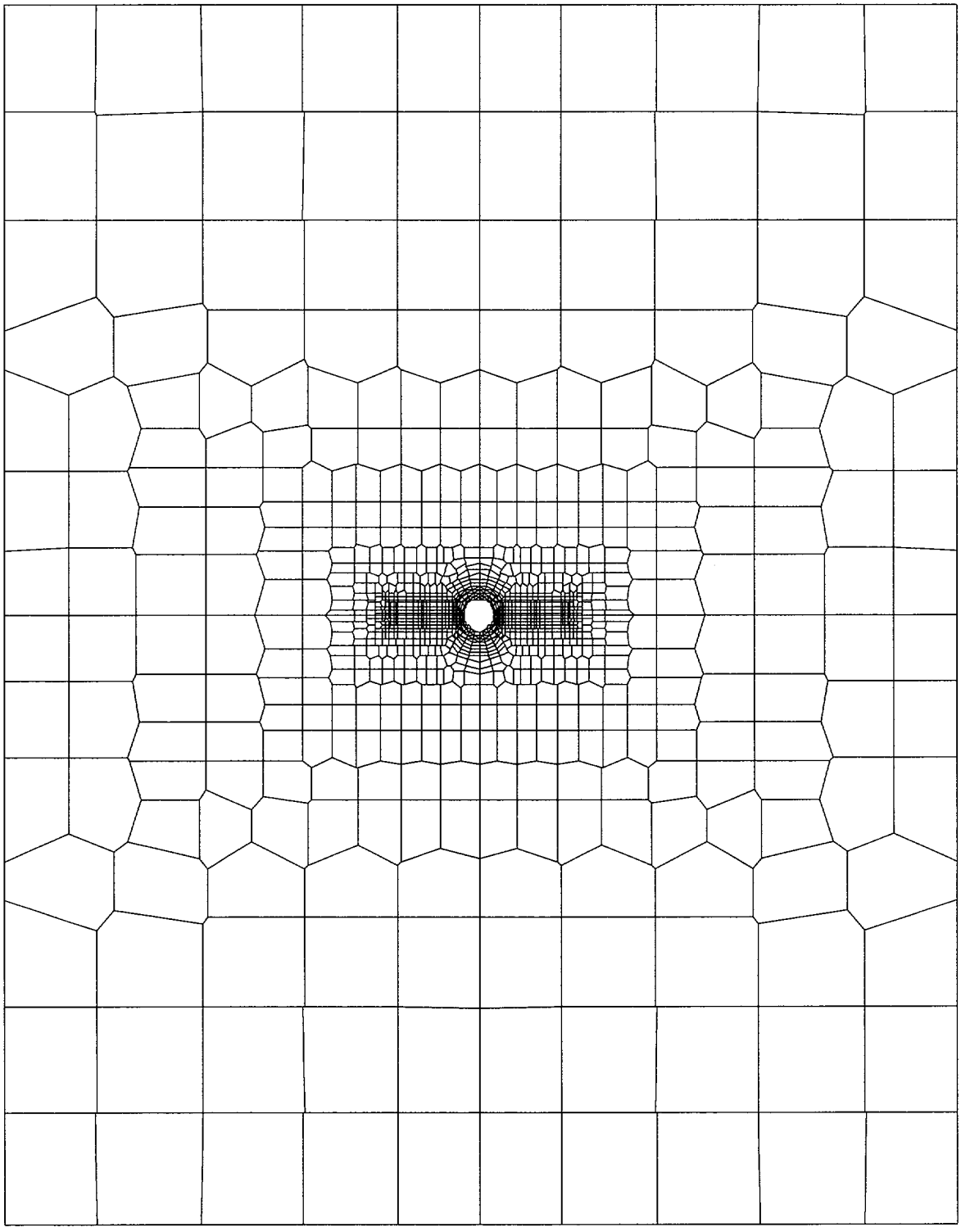

Figure 3-3. Unstructured grid discretization of the drift-scale

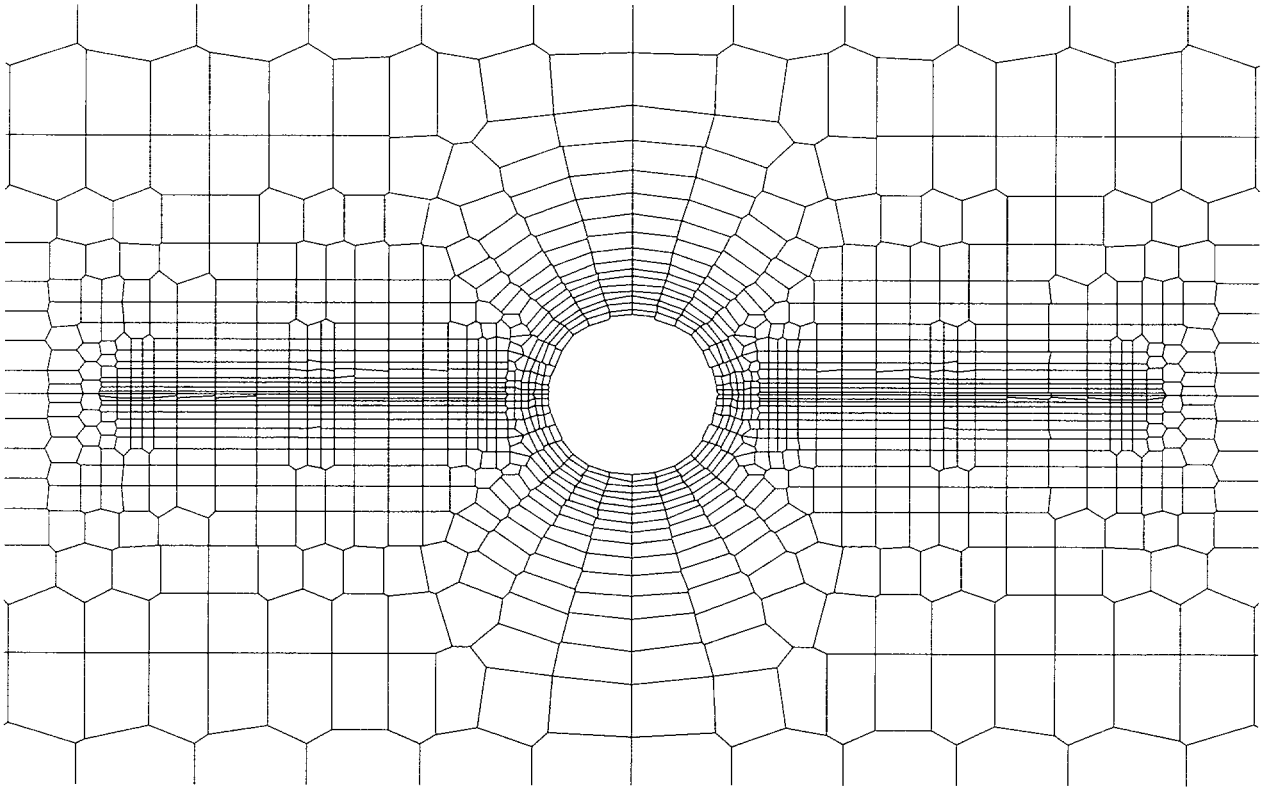

Figure 3-4. Close-up view of drift-scale model discretization

Table 3-1. Matrix hydraulic properties taken from Total System Performance Assessment-Viability Assessment thermal-hydrological parameter set (TRW Environmental Safety Systems, Inc., 1998a)

Unit	Porosity	Permeability (m^2)	Residual Saturation	α (Pa^{-1})	m
TSw33	0.135	2.04×10^{-17}	0.06	6.21×10^{-6}	0.2479
TSw34	0.089	4.08×10^{-18}	0.18	1.19×10^{-6}	0.3212
TSw35	0.115	2.22×10^{-17}	0.08	4.01×10^{-6}	0.1983

Table 3-2. Fracture hydraulic properties from Total System Performance Assessment-Viability Assessment thermal-hydrological parameter set (TRW Environmental Safety Systems, Inc., 1998a)

Unit	Porosity	Permeability vertical (m^2)	Permeability horizontal (m^2)	S_r	α (Pa^{-1})	m
TSw33	1.05×10^{-4}	2.63×10^{-11}	8.91×10^{-13}	0.01	1.73×10^{-3}	0.667
TSw34	1.24×10^{-4}	6.76×10^{-12}	4.27×10^{-13}	0.01	9.34×10^{-4}	0.643
TSw35	3.29×10^{-4}	3.80×10^{-12}	9.12×10^{-13}	0.01	1.26×10^{-3}	0.667

Table 3-3. Matrix thermal and physical properties [from Total System Performance Assessment-Viability Assessment (TRW Environmental Safety Systems, Inc., 1998a)]

Unit	Thermal Conductivity-Wet (W/m-K)	Thermal Conductivity-Dry (W/m-K)	Rock Specific Heat (J/kg-K)	Rock Density (kg/m^3)
TSw33	1.80	0.71	883	2,510
TSw34	2.33	1.56	948	2,530
TSw35	2.02	1.20	900	2,540

prohibits gas or heat flow out of the top of the model. The mixed boundary condition allows gas and heat transport in or out of the model to maintain pressure and temperature as specified.

A sensitivity analysis was conducted to evaluate how different property assignments and boundary and initial conditions affect matrix saturation. The model was run until steady-state conditions were approximated. As demonstrated in the sensitivity analyses results, changes in these property values have a significant effect on predicted matrix saturation. A matrix saturation of 0.924 was assumed in the Thermal Tests Thermal-Hydrological Analyses/Model Abstraction (TRW Environmental Safety Systems, Inc., 2000) to be representative of ambient matrix saturations of the TSw34 at the DST. The upper and lower boundaries were initially set at temperatures of 22 and 26 °C and pressures of 93,361 and 101,325 Pa.

3.4 DRIFT-SCALE HEATER TEST MODELING RESULTS

Simulation of the DST was accomplished in a step-wise fashion. First, ambient conditions for the model were predicted for a variety of property values input in simulations run in the absence of heat from the DST. These sensitivity analyses were performed for a model assigned with basecase property values with the exception of the variable under investigation. The basecase property values used in these analyses are shown in tables 3-1 through 3-3.

Second, transient heat and mass transfer was predicted for the heating phase of the DST using the predicted ambient conditions as the initial conditions. Included in these transport analyses were simulations conducted to evaluate the effect of lower fracture permeability, higher thermal conductivity in the host rock, variations in the infiltration rate, and the potential effect of mass loss through the DST thermal bulkhead.

3.4.1 Ambient Conditions Simulations

Numerical analyses were conducted using MULTIFLO to evaluate model parameters that influence ambient conditions and, in particular, matrix saturation. Ambient matrix saturation was selected as the key state variable to evaluate the appropriateness of the pretest conditions for the conceptual and numerical models used to simulate the DST because of the sensitivity to changes in model design and the ability to measure saturation in the field. Ambient matrix saturation for TSw34 is documented as 0.924 in the Thermal Tests Thermal-Hydrological Analysis Model Report (TRW Environmental Safety Systems, Inc., 2000).

Ambient saturation was determined by simulating flow in the absence of heating at the DST for sufficiently long periods of time that steady-state flow conditions were approximated. Steady-state flow conditions were usually approximated in 300,000 to 700,000 yr although steady state was approximated in as little as 100,000 yr for models with reduced fracture permeability. The heater drift was not explicitly included in the model. The heater drift was modeled as a no-flow boundary and heat from the floor canisters was applied directly to the heater drift walls. The effect of the no-flow boundary, at the heater drift wall on the predicted ambient saturation is assumed to be minimal except in the near field below the drift. The wing heaters have the same hydraulic properties as the adjoining rock (Tptpmn) and should not affect ambient saturation predictions.

Ambient matrix saturation was predicted for a range of values for several different model parameters. Model parameters evaluated in this study were infiltration rate, block size, liquid flow from matrix to fracture interaction area (i.e., A^*_{mod}), the upper boundary condition, and fracture permeability. Specific changes to model parameters that were evaluated were as follows:

- Surface boundary changed from Neumann to mixed
- Block size varied from 0.25 to 20 m, infiltration flux at the surface varied from 0.00036 to 3.6 mm/yr
- Liquid flow from matrix to fracture interaction area (A^*_{mod}) varied from 1.0 to 5.0×10^{-4}
- Anisotropic fracture permeability decreased up to three orders of magnitude in the x-, y-, and z-directions from the basecase values

As will be demonstrated, changes in block size and the surface boundary condition proved to have a significant effect on ambient matrix saturation. Changes in infiltration rate had a significant effect when the upper boundary condition was a Neumann type. Changes in values assigned to fracture permeability had no effect on ambient saturation but did affect temperatures and saturations predicted for the heating phase of the DST. Changes in A^*_{mod} did not result in significant changes in ambient matrix saturation. Matrix saturation predicted for the Tptpmn (TSw34) at a height of 8.9 directly above the drift crown was selected for comparison.

Ambient matrix saturation was simulated for two boundary conditions assigned to the top of the model: (i) a Neumann condition with a fixed liquid flux and (ii) mixed conditions with specified gas pressure, temperature, and liquid flux. The model bottom was maintained as a Dirichlet boundary with matrix and fracture saturations of 0.9 and 0.05 after cursory analyses indicated that changes to the lower boundary condition had minimal effect on ambient model conditions. Evaluation of the mixed boundary condition was not complete at the time of this report and will be documented in a subsequent report. All results reported here are predicated on a Neumann upper boundary condition.

Designating the model top as a Neumann boundary with a fixed liquid flux prohibited the flow of gas and liquid either into or out of the model domain through the surface boundary. Although a buildup in gas pressure near the surface was not encountered, assumption of a Neumann boundary condition at the top of the model did lead to a significant error in the mass balance of air in one simulation reported in this study

(i.e., heating period simulation for infiltration at 3.6 mm/yr and a reduced fracture permeability). The significance of this mass balance error has not yet been fully evaluated.

Simulations were conducted to evaluate the effect of the upper boundary condition on ambient matrix saturation relative to a variety of changes in other variables of interest. In general, specifying the top of the model as a mixed boundary condition resulted in consistently high ambient matrix saturations, typically above 0.99 at the reference point located 8.9 m above the top of the heater drift, irrespective of values assigned to the other variables. The high ambient saturations persisted for low infiltration rates (i.e., 0.0036 mm/yr) and block sizes up to 1.0 m on a side. Significantly lower matrix saturations were encountered for a Neumann boundary condition specified at the top of the model. Matrix saturation at the reference point 8.9 m above the heater drift varied from 0.859 at an infiltration of 0.036 mm/yr up to 0.9997 at an infiltration of 3.6 mm/yr. A block size of 0.25 m an A^*_{mod} of 5.0×10^{-4} were specified in these Neumann boundary condition simulations. Varying the A^*_{mod} had a negligible effect on the ambient saturations predicted for the Neumann upper boundary condition simulations.

Increasing the block size was the only parameter variation for a mixed upper boundary condition that simulated reduced matrix saturations at the reference point located 8.9 m above the heater drift. Matrix saturations were predicted for block sizes of 0.25 m to 20.0 m. (Note that all three sides of the blocks are assigned a length equal to the size indicated in figure 3-5.) An infiltration rate of 3.0 mm/yr was assumed in

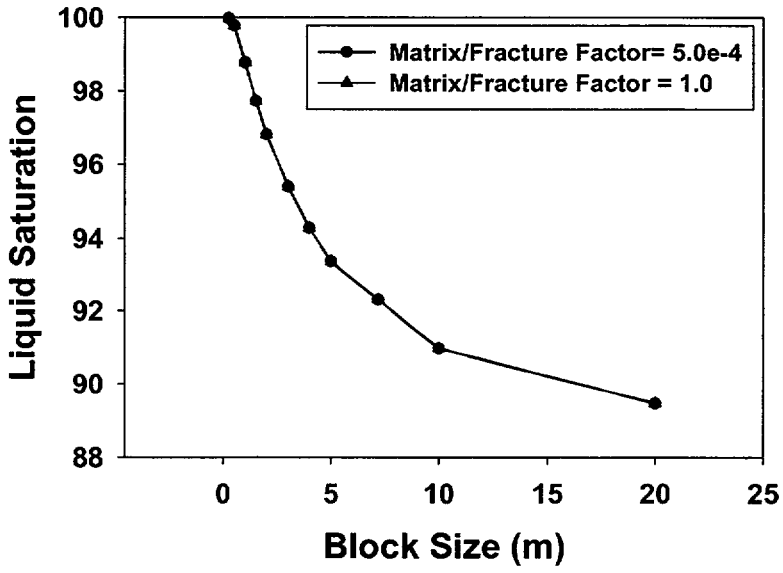

Figure 3-5. Ambient matrix saturation at a reference point 8.9 m above the heater drift crown versus change in block size for an A^*_{mod} of 1.0 and 5.0×10^{-4}

these simulations. The simulations were run for an A^*_{mod} of 1.0 and 5.0×10^{-4}. As illustrated in figure 3-5, the matrix saturation was reduced from 0.9997 for a block size of 0.25 m to 0.8953 for a block size of 20.0 m. The lower saturation is attributed to the reduced matrix/fracture interfacial area and the decreased pressure gradient between the two continua. Variation in A^*_{mod} had negligible effect on saturation in these simulations.

The effect of changes in the infiltration rate from 0.00036 mm/y to 3.6 mm/y was evaluated. A block size of 0.25 m and an A^*_{mod} of 5.0×10^{-4} were assumed in these analyses. The rate of infiltration has a pronounced effect on matrix saturation for a Neumann boundary condition assigned to the model top. The matrix saturation at the reference point located 8.9 m above decreased from 0.9997 to 0.9549 and 0.8593 for a decrease in infiltration from 3.6 mm/yr to 0.36 and 0.036 mm/yr, respectively. A block size of 0.25 m and an A^*_{mod} of 5.0×10^{-4} were assigned in these calculations.

The permeability assigned to the fractures in the DCM conceptualization did not have a significant effect on predicted ambient saturation. Matrix saturation at the reference location was predicted for the basecase fracture permeabilities and up to a three order-of-magnitude decrease in fracture permeabilities compared to the basecase values in table 3-2. In all simulations, the anisotropic fracture permeabilities of all three modeled units, TSw33, TSw34, TSw35, were uniformly reduced. At an infiltration rate of 0.00036 mm/yr, matrix saturations at the reference location decreased slightly from 0.7927, to 0.7921, and 0.7917 for three different fracture permeability values (i.e., basecase, 0.01 × basecase, and 0.001 × basecase). At a greater infiltration rate of 3.6 mm/yr, matrix saturations at the reference location for simulations with the same three fracture permeabilities were 0.9997, 0.9999, and 0.9999. A block size of 0.25 m and an A^*_{mod} of 1.0 with a Neumann boundary condition at the model top were assumed in these simulations.

Some model assumptions evaluated in this report obviously do not predict ambient matrix saturations that approach the documented values (i.e., 0.924) (TRW Environmental Safety Systems, Inc., 2000). The inability to predict matrix saturations consistent with the published values may suggest that either the conceptual model is in error or that assigned model input values are inappropriate. Conversely, the inability to match documented ambient saturations raises some doubt that the documented saturation values are representative. All three of these possibilities should be considered for those occurrences (i.e., input parameter combinations) where predicted matrix saturations fail to match documented saturation values.

Several simulations led to matrix saturations consistent with the documented value of 0.924. An infiltration rate of about 0.25 for a block size of 0.25 m predicted TSw34 matrix saturations similar to the measured values. Greater infiltration rates can be achieved for larger block sizes. The ability to predict moderate matrix saturations (i.e., less than 0.95) for an upper Neumann boundary condition, but not for a mixed boundary condition, raises doubts about the appropriateness in the implementation of the conceptual model. This issue is still being evaluated. Additional measurement of matrix saturation should be pursued, preferably using independent methods if available.

3.4.2 Transient Nonisothermal Simulations

Heat and mass transfer at the DST was simulated with MULTIFLO Version 1.2 (Lichtner et al., 2000) using the steady-state predictions discussed previously as the initial conditions. Combinations of input parameters were selected for analysis to span the range of values considered reasonable for the DST.

3.4.2.1 Model Heat Source

Heat was introduced into the model at the heated drift and at the inner and outer wing heaters. All three heat sources supplied a heat rate (W) per grid block to the elements surrounding the interior, no-flow boundary representing the heated drift. The heated drift cavity was not explicitly included in the model because of difficulties associated with representing the air space within the drift, radiative and convective heat transfer between the heater canisters and the drift wall, and the physics of heat and mass transfer at the drift cavity/drift wall boundary. The disadvantage to this simplification is that coupled TH processes at the drift wall cannot be directly or easily investigated using this model. The heat source levels were ramped up over 4 hr to the maximum heat load applied uniformly to each of the 36 drift boundary elements at the 5-m-diameter drift wall. The inner and outer cylindrical wing heaters were represented as individual rectangular slabs, thereby smearing the heat in the y-direction of the model. The 4.65-m-long inner wing heater was set at a distance of 1.62 m from the drift wall. The 4.45-m-long outer heater was separated from the inner heater by 0.82 m. Both wing heaters were assigned a vertical thickness of 0.2 m. These dimensions are consistent with those provided in the as-built report (TRW Environmental Safety Systems, Inc., 1998b), with the exception of the wing heater thickness. The wing heaters were modeled as 0.2 m thick, rather than the reported diameter of 24 mm, because of constraints on mesh resolution. Increasing the thickness of the wing heaters will distort the resulting TH regime in the region close to the heat source, however, the effect should be negligible beyond a few tens of centimeters.

The design thermal load for the DST was 68.0 kW for the canister heaters and 143.0 kW for the cumulative wing heaters (85.8 kW at the outer wing heater and 57.2 kW for the inner wing heaters) for a total of 211 kW (TRW Environmental Safety Systems, 1998b). The DST has experienced measured heat loads that deviate significantly (less) from the levels of the design heat loads since energizing in December 1997 (figure 3-6). At the time of energizing, the canister heat load was about 52.8 kW and the cumulative wing heater heat load was about 137 kW (TRW Environmental Safety Systems, Inc., 1998c). These power levels decreased after heating started, however, the precise magnitude of decrease is not well defined. Conflicting measurements between qualified and currently nonqualified data suggest the heat load values decreased to between 49.4 (nonqualified) to 51.8 (qualified) kW for the canisters and between 130.8 (nonqualified) to 133.3 (qualified) kW for the wing heaters by day 179 after heating started. Qualified canister heat load measurements continued to decrease to about 51 kW by day 244, but then increased to about 53.5 kW over the next 26 days until day 270 (TRW Environmental Safety Systems, Inc., 1998d). After day 270, the canister heat load resumed a gradual, consistent decline, decreasing to 51.5 kW by day 700 (TRW Environmental Safety Systems, Inc., 1999b). The canister heat load increase over days 244 to 270 is attributed to a modification in the access drift and heat drift (outside the thermal bulkhead) ventilation system.

The wing heaters also experienced an increase in heat load soon after day 244, however, this increase followed a rather precipitous decrease in the (qualified) heater load from about 133 kW at day 185 to less than 130 kW by day 244 (TRW Environmental Safety Systems, Inc., 1998d). The cause of this precipitous heat load decrease is attributed to the loss of power to wing heater 29. Measured (qualified) heater load values continued to decrease to about 52.3 kW for the canisters and to slightly over 130 kW for the wing heaters by day 480 (TRW Environmental Safety Systems, Inc., 1999a) and to about 51.5 kW for the canisters and 128.2 kW for the wing heaters by day 700 (TRW Environmental Safety Systems, Inc., 1999b).

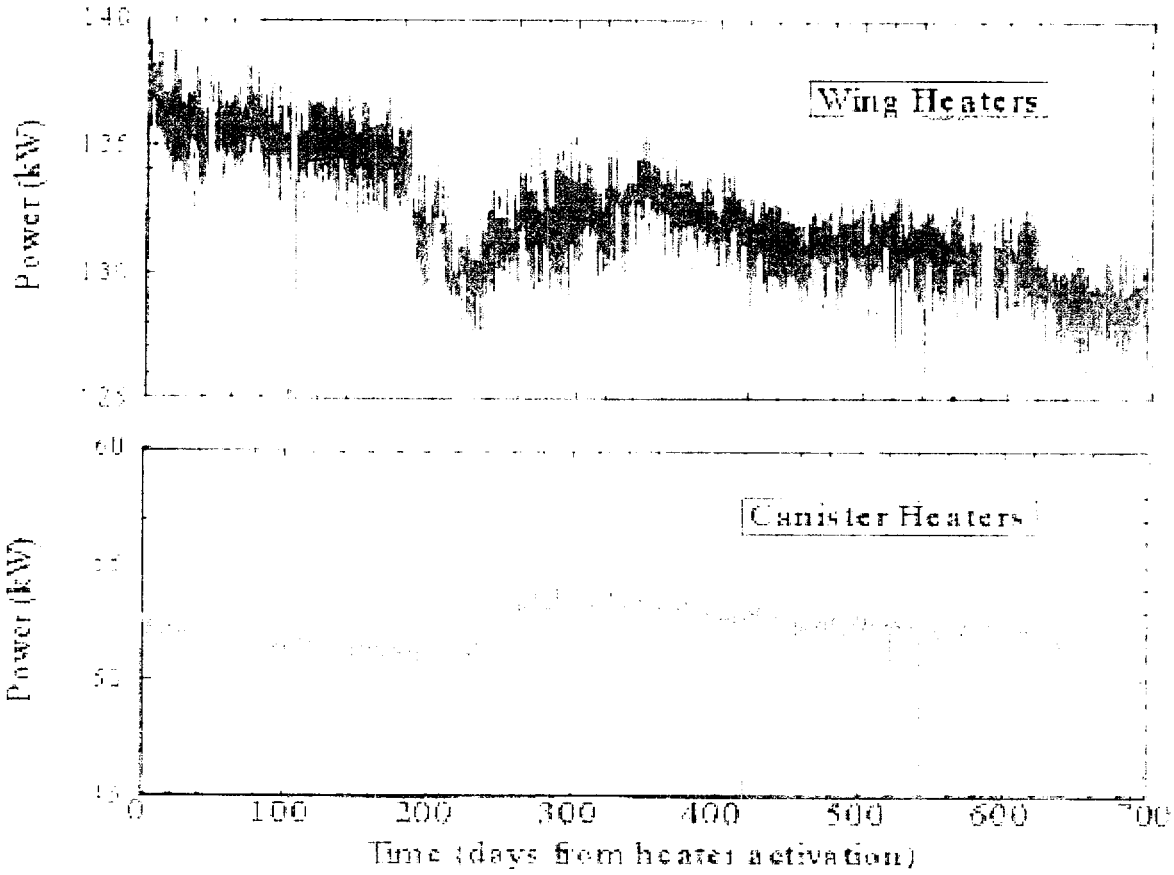

Figure 3-6. Total power measurements (Q) for the wing heaters and canister heaters

Heat loads consistent with measured levels were assigned to the model in the TH evaluations. The thermal loads were ramped up to their starting power levels over a period of about 4.2 hr to avoid stability problems. Heat loads were established to resemble the (qualified) heat loads measured for the first 1.9 yr of heating (TRW Environmental Safety Systems, Inc., 1999b). The measured cumulative heat load for the canister heaters was estimated to remain constant at 52 kW up to day 700 of the test. Transient effects from deviations in the canister heat load from 52 kW, which decreased to about 51 kW by day 230 and increased to about 53.8 kW by day 280, are presumed to be negligible with respect to the scale of investigation. The overall reduction in the cumulative canister heat load was 23.5 percent from the design level of 68 kW to the actual measured level of 52 kW.

The measured cumulative heat load for the wing heaters demonstrated a defined decreasing trend, with some deviation, for the first 700 days of heating. Deviations of actual heat loads from a linear decline in cumulative wing heater heat load between days 180 to 240 have been neglected, and a constant linear decrease in cumulative wing heater heat load from 136.5 kW at the onset of heating to 128.2 kW at day 700 was assumed. It was assumed that the decrease in cumulative heat load for the wing heaters occurred uniformly over both the inner and outer wing heaters. Accordingly, the inner wing heaters decreased from 54.6 to 51.3 kW, and the outer wing heaters decreased from 81.9 to 76.9 kW during the first 1.9 yr of heating.

The decrease in heating of the wing heaters varied from a 4.5-percent decrease from the design basecase values heat of 143 kW at the start of heating to a 10.3-percent decrease at day 700.

3.4.2.2 Thermal-Hydrological Simulation Cases

Heat and mass transfer at the DST was predicted for nine different combinations of model parameters. The parameters selected for this analysis were those that resulted in the greatest change in thermal-hydrologic response when varied. In six of the cases, the varied parameters were infiltration rate (0.036 and 3.6 mm/yr), fracture permeability (basecase values and two orders of magnitude less than basecase values), and effect of the thermal bulkhead (no mass loss and 80 or 200 mL/hr mass loss). The other two cases evaluated the effect of a one-third increase in thermal conductivity values assigned to all three model units. The modified values for thermal conductivity are summarized in table 3-4. An infiltration rate of 0.036 mL/hr and low fracture permeabilities were assumed for the elevated thermal conductivity cases. A block size of 0.25 m, a Neumann upper boundary condition, and an A^*_{mod} of 1.0 were assumed in all calculations. Parameter values for these cases are summarized in table 3-5.

Table 3-4. Basecase and modified values assigned to thermal conductivity [W/(m °C)]

Unit	TSw33 (Tptpul)		TSw (Tptpmn)		TSw (Tptpll)	
Saturation	Dry	Wet	Dry	Wet	Dry	Wet
Basecase	0.71	1.80	1.56	2.33	1.20	2.02
Modified	0.94	2.39	2.07	3.10	1.60	2.69

Table 3-5. Summary of parameter values assigned to thermal-hydrological simulations of the Drift-Scale Heater Test. Basecase values are listed in tables 3-1, 3-2, and 3-3.

Permeability (m^2)	Infiltration Rate (mm/yr)	Bulkhead Mass Loss (mL/hr)	Thermal Conductivity (W/m-°C)
Basecase values	0.036	None	Basecase values
Basecase values	0.036	80	Basecase values
10^{-2} reduction	3.6	None	Basecase values
10^{-2} reduction	3.6	80	Basecase values
10^{-2} reduction	0.036	None	Basecase values
10^{-2} reduction	0.036	80	Basecase values
10^{-2} reduction	0.036	None	one-third increase in κ_r
10^{-2} reduction	0.036	80	one-third increase in κ_r
10^{-2} reduction	0.036	80	one-third decrease in κ_r

Effects from the boundary condition represented by the thermal bulkhead were indirectly incorporated into the 2D model by placing mass sink terms uniformly in the elements at the drift wall boundary. The rate of mass loss through the bulkhead has been roughly estimated to be 200 mL/hr.[2] The actual rate of mass loss is unknown. A mass flux rate of 80 mL/hr was assigned to these test cases. Mass removal in MULTIFLO is restricted to the liquid phase. This limits the mass of water removed in the simulation to the mass of liquid water present in the heater drift wall elements from which mass is removed. MULTIFLO, as currently implemented, cannot extract vapor phase water. Attempts to extract water at rates in excess of 80 mL/hr failed when all liquid phase water was removed from any element. Nonetheless, the effect of the removal of limited amounts of water can be evaluated with these simulations.

3.4.3 Comparison of Drift-Scale Heater Test Modeling by the Center for Nuclear Waste Regulatory Analyses with Drift-Scale Heater Test Data

Matrix temperatures and saturations simulated for the DST basecase are compared to temperatures in two boreholes, No. 158 and No. 160, measured after 1 yr of heating. Borehole 158 is located at the midpoint of the drift and is oriented vertically upward from the drift crown. Borehole 160 is also located at the midpoint of the heater drift but is horizontally oriented from the springline of the heater drift toward the DST observation drift. Borehole 160 is placed about 0.2 m above the wing heaters. Both boreholes are 20 m in length. Contour plots for temperature and saturation for both the matrix and fracture continua are presented for the two cases.

Basecase simulations with an infiltration rate of 0.036 mm/yr for the heating phase of the DST predicted temperatures different from temperatures observed in Boreholes 158 and 160 (figure 3-7a,b). A significant heat pipe was predicted for a zone above the heater drift to a depth of approximately 4.5 m into the rock after 1 yr of heating. In contrast, temperatures recorded in Borehole 158 indicate the formation of a slight heat pipe at a depth of approximately 3.5 m into the rock. Measured temperatures of the rock above the heat pipe are greater than those predicted for the model (note that simulated matrix temperatures equal fracture temperatures, this is mostly because of the value of unity assigned to A^*_{mod}). Similarly, along Borehole 160, with the exception of the heat source element located at the heater drift wall, simulated temperatures were as much as 40 °C less than above the inner wing heater and 25 °C less than above the outer wing heater (figure 3-7b). Simulated temperatures beyond the outer heater were in agreement with measured temperatures. Contour plots of matrix and fracture temperature and saturation for the basecase are illustrated in figure 3-8a,b,c,d. Temperatures for the matrix are similar to those for fracture (figure 3-8a,b) with the highest temperatures observed at the springline of the heater drift and slightly lower temperatures observed in the outer wing heaters. This similarity between matrix and fracture temperatures is consistent with a value of unity assigned to A^*_{mod} . A general increase in fracture saturation is observed above the DST with the greatest increase located above the heater drift although the maximum predicted fracture saturation is approximately 0.2 (figure 3-8d). There is also an increase in fracture saturation that extends approximately 70 m below the DST horizon. Predictions of matrix saturation indicate a distinct zone of dryout formed both above and below the DST to a distance of several meters although less than complete dryout was observed in the area immediately above the heater drift (figure 3-8c). A zone of increased saturation formed beyond the dryout zone. These zones were slightly nonsymmetric relative to a horizontal plane through the DST. Both the extent and the area of increased saturation were greater below the DST compared to above. The basecase model also predicted a large temperature difference between the springline and at the heater drift

[2]TRW Environmental Safety Systems, Inc., Interoffice correspondence memo dated October 21, 1999.

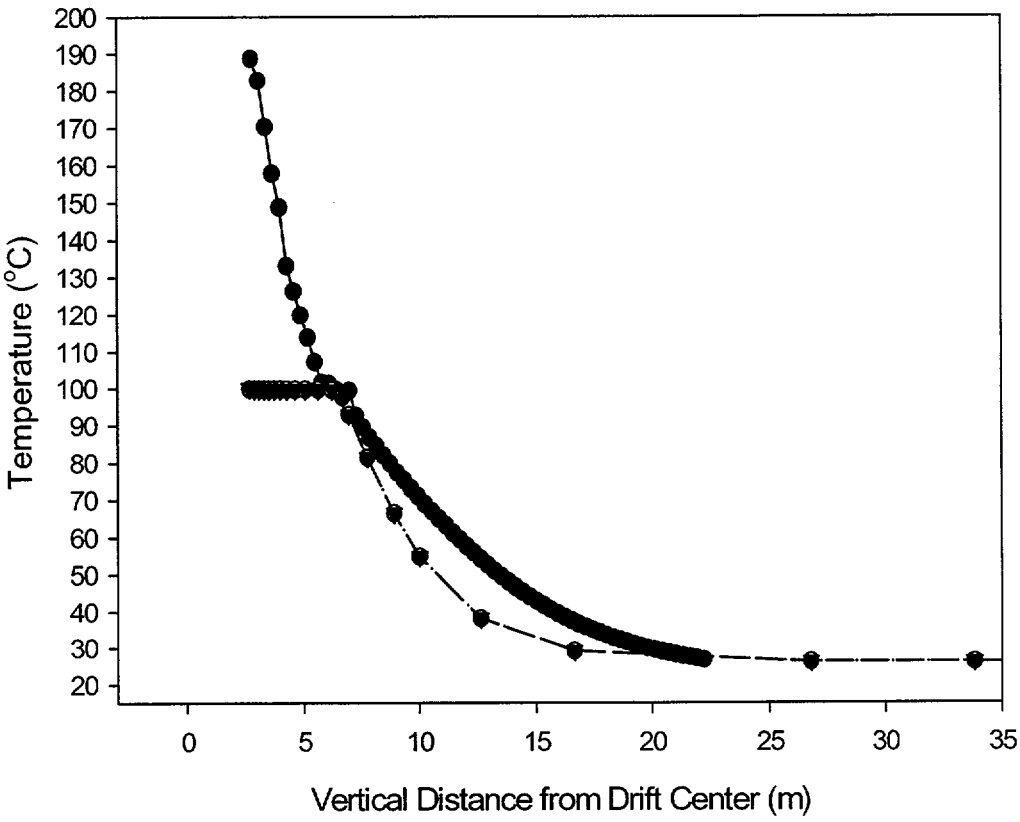

Figure 3-7a. Comparison of measured temperatures (solid circle) versus simulated temperatures in the matrix (closed triangle) and fracture (open circle) for vertical Borehole 158 for basecase property values and an infiltration rate of 0.036 mm/yr

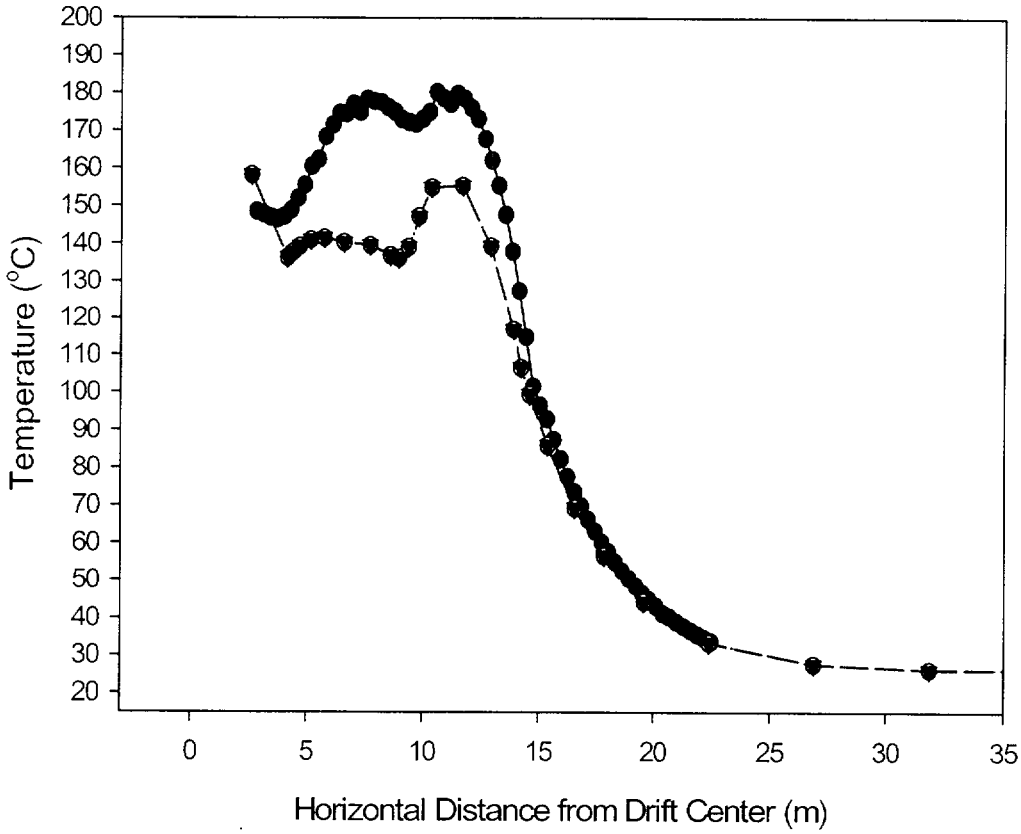

Figure 3-7b. Comparison of measured temperatures (solid circle) versus simulated temperatures in the matrix (closed triangle) and fracture (open circle) for horizontal Borehole 160 for basecase property values and an infiltration rate of 0.036 mm/yr

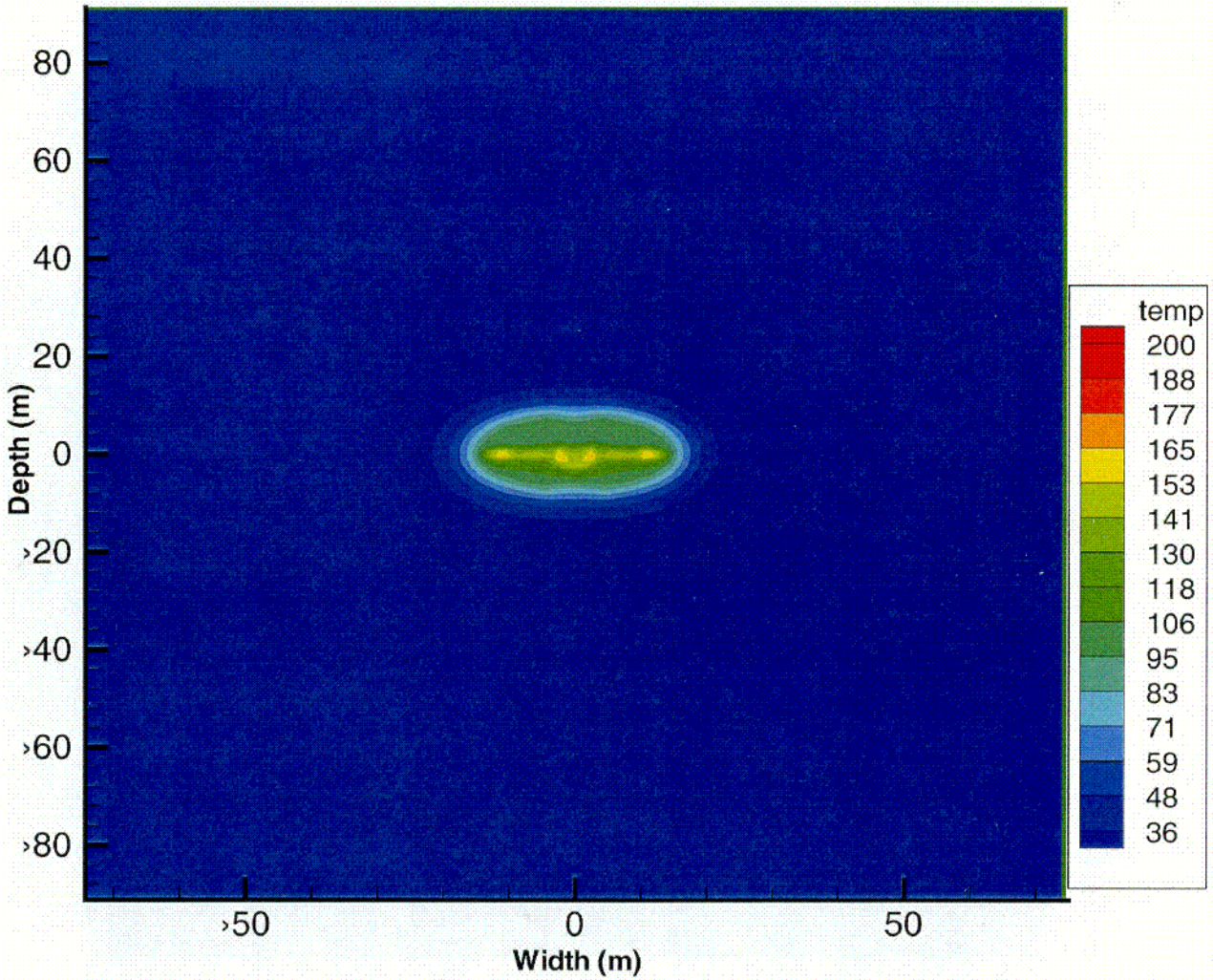

Figure 3-8a. Contour plot of simulated matrix temperature for basecase property values and an infiltration rate of 0.036 mm/yr

C01

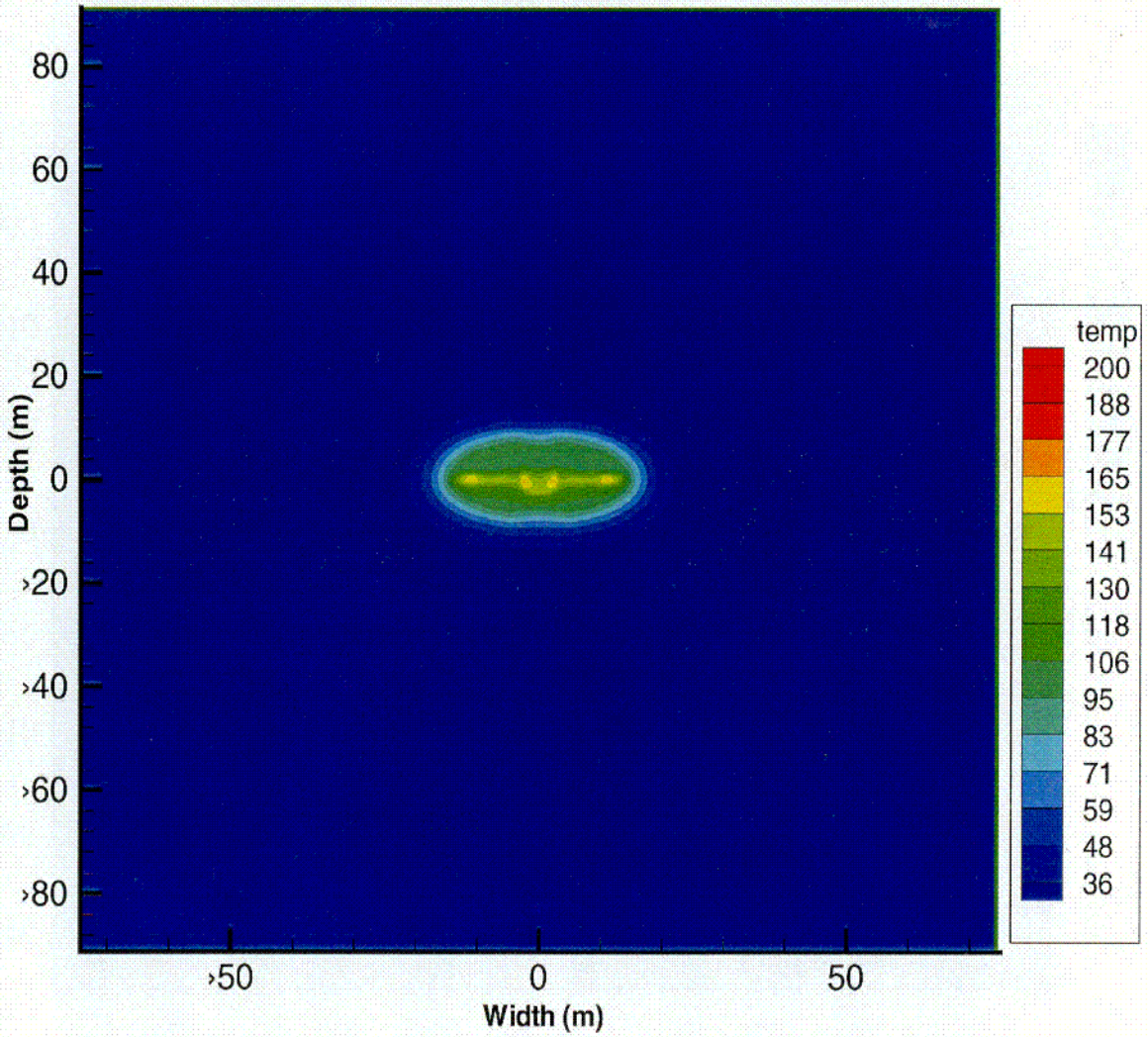

Figure 3-8b. Contour plot of simulated fracture temperature for basecase property values and an infiltration rate of 0.036 mm/yr

C02

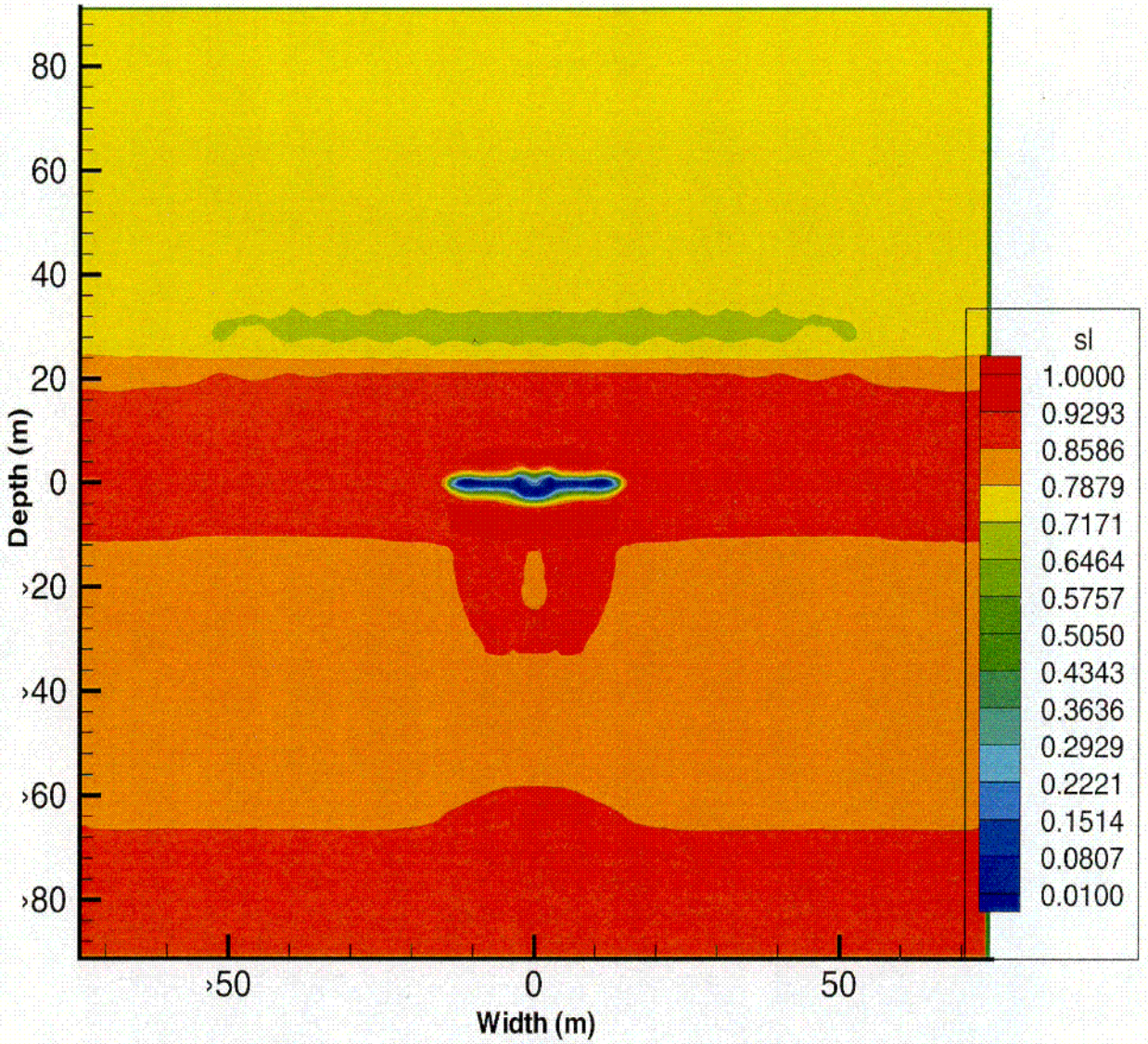

Figure 3-8c. Contour plot of simulated matrix saturation for basecase property values and an infiltration rate of 0.036 mm/yr

C03

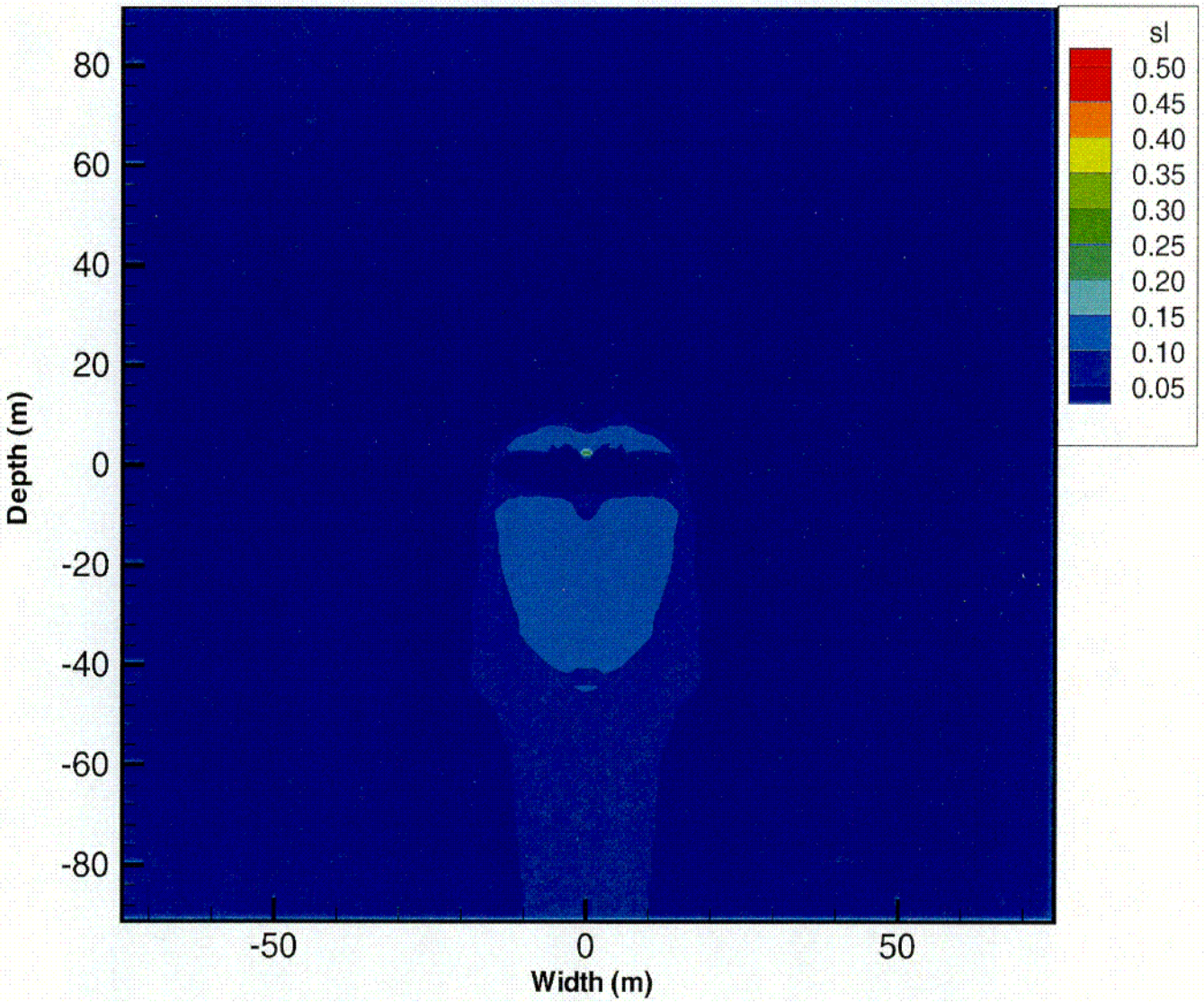

Figure 3-8d. Contour plot of simulated fracture saturation for basecase property values and an infiltration rate of 0.036 mm/yr

C04

crown. This difference may be an artifact of the manner in which the heat source was applied to the drift wall.

Simulations of a mass removal of 80 mL/hr from the heater drift wall for the basecase simulations had a negligible effect on predicted temperature (figure 3-9a,b). The only observable effect on the simulation was a 5 °C increase in temperature at the heater drift wall for Borehole 160 (figure 3-9b). There was no distinguishable difference between the temperatures and saturations predicted for a mass removal of 80 mL/hr (figure 3-10a,b,c,d) and those for the basecase with no mass removal (figure 3-8).

A reduction in fracture permeability and an increase in infiltration rate from 0.036 to 3.6 mm/yr had a noticeable effect on simulated temperatures (figure 3-11a,b). The effect of the predicted heat pipe in Borehole 158 was reduced allowing temperatures at the heater drift crown to increase to approximately 110 °C. Nonetheless, the simulated temperatures still underestimate the observed temperatures by approximately 80 °C. In addition, temperatures predicted over the inner and outer wing heaters decreased by approximately 5 °C (figure 3-11b). The decreased temperatures are attributed to the increased ambient matrix saturation from approximately 0.86 to near full saturation caused by the higher rate of infiltration. The higher ambient saturations of this case did not result in observable changes to predicted matrix or fracture temperatures (figure 3-12a,b) compared to the basecase. A distinct dryout zone formed in the matrix around the DST even at the higher ambient saturations although the zone of matrix dryout was restricted to a couple of meters (figure 3-12c). The higher matrix saturations also led to a more distinctly formed zone of increased fracture saturation that extended below the DST to at least the bottom of the model and obviously much farther (figure 3-12d).

A mass removal of 80 mL/hr for the case of reduced fracture permeability, and an infiltration rate of 3.6 mm/yr, had negligible effects of predicted temperature profiles either above the heater drift (Borehole 158) (figure 3-13a) or along the wing heaters (Borehole 160) (figure 3-13b). Similarly, contour plots for temperature and saturation for the case with high infiltration and 80 mL/hr mass removal (figure 3-14a,b,c,d) are indistinguishable from those with no mass removal (figure 3-12a,b,c,d).

A reduction in fracture permeability and a low rate of infiltration (i.e., 0.036 mm/yr) resulted in a further decrease in the simulated heat pipe (figure 3-15a,b). The predicted temperature at the heater drift crown was increased to above 120 °C at 1 yr, however, this temperature is still 70 °C less than the observed. Differences in temperature along Borehole 160 were reduced to 30 °C over the inner wing heater and to approximately 20 °C over the outer wing heater (figure 3-15b). Matrix and fracture temperature contour plots for the case with reduced fracture permeability (figure 3-16a,b) are indistinguishable from temperature contour plots for the basecase with regular fracture permeability (figure 3-8a,b) although saturation plots differ significantly. In particular, matrix saturation for the case with reduced fracture permeability indicates more distinctly formed vertical asymmetry (figure 3-16c). The zone of increased matrix saturation below the DST is better defined for the case with a decrease in fracture permeability. The zone of increased fracture saturation for this case (figure 3-16d) is limited in depth below the DST to approximately 20 m, however, fracture saturations both above and below the DST are much greater (i.e., 0.45) when fracture permeabilities are reduced compared to a saturation of 0.15 for basecase fracture permeabilities.

Simulations of a mass removal of 80 mL/hr from the heater wall for the case with reduced fracture permeability and a low rate of infiltration had a small, but distinguishable effect on temperature above the heater drift (figure 3-17a). The effect of the simulated heat pipe above the heater drift was only slightly reduced compared to the same case but with no mass removal, however, the predicted temperature at the heater drift crown increased by about 5 °C (figure 3-17a) reducing the difference between simulated and

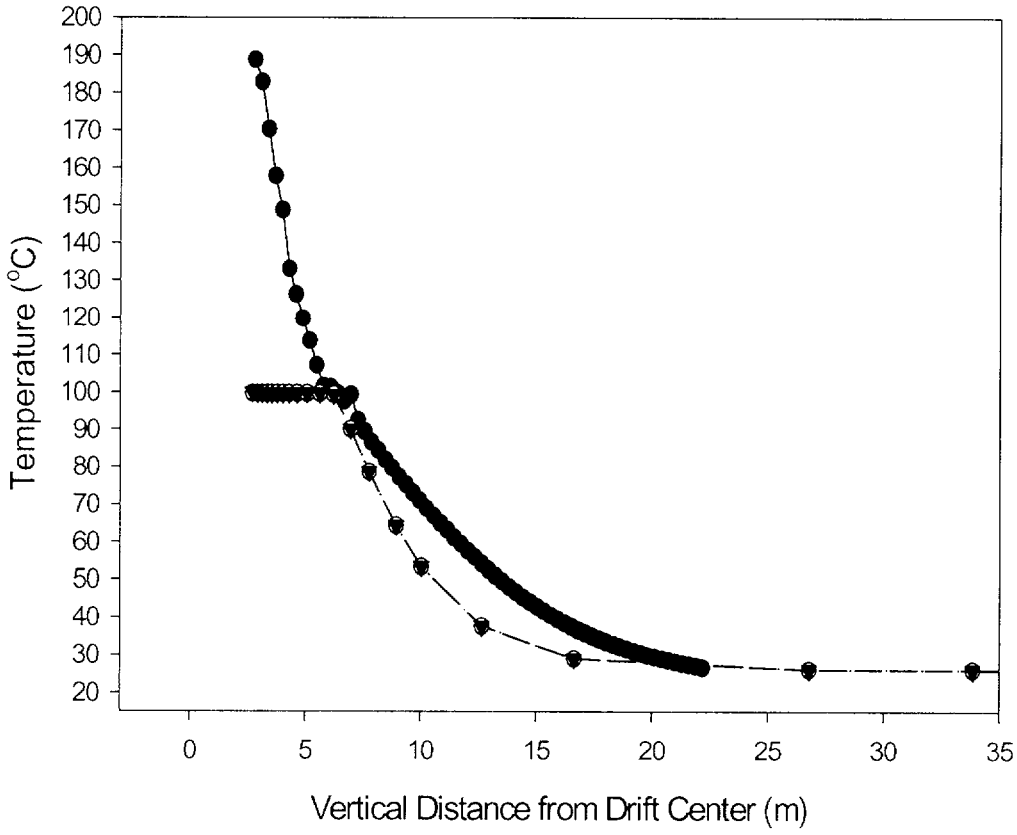

Figure 3-9a. Comparison of measured temperatures (solid circle) versus simulated temperatures in the matrix (closed triangle) and fracture (open circle) for vertical Borehole 158 for basecase property values, an infiltration rate of 0.036 mm/yr, and a mass loss rate of 80 mL/hr through the thermal bulkhead

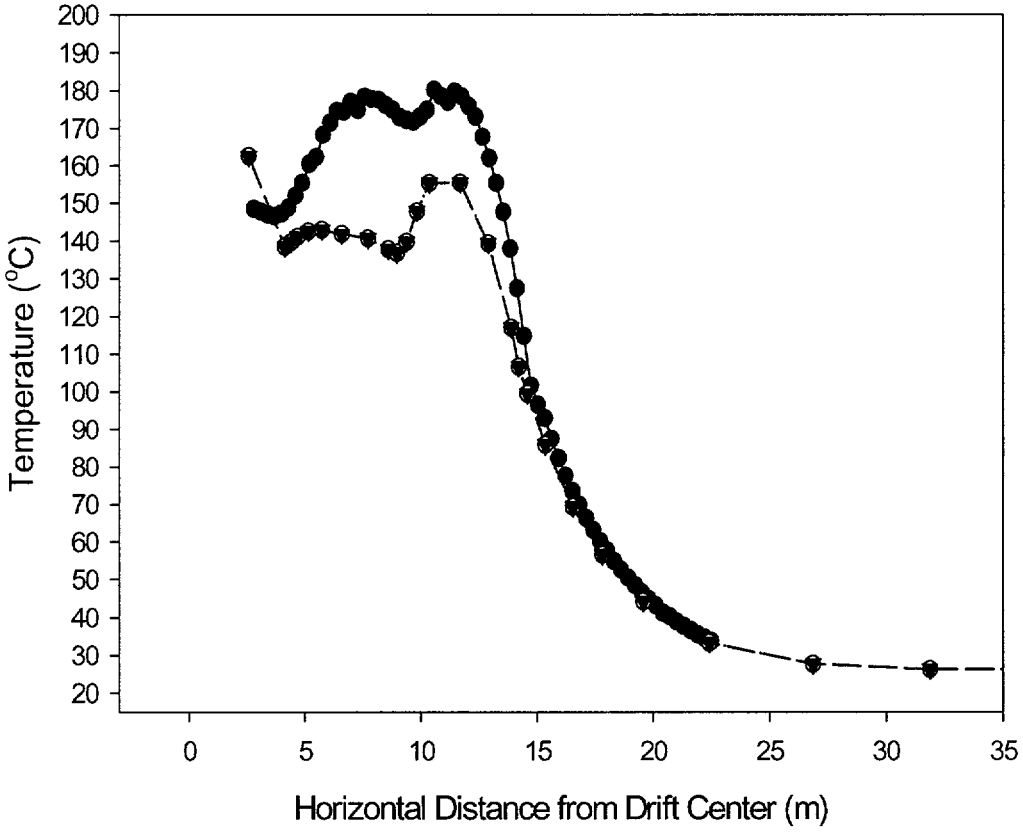

Figure 3-9b. Comparison of measured temperatures (solid circle) versus simulated temperatures in the matrix (closed triangle) and fracture (open circle) for horizontal Borehole 160 for basecase property values, an infiltration rate of 0.036 mm/yr, and a mass loss rate of 80 mL/hr through the thermal bulkhead

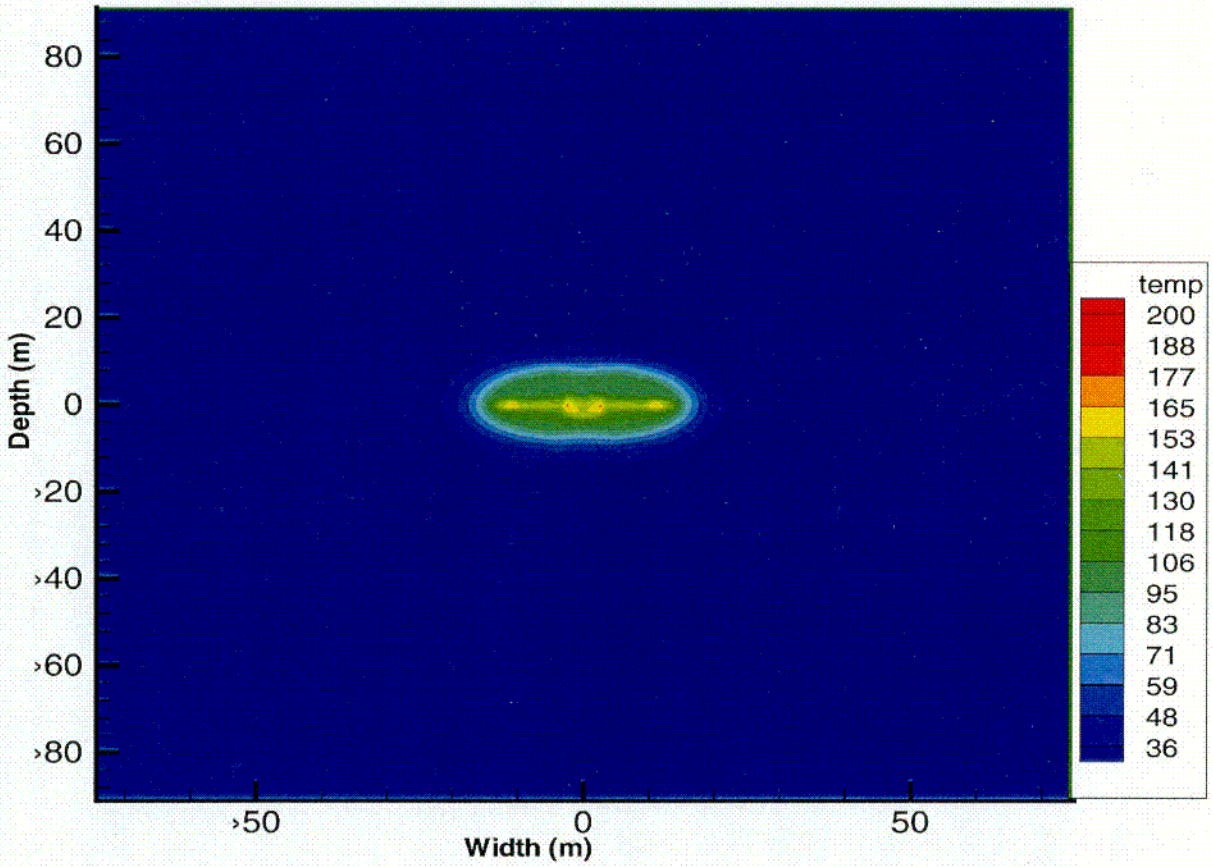

Figure 3-10a. Contour plot of simulated matrix temperature for basecase property values, an infiltration rate of 0.036 mm/yr, and a mass loss rate of 80 mL/hr through the thermal bulkhead

C05

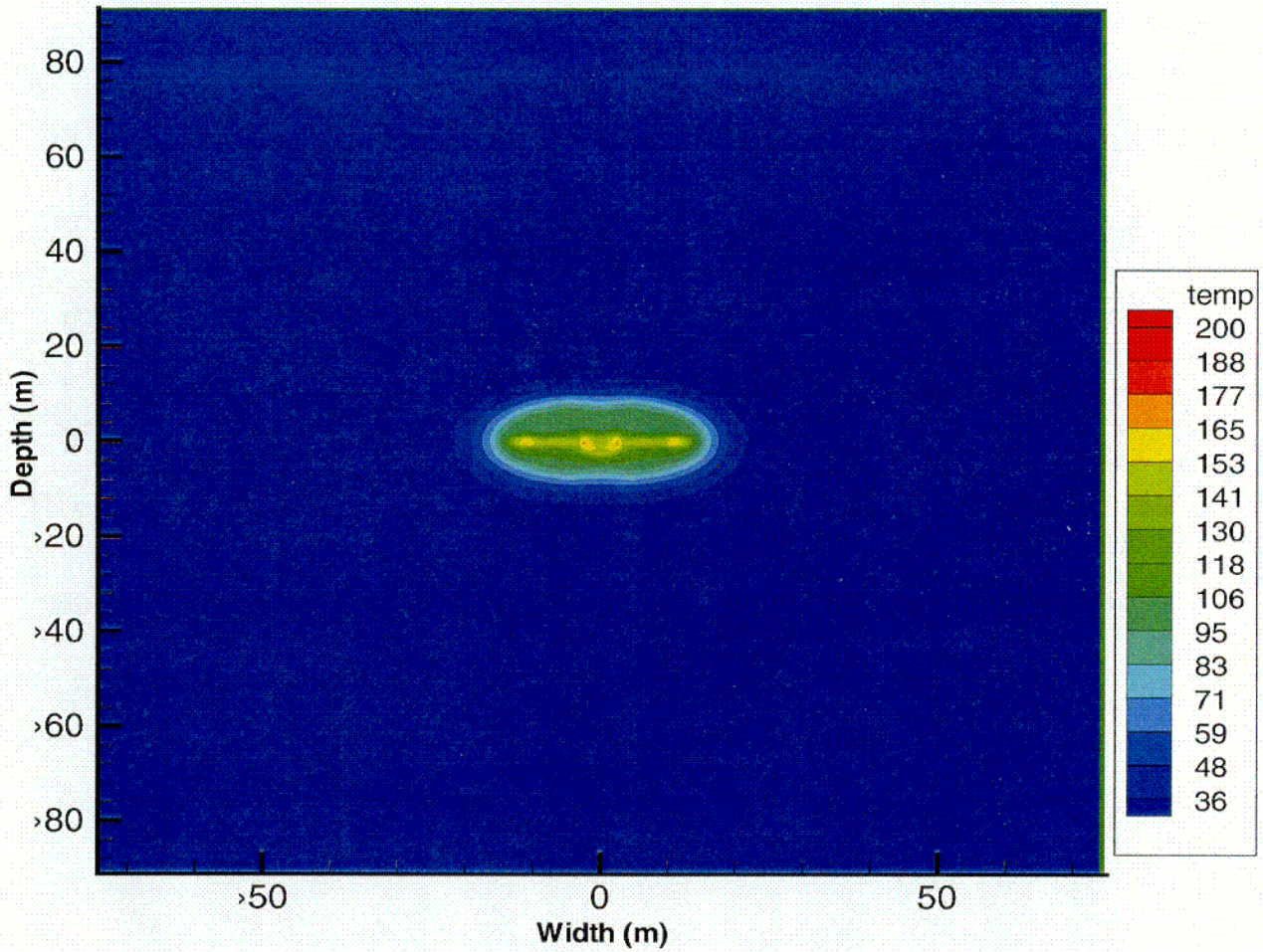

Figure 3-10b. Contour plot of simulated fracture temperature for basecase property values, an infiltration rate of 0.036 mm/yr, and a mass loss rate of 80 mL/hr through the thermal bulkhead

C-06

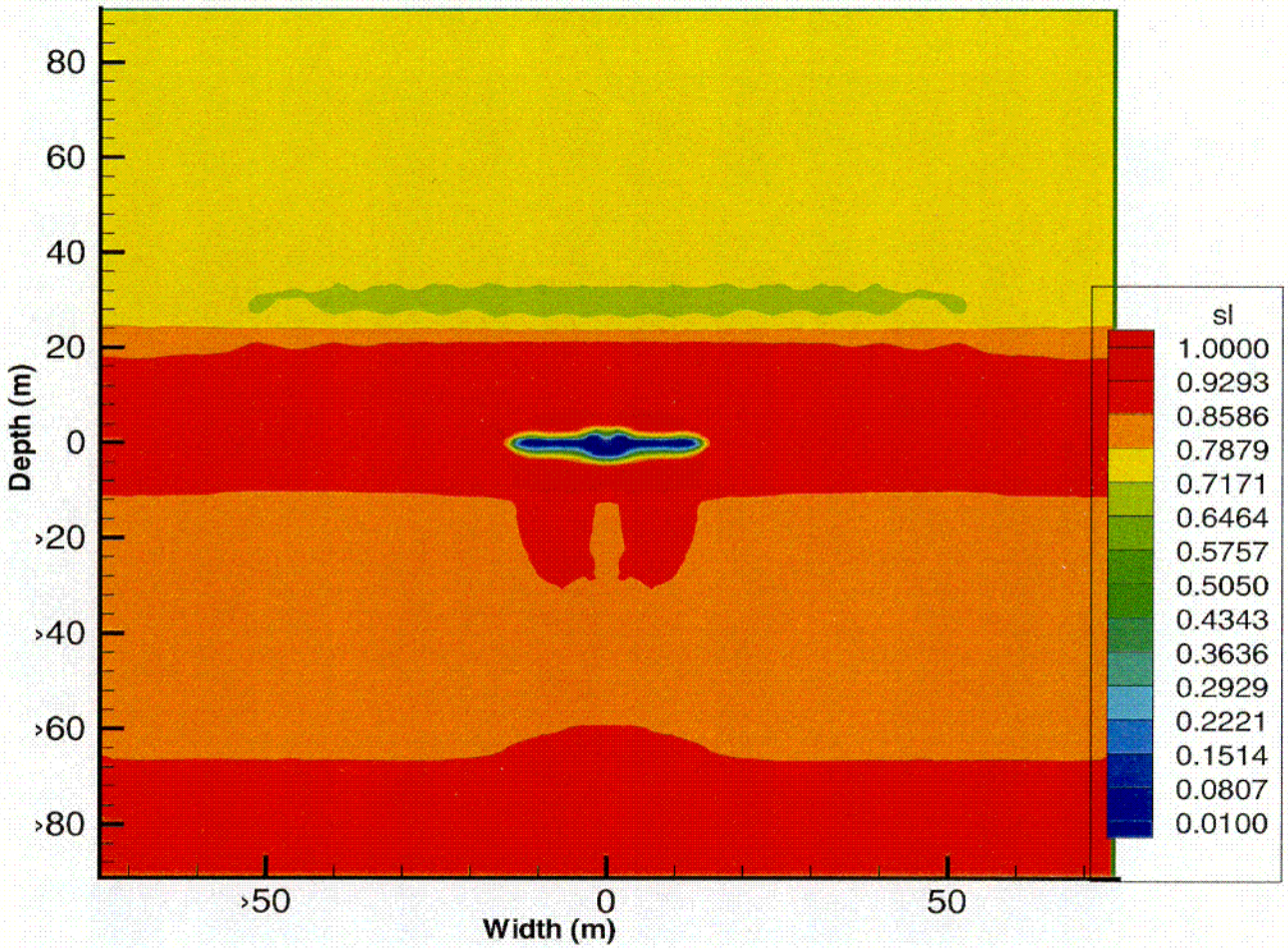

Figure 3-10c. Contour plot of simulated matrix saturation for basecase property values, an infiltration rate of 0.036 mm/yr, and a mass loss rate of 80 mL/hr through the thermal bulkhead

C07

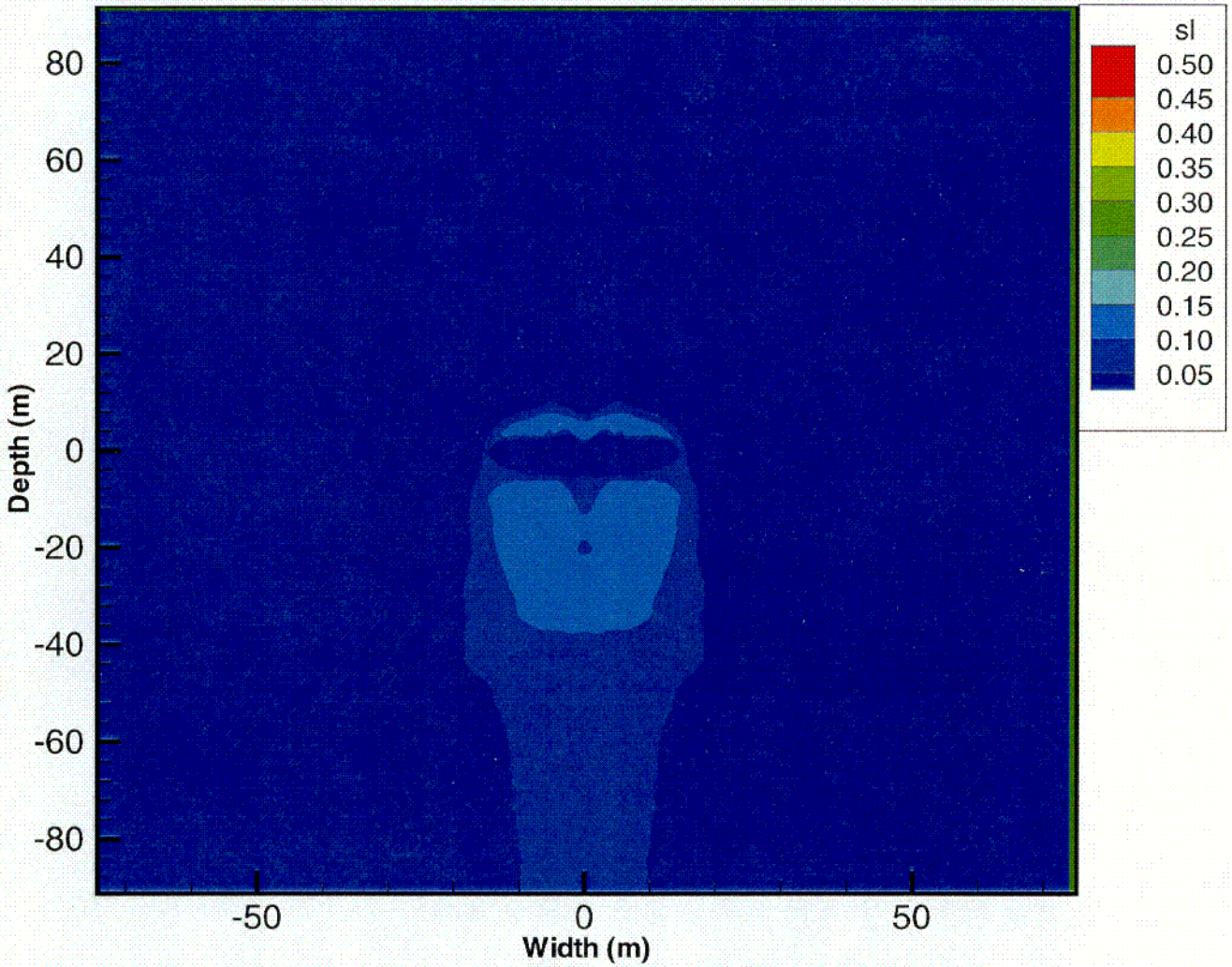

Figure 3-10d. Contour plot of simulated fracture saturation for basecase property values, an infiltration rate of 0.036 mm/yr, and a mass loss rate of 80 mL/hr through the thermal bulkhead

C08

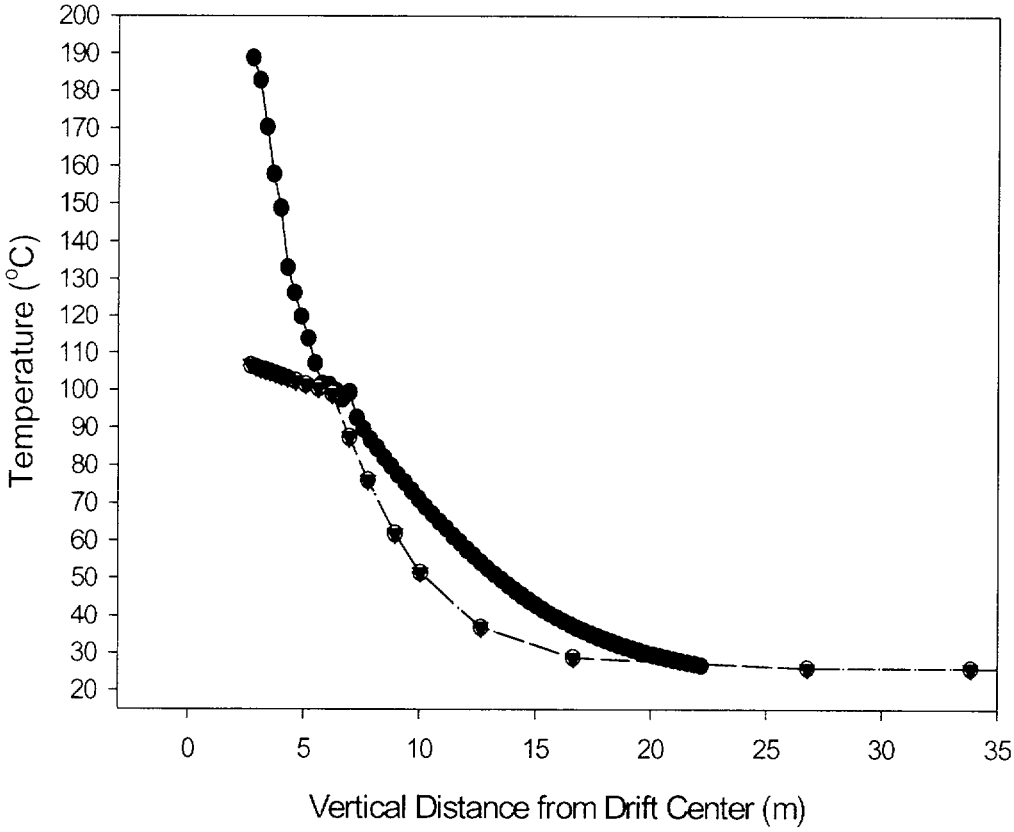

Figure 3-11a. Comparison of measured temperatures (solid circle) versus simulated temperatures in the matrix (closed triangle) and fracture (open circle) for vertical Borehole 158 for a 10^{-2} reduction in fracture permeability and an infiltration rate of 3.6 mm/yr

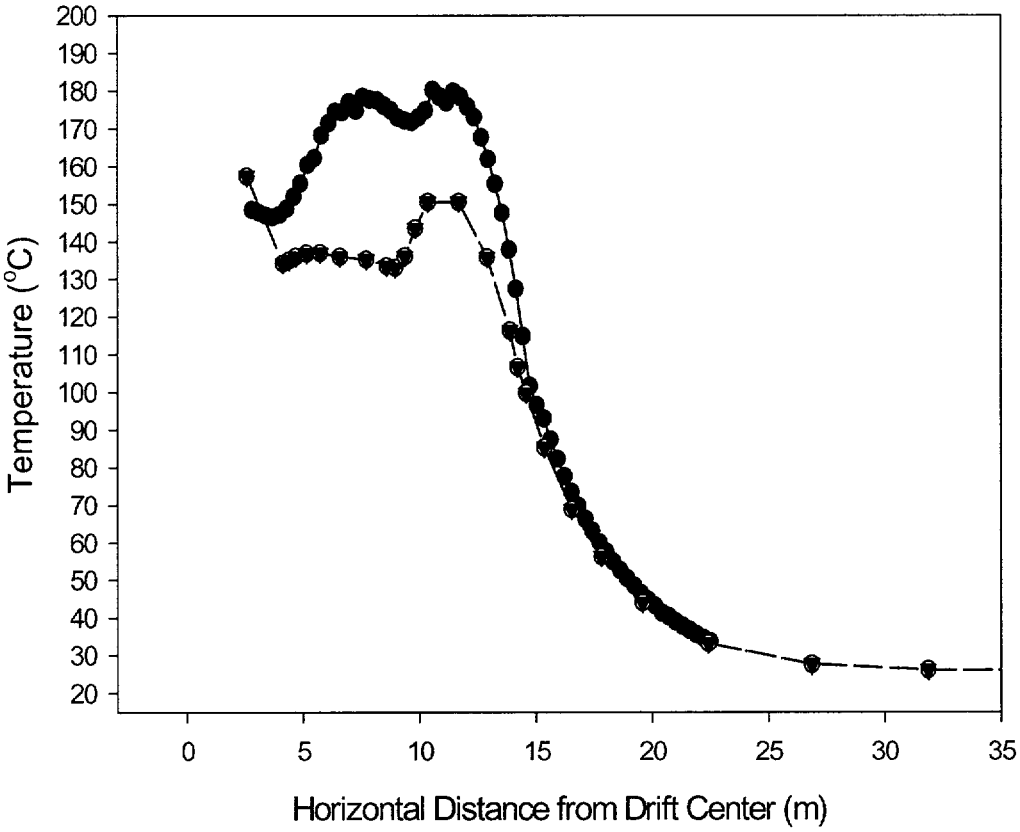

Figure 3-11b. Comparison of measured temperatures (solid circle) versus simulated temperatures in the matrix (closed triangle) and fracture (open circle) for horizontal Borehole 160 for a 10^{-2} reduction in fracture permeability and an infiltration rate of 3.6 mm/yr

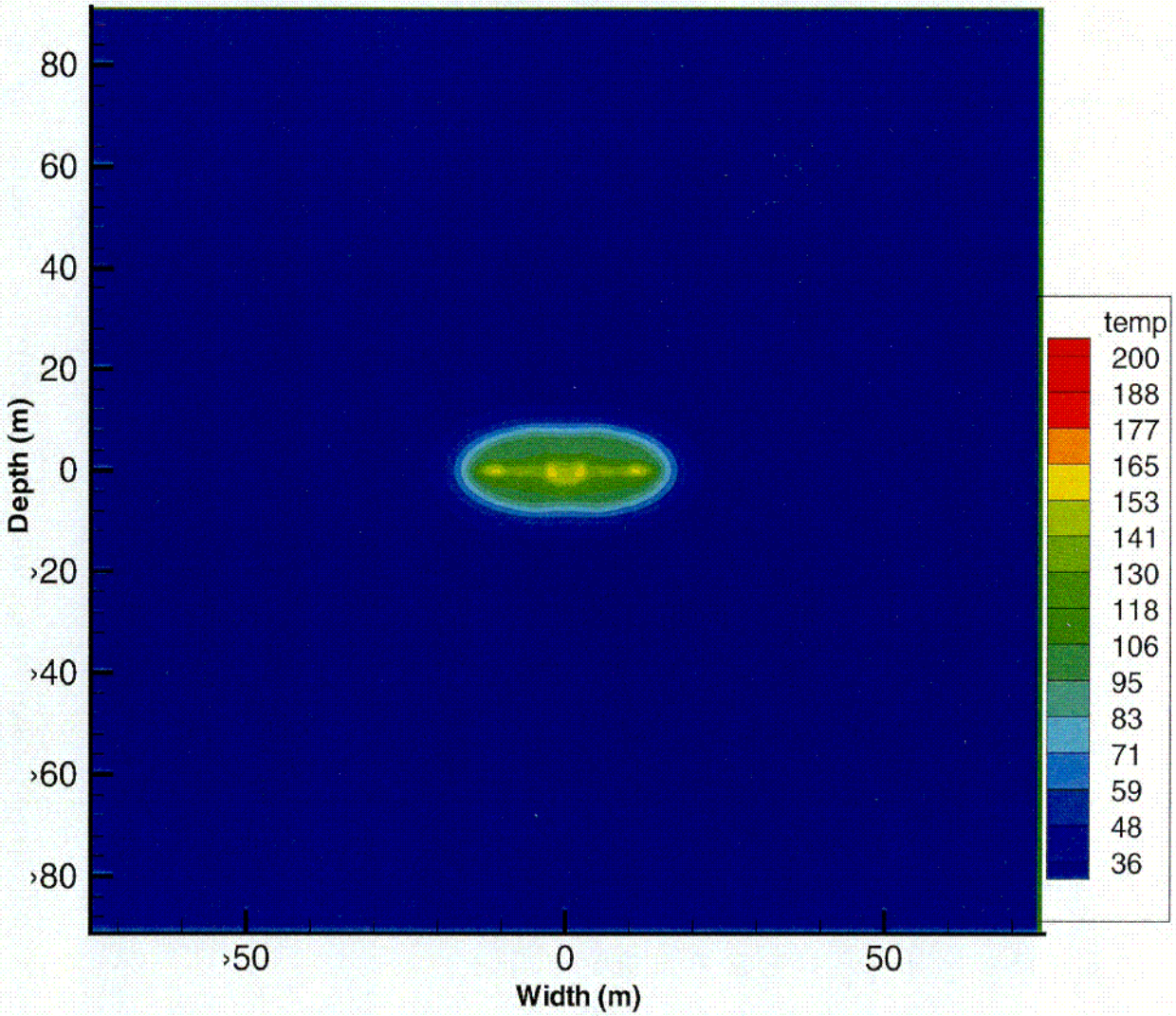

Figure 3-12a. Contour plot of simulated matrix temperature for a 10^{-2} reduction in fracture permeability and an infiltration rate of 3.6 mm/yr

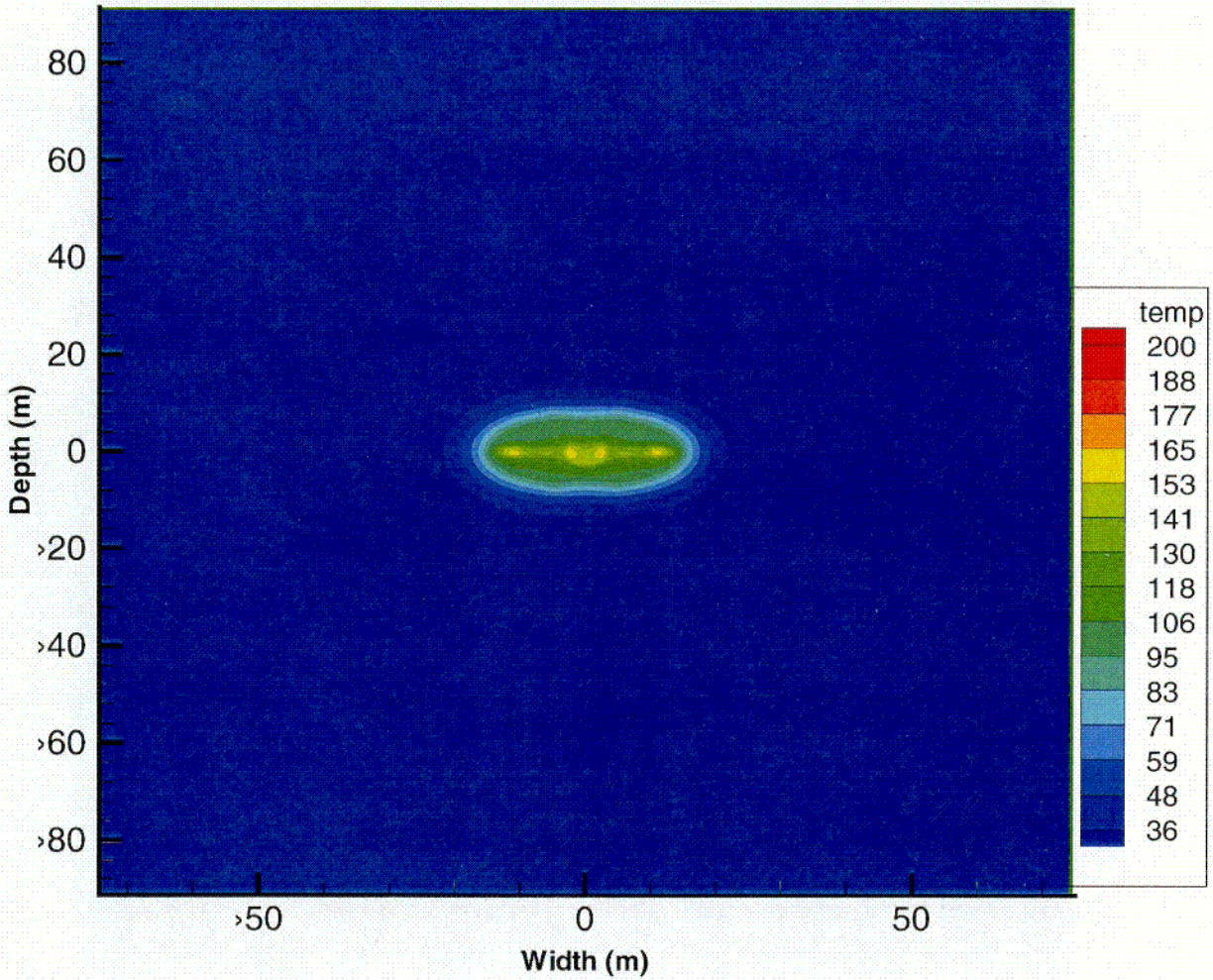

Figure 3-12b. Contour plot of simulated fracture temperature for a 10^{-2} reduction in fracture permeability and an infiltration rate of 3.6 mm/yr

C10

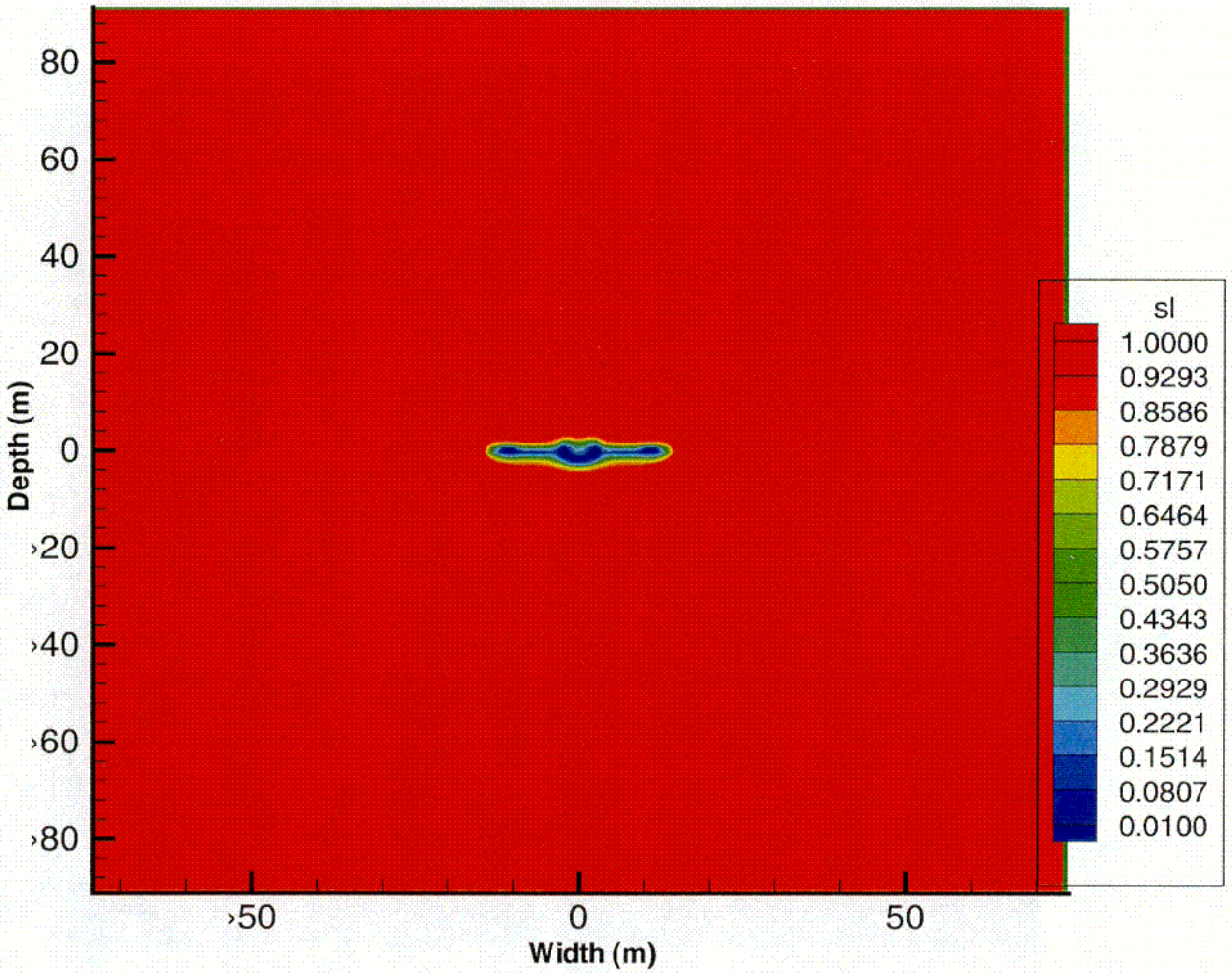

Figure 3-12c. Contour plot of simulated matrix saturation for a 10^{-2} reduction in fracture permeability and an infiltration rate of 3.6 mm/yr

C11

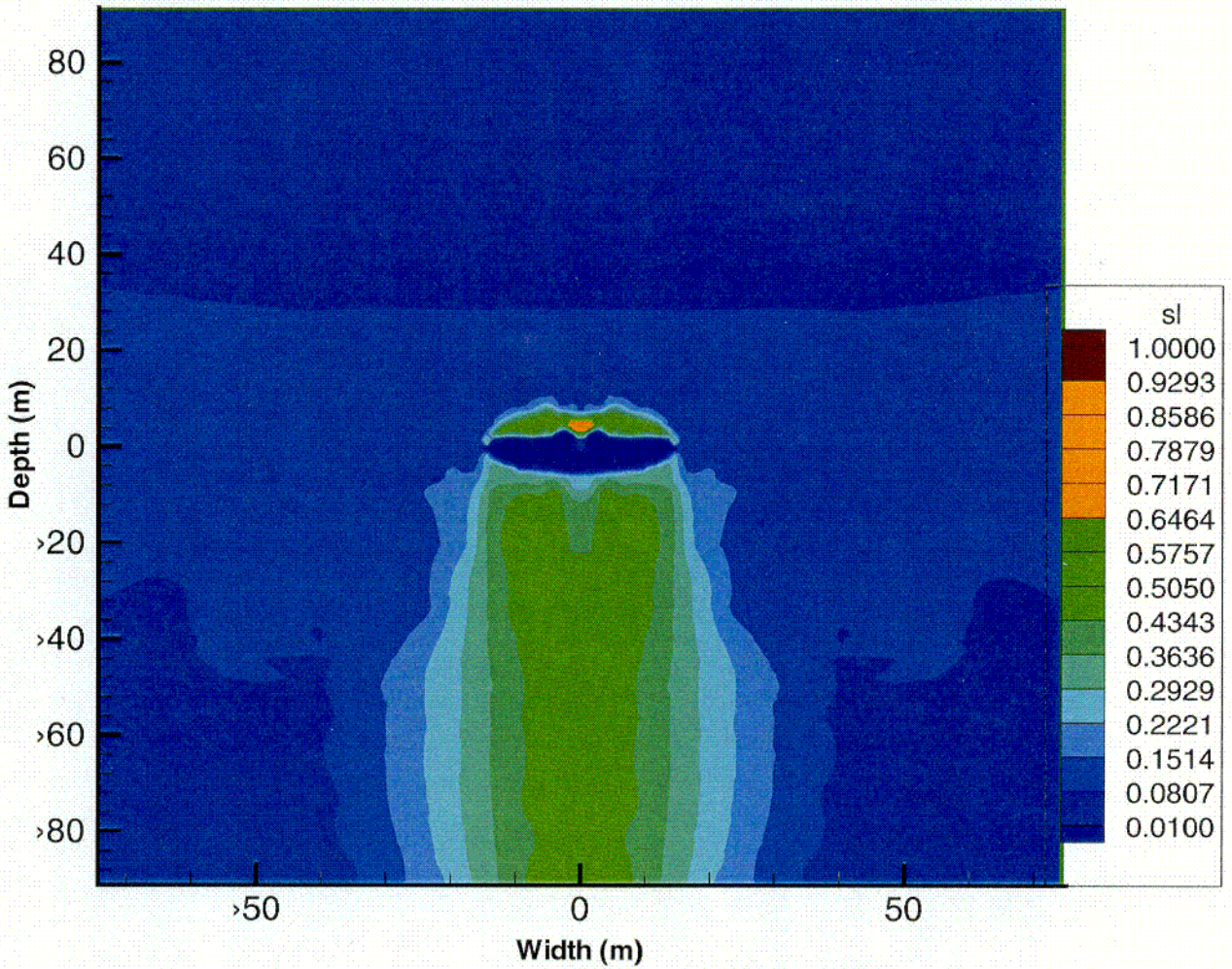

Figure 3-12d. Contour plot of simulated fracture saturation for a 10^{-2} reduction in fracture permeability and an infiltration rate of 3.6 mm/yr

C12

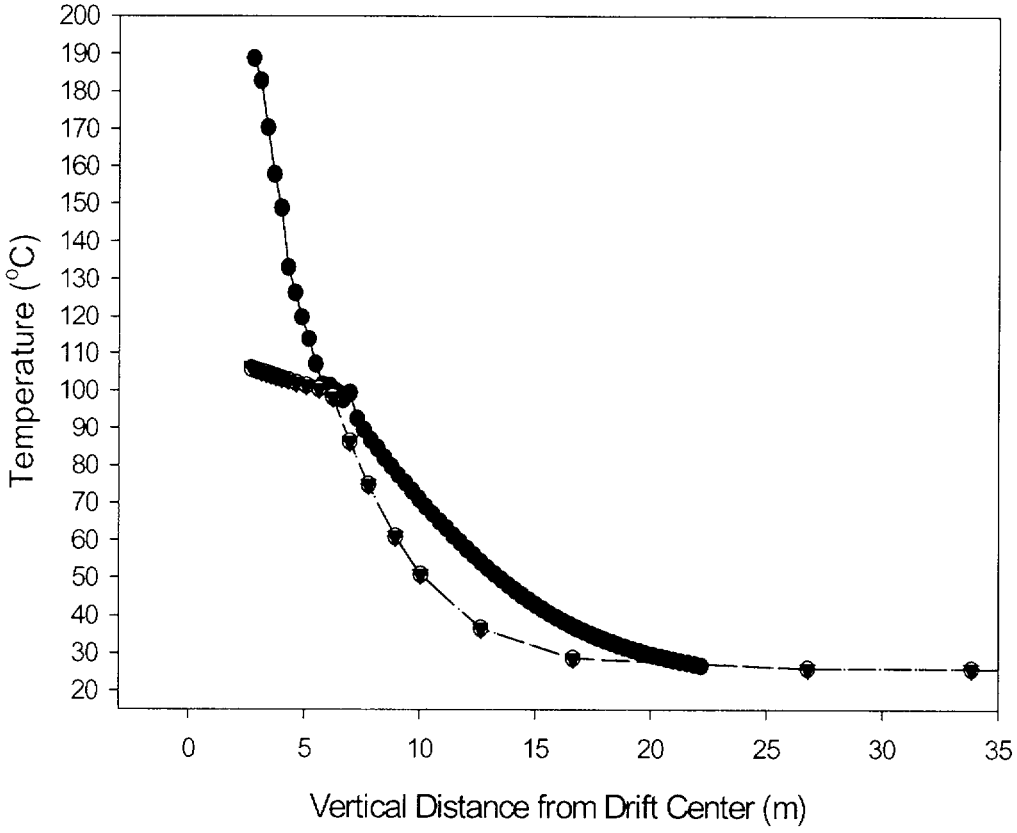

Figure 3-13a. Comparison of measured temperatures (solid circle) versus simulated temperatures in the matrix (closed triangle) and fracture (open circle) for vertical Borehole 158 for a 10^{-2} reduction in fracture permeability, an infiltration rate of 3.6 mm/yr, and a mass loss rate of 80 mL/hr through the thermal bulkhead

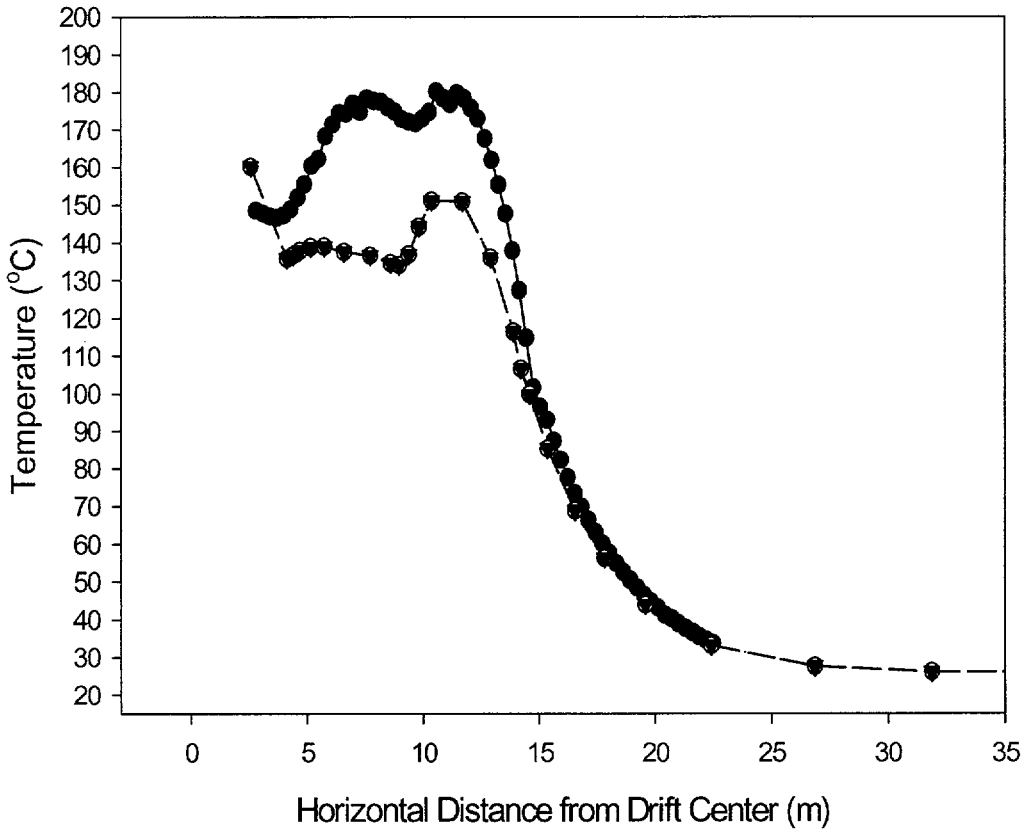

Figure 3-13b. Comparison of measured temperatures (solid circle) versus simulated temperatures in the matrix (closed triangle) and fracture (open circle) for horizontal Borehole 160 for a 10^{-2} reduction in fracture permeability, an infiltration rate of 3.6 mm/yr, and a mass loss rate of 80 mL/hr through the thermal bulkhead

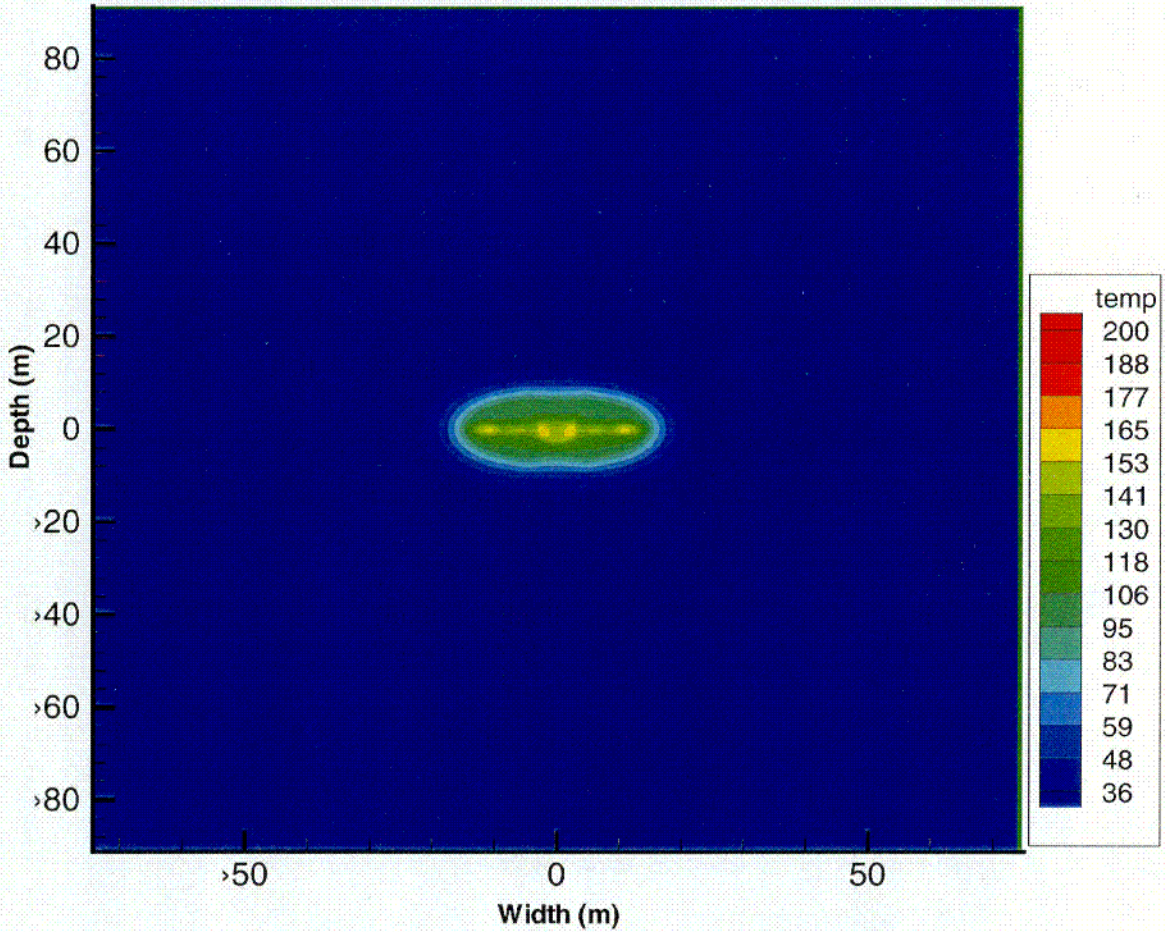

Figure 3-14a. Contour plot of simulated matrix temperature for a 10^{-2} reduction in fracture permeability, an infiltration rate of 3.6 mm/yr, and a mass loss rate of 80 mL/hr through the thermal bulkhead

C|3

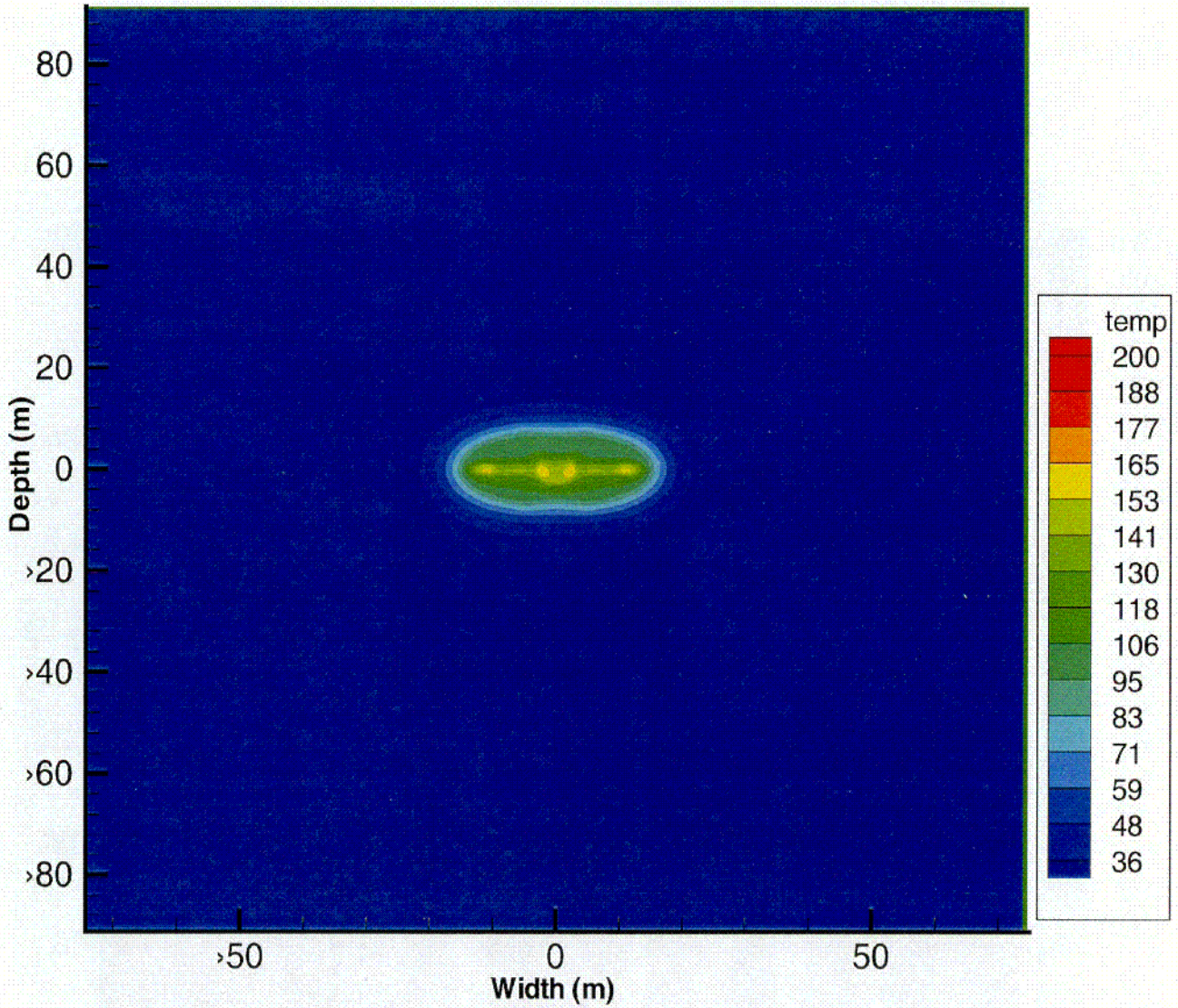

Figure 3-14b. Contour plot of simulated fracture temperature for a 10^{-2} reduction in fracture permeability, an infiltration rate of 3.6 mm/yr, and a mass loss rate of 80 mL/hr through the thermal bulkhead

C14

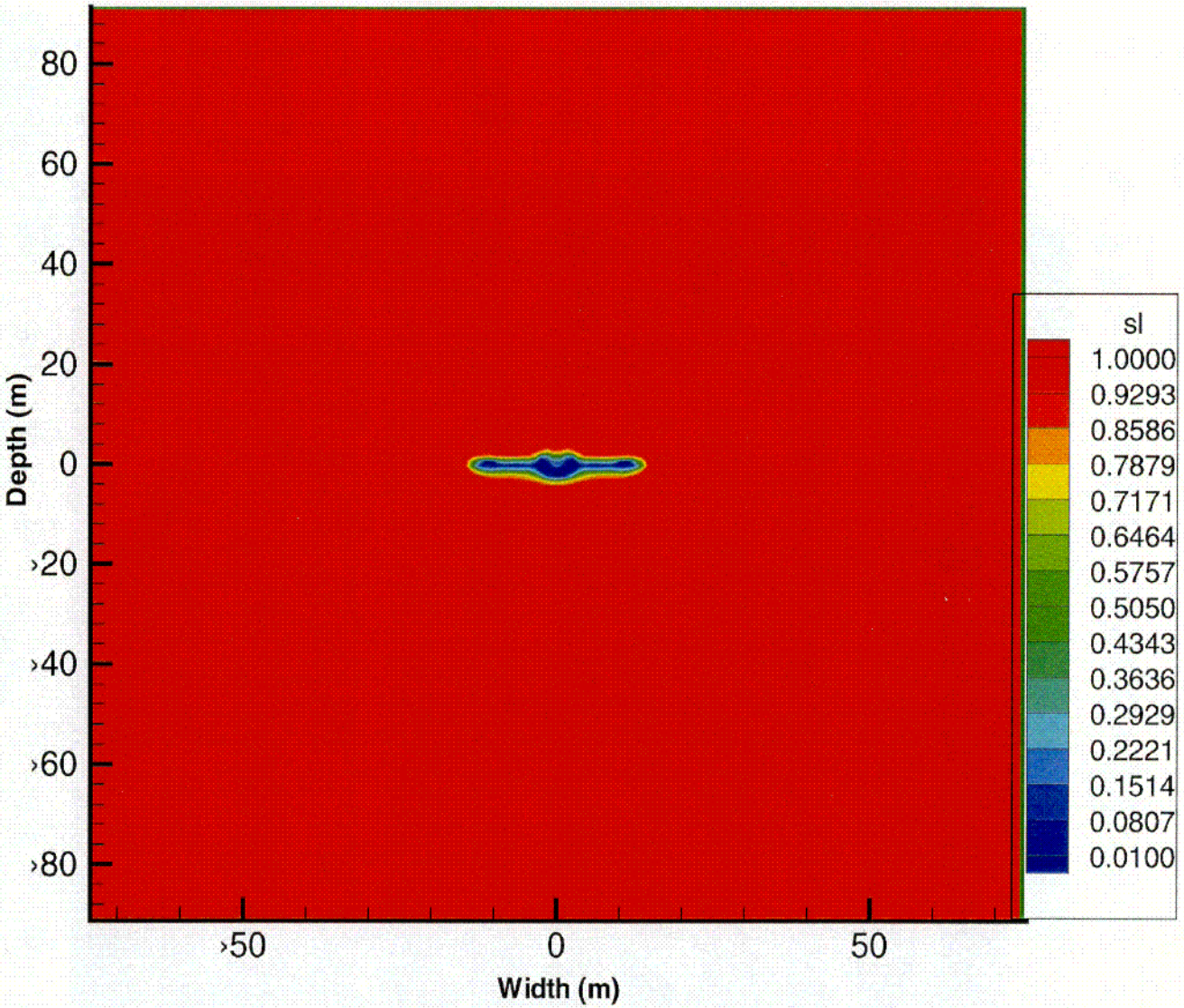

Figure 3-14c. Contour plot of simulated matrix saturation for a 10^{-2} reduction in fracture permeability, an infiltration rate of 3.6 mm/yr, and a mass loss rate of 80 mL/hr through the thermal bulkhead

C15

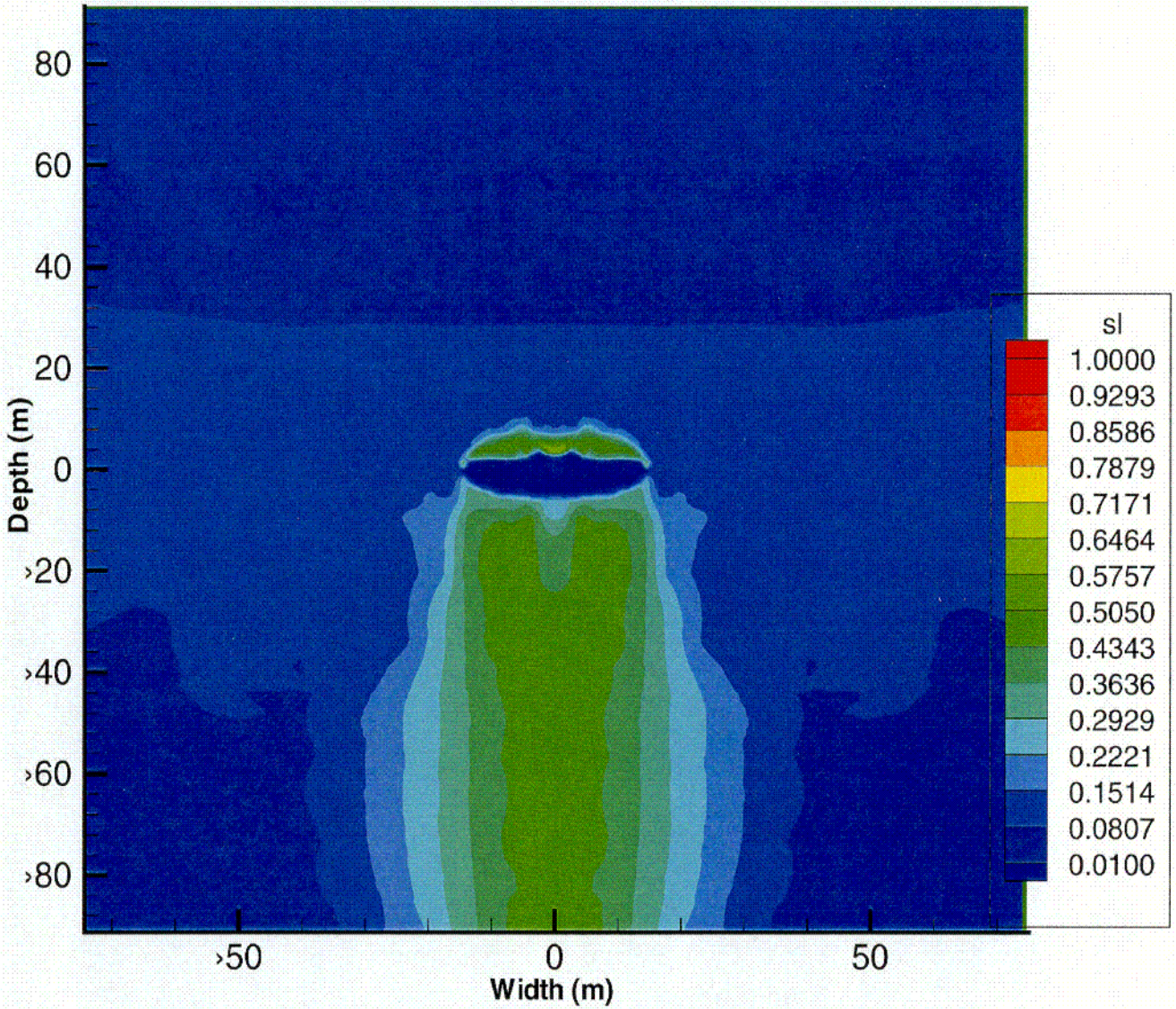

Figure 3-14d. Contour plot of simulated fracture saturation for a 10^{-2} reduction in fracture permeability, an infiltration rate of 3.6 mm/yr, and a mass loss rate of 80 mL/hr through the thermal bulkhead

C16

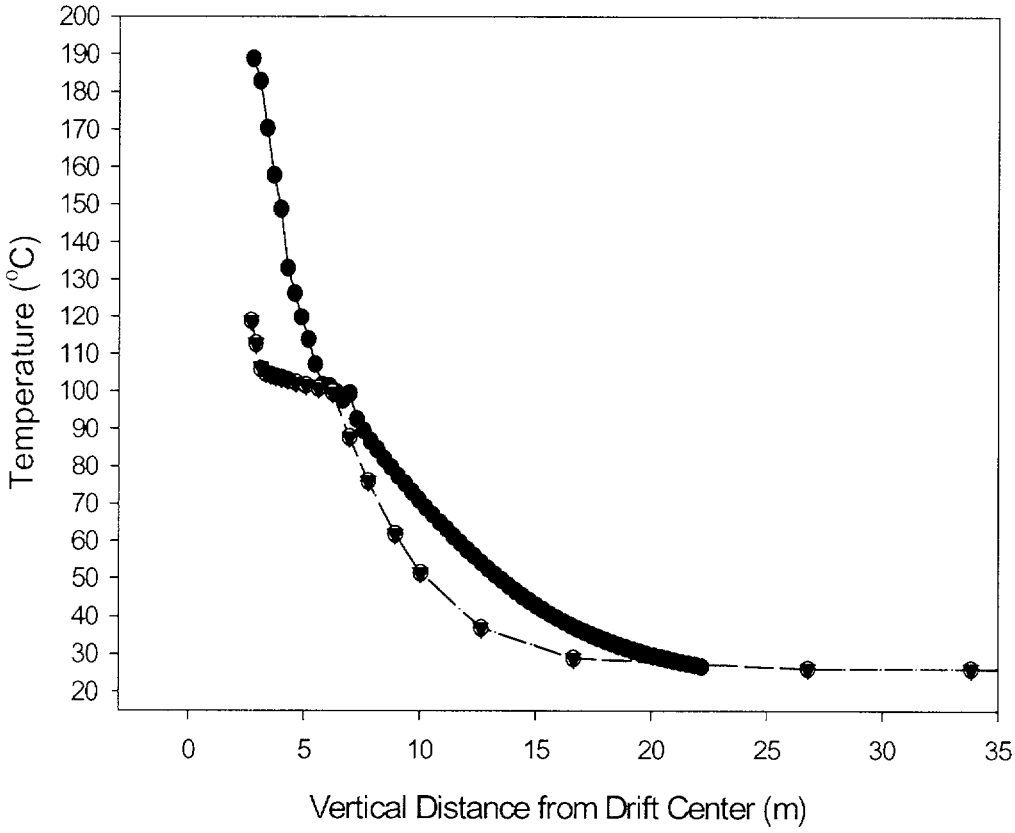

Figure 3-15a. Comparison of measured temperatures (solid circle) versus simulated temperatures in the matrix (closed triangle) and fracture (open circle) for vertical Borehole 158 for a 10^{-2} reduction in fracture permeability and an infiltration rate of 0.036 mm/yr

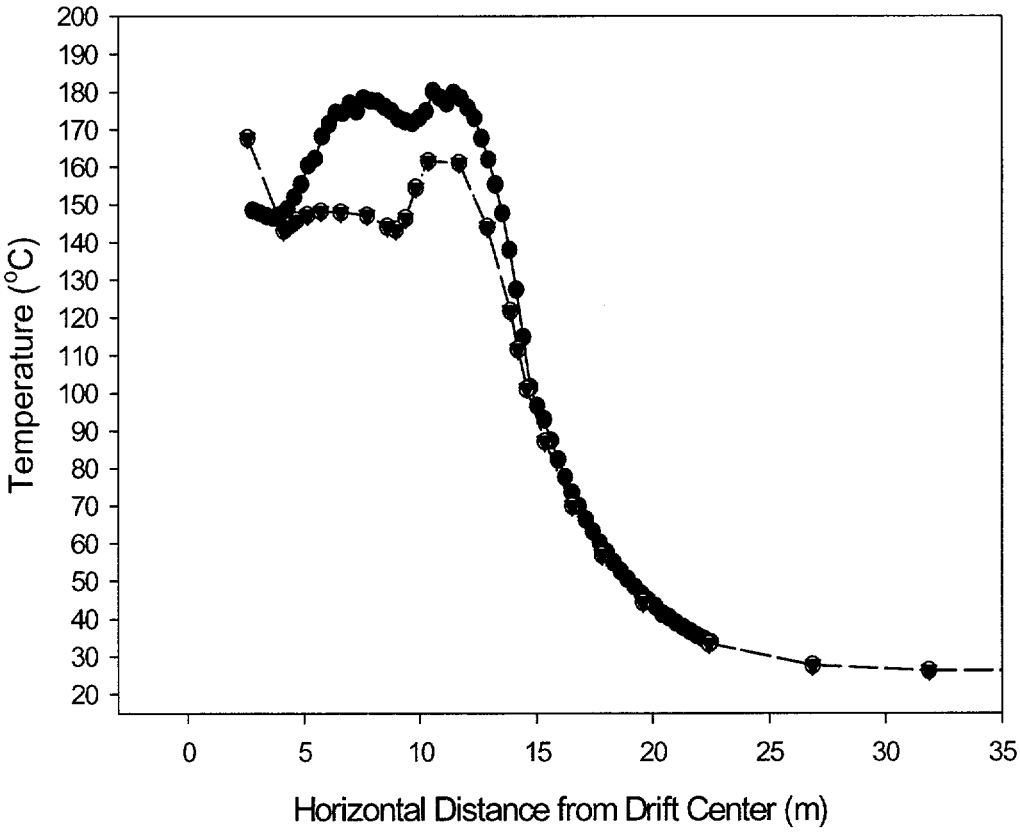

Figure 3-15b. Comparison of measured temperatures (solid circle) versus simulated temperatures in the matrix (closed triangle) and fracture (open circle) for horizontal Borehole 160 for a 10^{-2} reduction in fracture permeability and an infiltration rate of 0.036 mm/yr

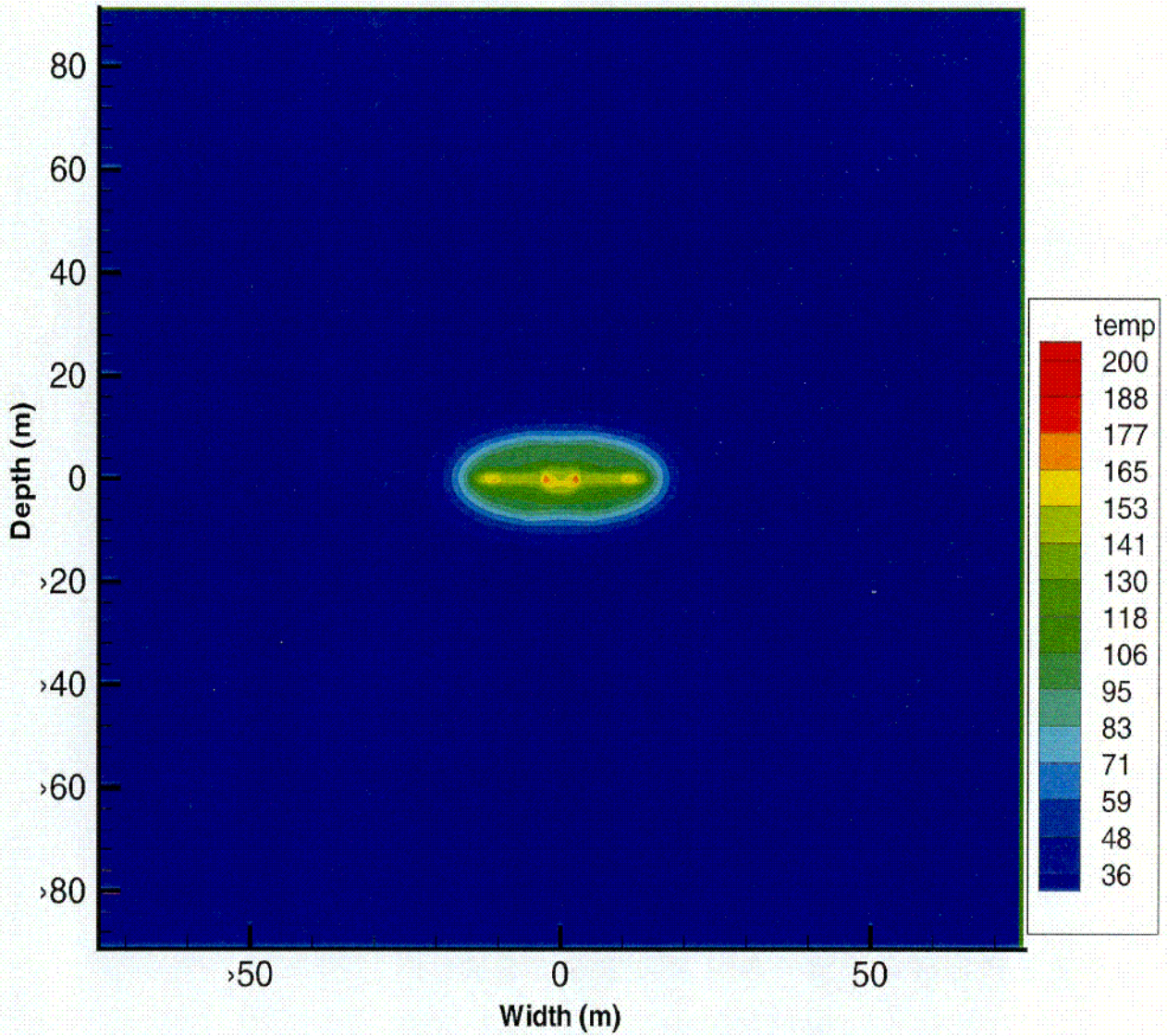

Figure 3-16a. Contour plot of simulated matrix temperature for a 10^{-2} reduction in fracture permeability an infiltration rate of 0.036 mm/yr

C17

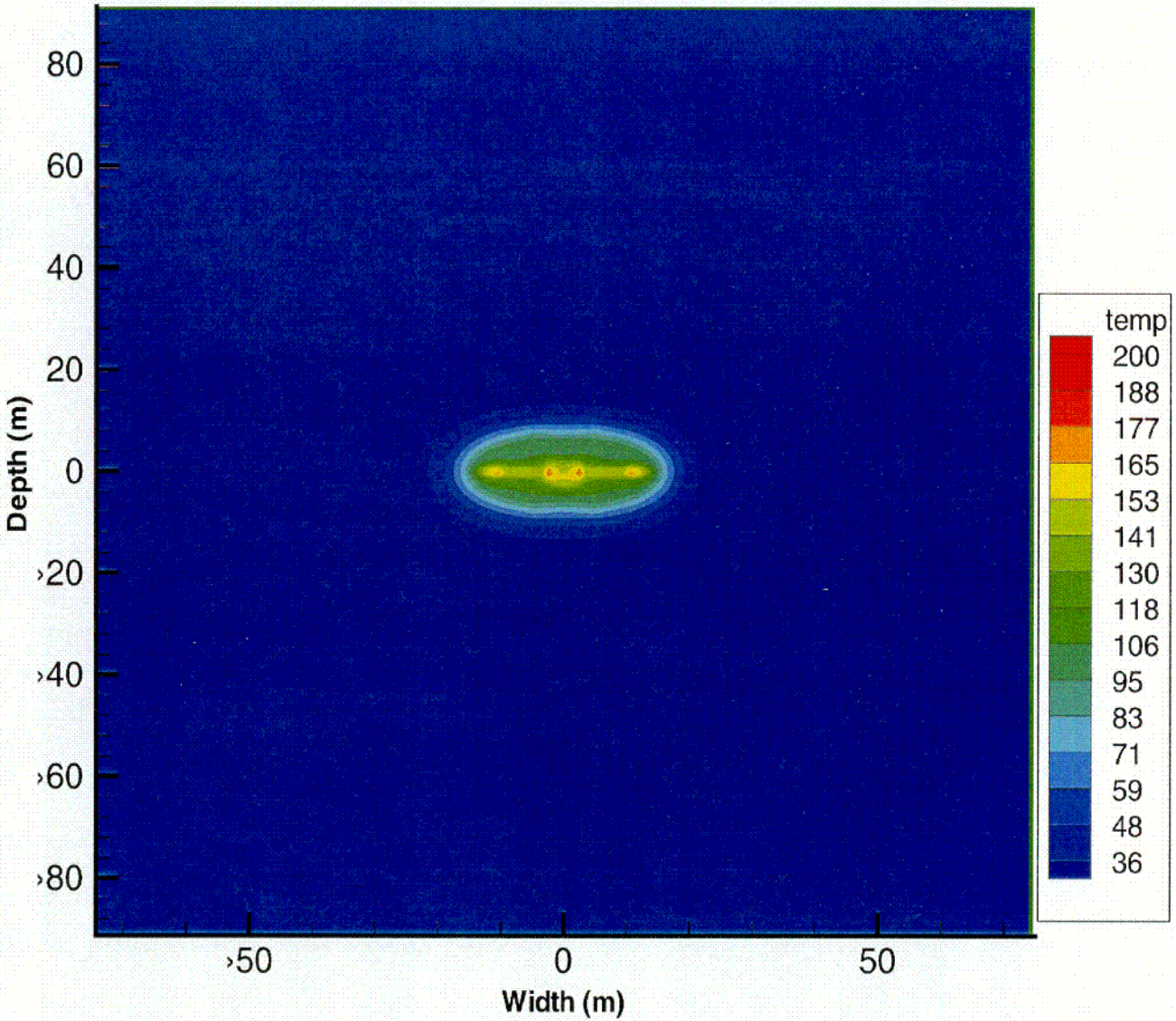

Figure 3-16b. Contour plot of simulated fracture temperature for a 10^{-2} reduction in fracture permeability and an infiltration rate of 0.036 mm/yr

C18

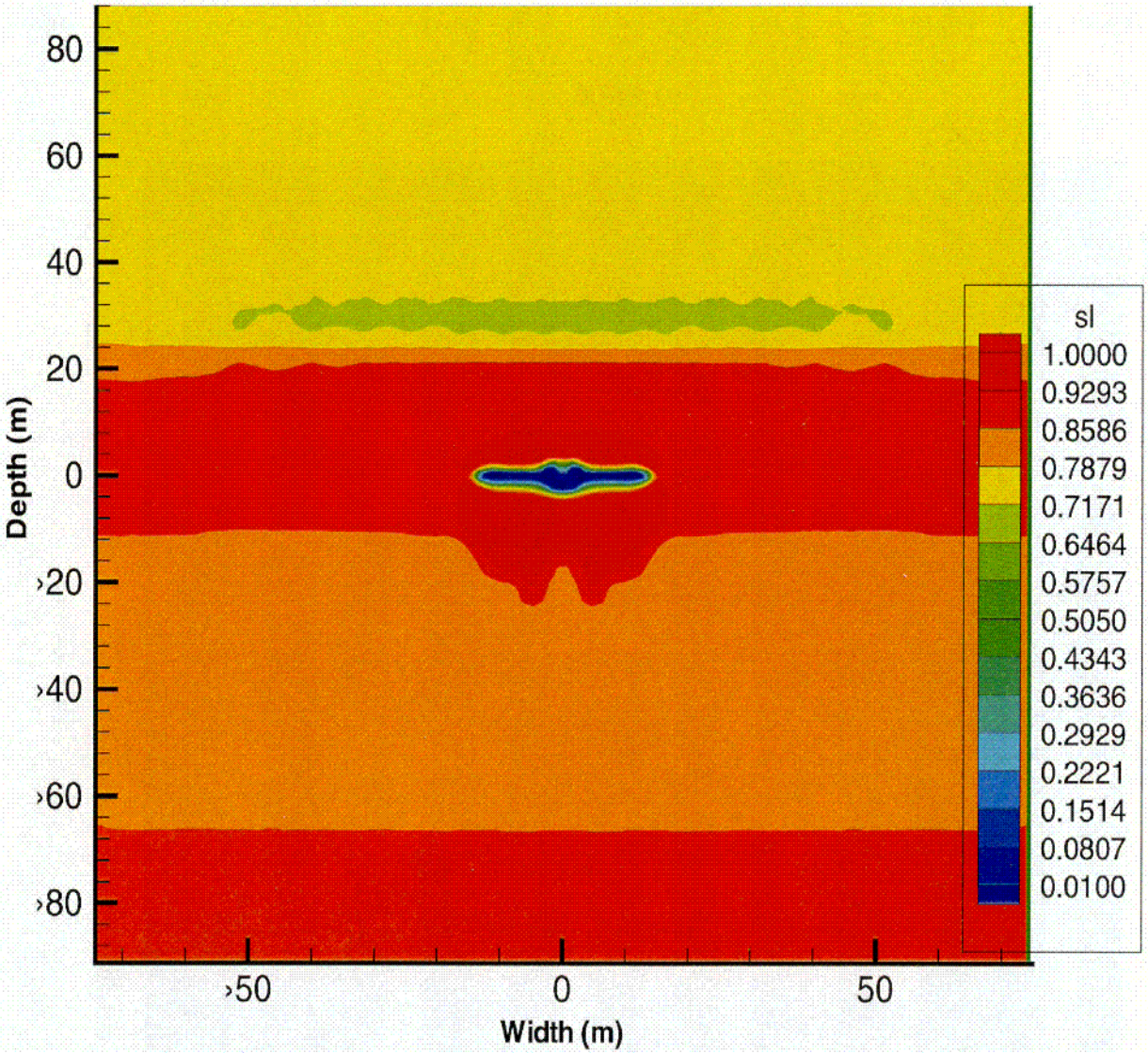

Figure 3-16c. Contour plot of simulated matrix saturation for a 10^{-2} reduction in fracture permeability and an infiltration rate of 0.036 mm/yr

C19

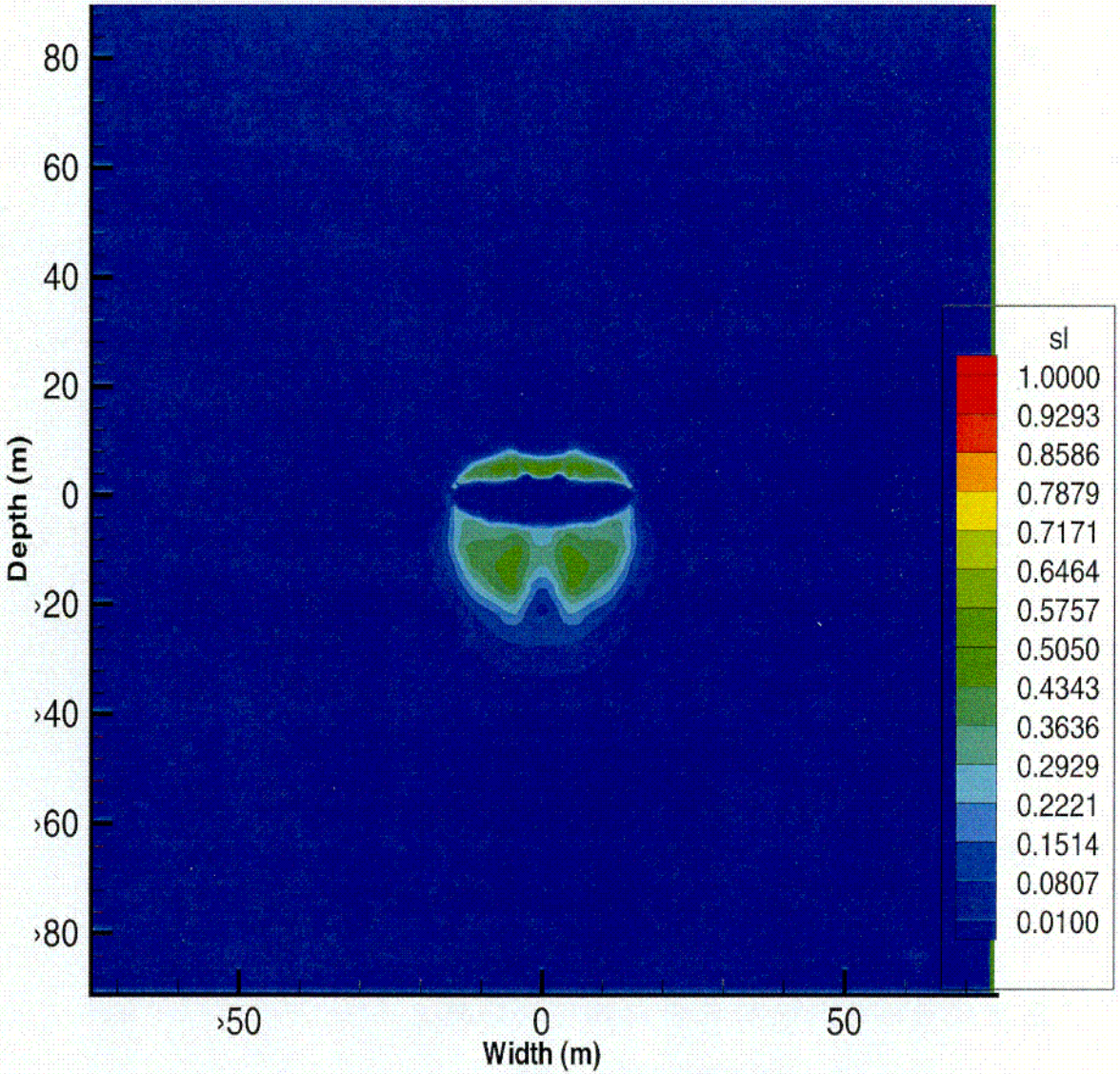

Figure 3-16d. Contour plot of simulated fracture saturation for a 10^{-2} reduction in fracture permeability and an infiltration rate of 0.036 mm/yr

C20

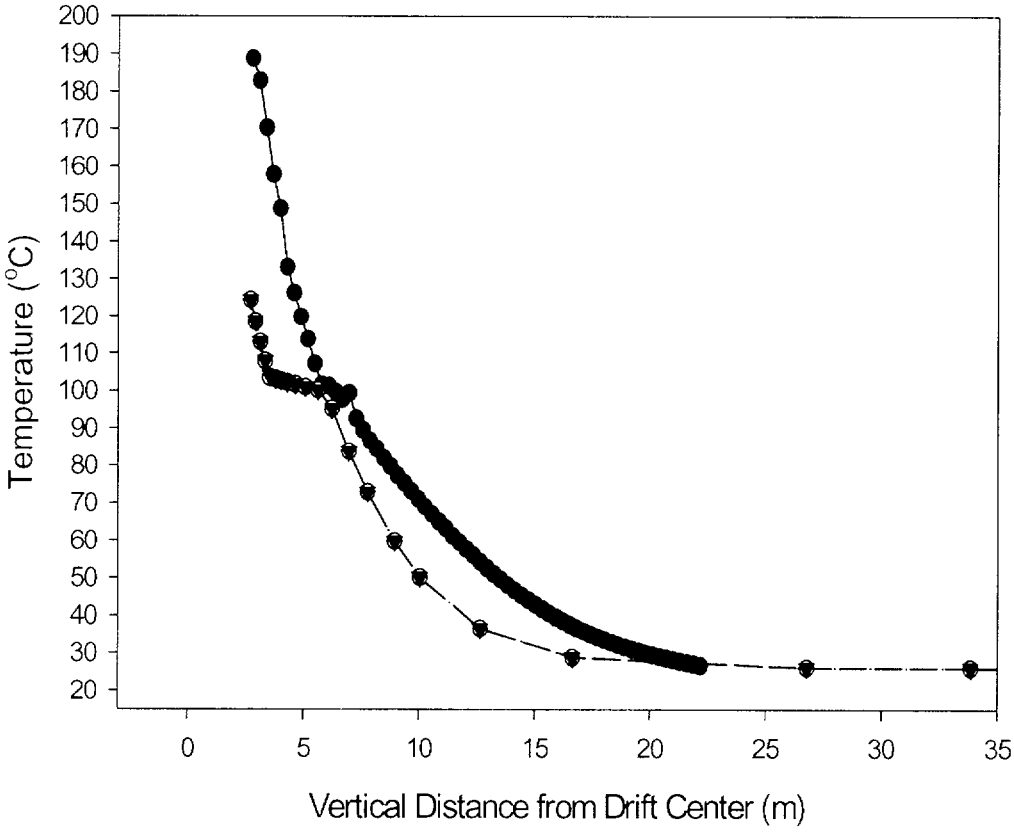

Figure 3-17a. Comparison of measured temperatures (solid circle) versus simulated temperatures in the matrix (closed triangle) and fracture (open circle) for vertical Borehole 158 for a 10^{-2} reduction in fracture permeability, an infiltration rate of 0.036 mm/yr, and a mass loss rate of 80 mL/hr through the thermal bulkhead

observed temperatures to about 55 °C. There also was a slight increase (i.e., about 5 °C at the drift wall springline diminishing to no change at a distance of 5 m from the drift wall) in simulated temperatures compared with those observed along Borehole 160 (figure 3-17b). Matrix and fracture temperatures and saturations for the case with reduced fracture permeability are not affected by a mass loss of 80 mL/hr with the notable exception of saturation directly above the heater drift (figure 3-18a,b,c,d). Comparison of matrix saturation above the heater drift for the cases of reduced fracture permeability with (figure 3-18c) and without a mass loss of 80 mL/hr (figure 3-16c) indicates that the mass is mostly removed from the heater drift crown.

This loss is further illustrated in profiles of predicted saturation along Borehole 158 for these two cases (figure 3-19). As illustrated, the predicted saturation in the heater drift crown is decreased from 0.80 to 0.35 in the matrix by the mass removal. The zone of dryout in the fracture continuum is depressed slightly deeper into the rock unit, and the maximum fracture saturation observed in the fractures in the condensation zone above the heater drift is decreased from approximately 0.55 to 0.47 by a mass removal of 80 mL/hr. The total mass of water in the condensation zone in the fracture continuum is reduced by the 80 mL/hr mass removal as indicated by the reduced area of increased fracture saturation. The condensation zone for the matrix continuum, however, is similar for the cases with and without mass removal with the exception of reduced matrix saturation near the drift crown caused by the mass removal.

A one-third increase in the thermal conductivity of all three model units did not significantly alter the temperature simulated above the heater drift along Borehole 158 (figures 3-20a). Simulated temperatures along the horizontally oriented Borehole 160, however, were significantly decreased by an increase in thermal conductivity (figure 3-20b). Temperatures above the inner wing heaters were reduced by about 15 °C and by as much as 20 °C above the outer wing heaters. Matrix and fracture temperatures and saturation contour plots for the case with increased thermal conductivity indicate the lower temperatures that formed at the DST (figure 3-21a,b) resulted in reduced zones of dryout around the heaters (figure 3-21c,d). The greatest zones of dryout were observed at the springline of the heater drift. There is a well-defined difference between predicted saturations for the cases of increased thermal conductivity with and without mass loss. The removal of 80 mL/hr from the heater drift wall resulted in a better defined dryout zone around the heater drift with the greatest decrease in saturation observed at the heater drift crown (figures 3-22a,b; 3-23a,b,c,d; and 3-24).

A one-third decrease in thermal conductivity and a mass loss of 80 mL/hr had a pronounced effect on predicted temperatures (figure 3-25a,b). In particular, the predicted temperature at the heater drift crown was increased to 135 °C, although still 45 °C less than observed. The predicted temperatures for Borehole 160 exceeded the observed temperature near the heater drift and at the outer wing heater. The difference between the temperature at the springline (210 °C) and at the drift crown (135 °C) persisted for this case. Contour plots for this case (figures 3-26a,b,c,d) are similar to the same case, but with basecase thermal conductivity values with the exception that temperatures were significantly increased.

Horizontally asymmetrical saturation is clearly discernable in the model results for both the matrix and fracture continua. Predictions of fracture saturations indicate that rapid flow through the fractures is experienced soon after the onset of heating. The increased fracture saturation above the heaters is attributed to condensation of water vapor in the fractures beyond where the fractures are at above boiling temperatures. The lateral extensions of elevated fracture saturation beyond the extent of the wing heaters and the presence of elevated saturation below the DST horizon beyond the ends of the wing heaters suggest that condensate shedding off the ends of the wing heaters occurs later in the 4-yr heating phase of the DST.

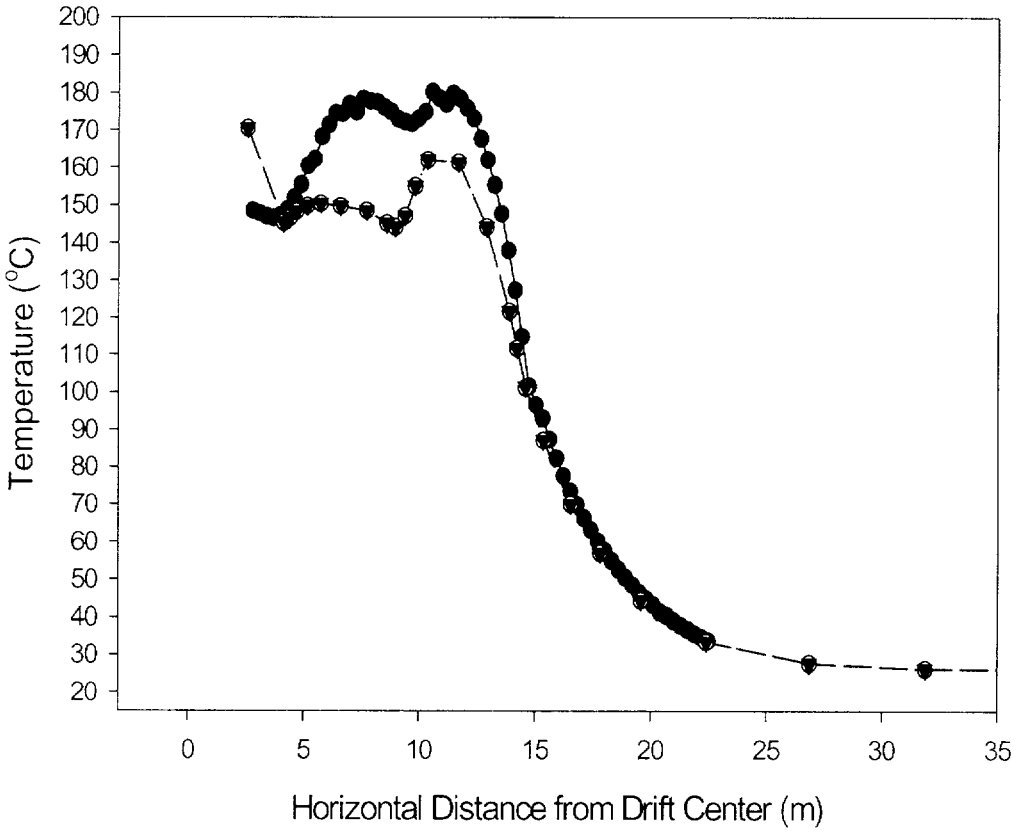

Figure 3-17b. Comparison of measured temperatures (solid circle) versus simulated temperatures in the matrix (closed triangle) and fracture (open circle) for horizontal Borehole 160 for a 10^{-2} reduction in fracture permeability, an infiltration rate of 0.036 mm/yr, and a mass loss rate of 80 mL/hr through the thermal bulkhead

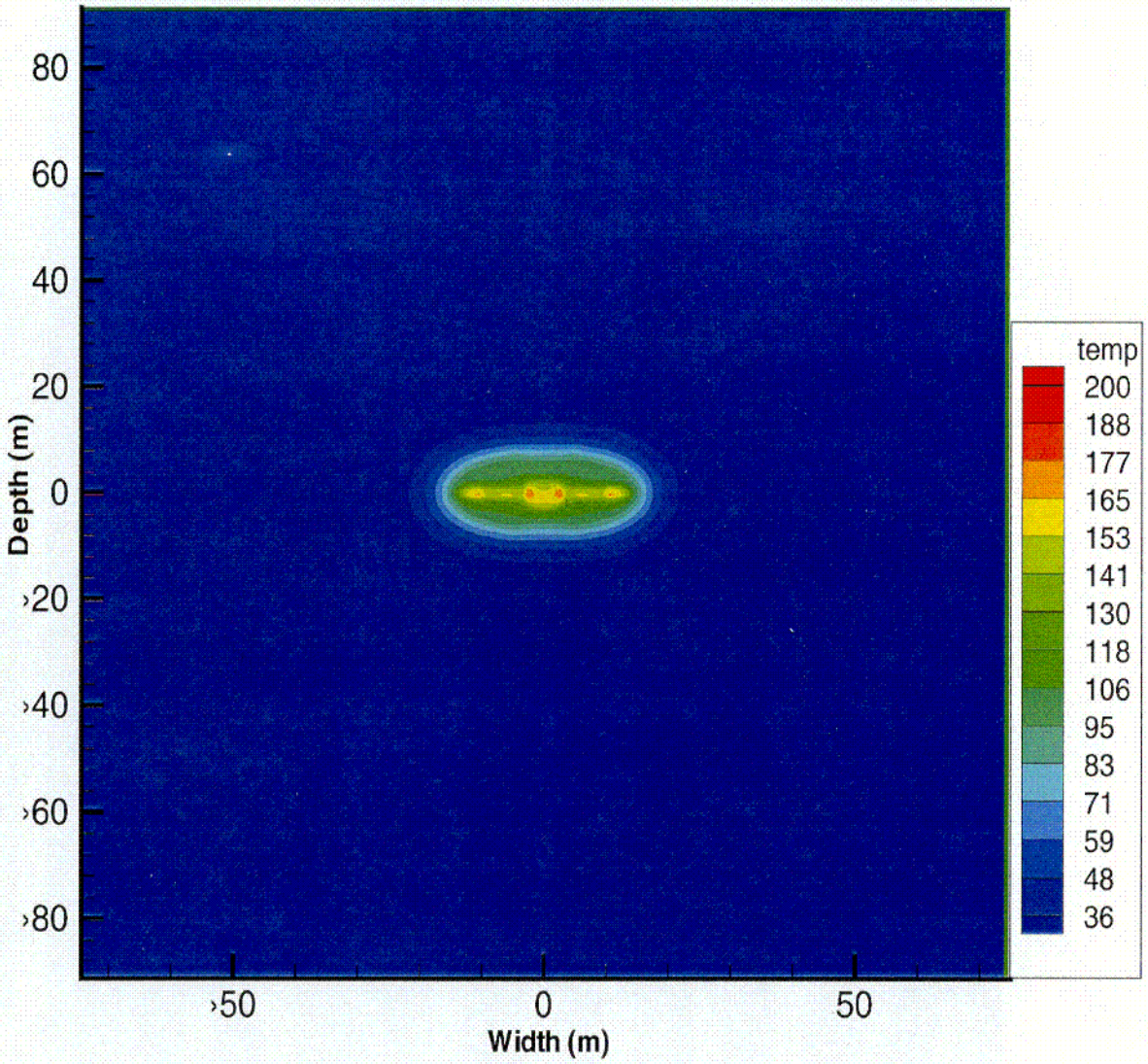

Figure 3-18a. Contour plot of simulated matrix temperature for a 10^{-2} reduction in fracture permeability, an infiltration rate of 0.036 mm/yr, and a mass loss rate of 80 mL/hr through the thermal bulkhead

C21

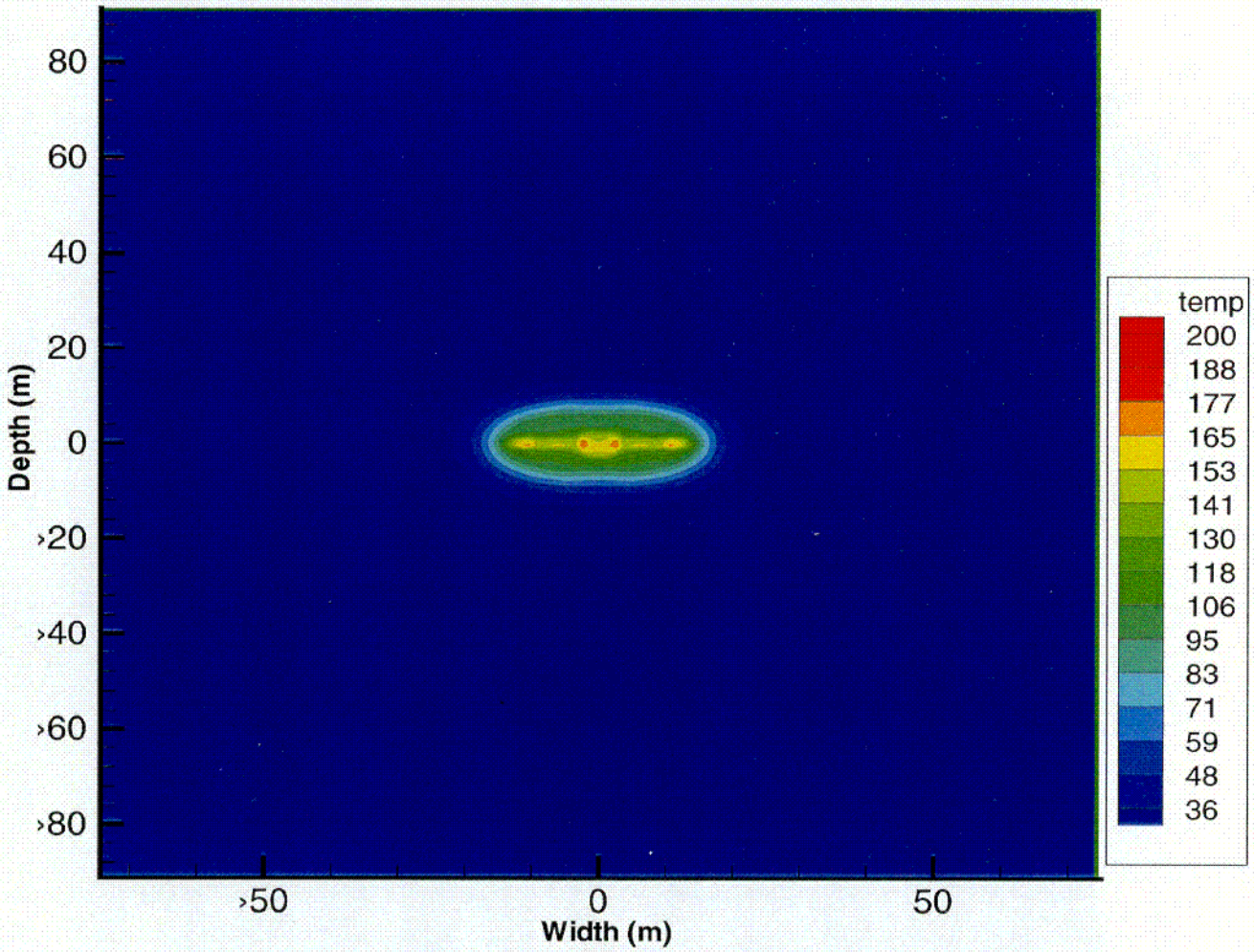

Figure 3-18b. Contour plot of simulated fracture temperature for a 10^{-2} reduction in fracture permeability, an infiltration rate of 0.036 mm/yr, and a mass loss rate of 80 mL/hr through the thermal bulkhead

C222

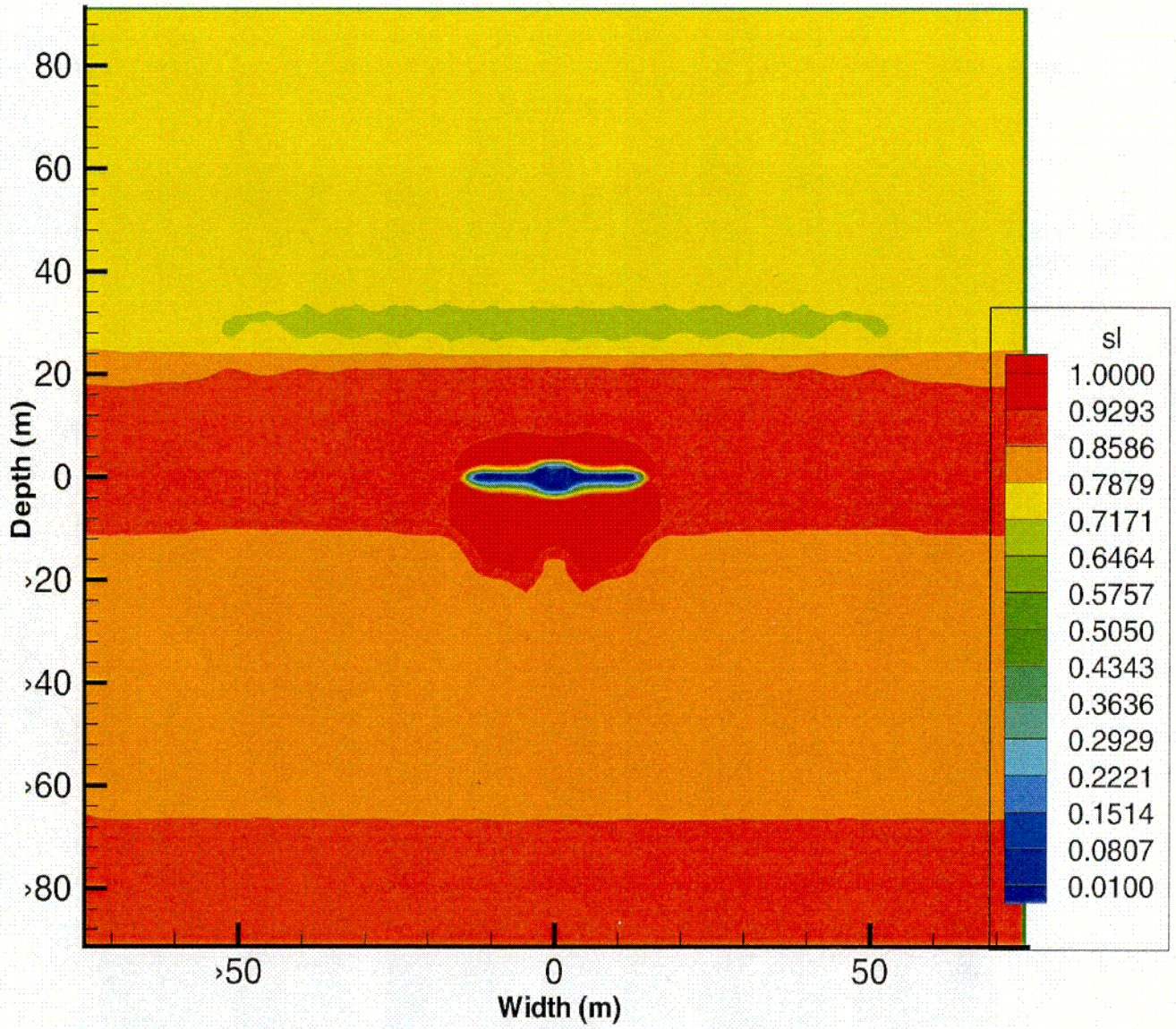

Figure 3-18c. Contour plot of simulated matrix saturation for a 10^{-2} reduction in fracture permeability, an infiltration rate of 0.036 mm/yr, and a mass loss rate of 80 mL/hr through the thermal bulkhead

C23

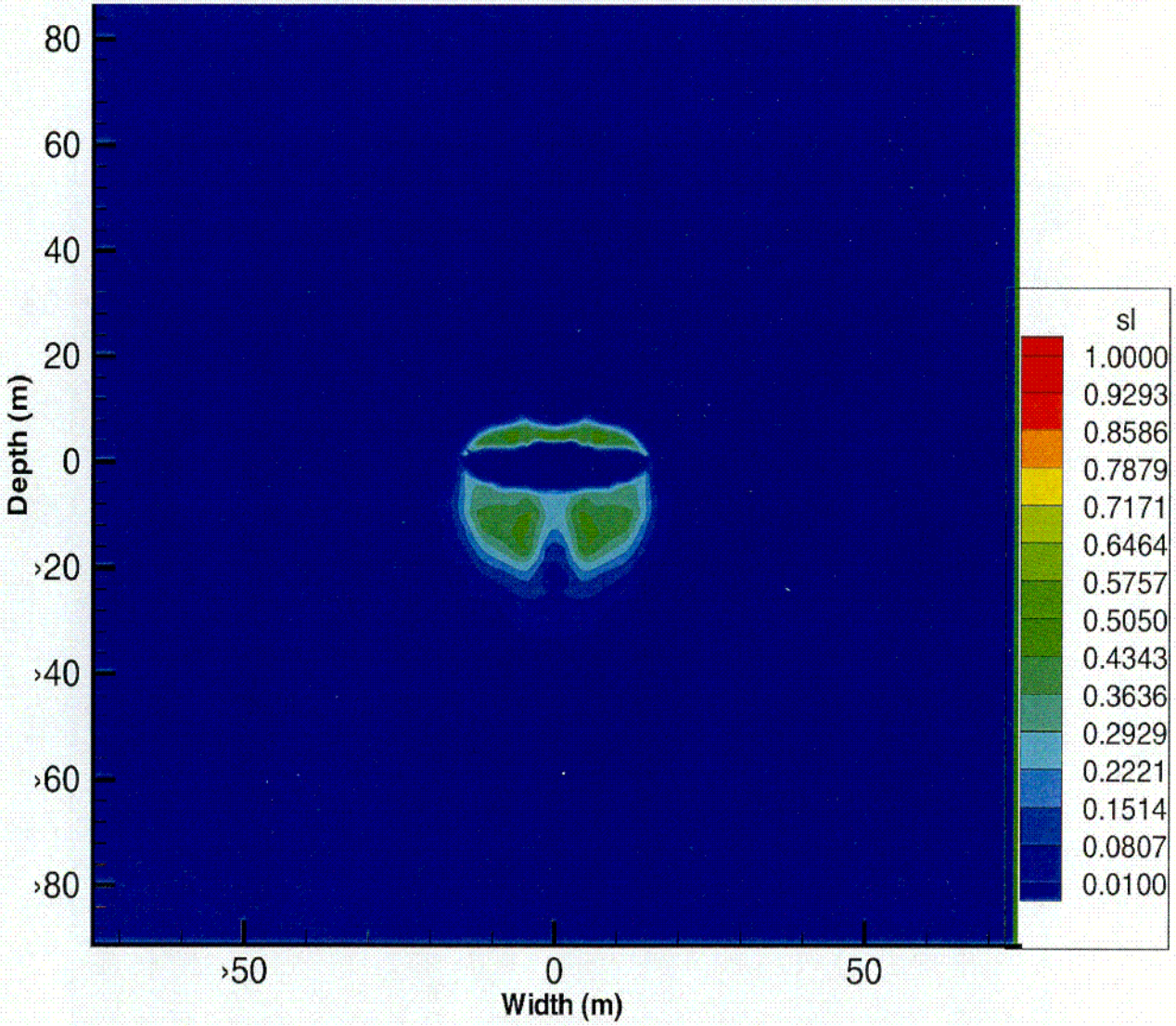

Figure 3-18d. Contour plot of simulated fracture saturation for a 10^{-2} reduction in fracture permeability, an infiltration rate of 0.036 mm/yr, and a mass loss rate of 80 mL/hr through the thermal bulkhead

C24

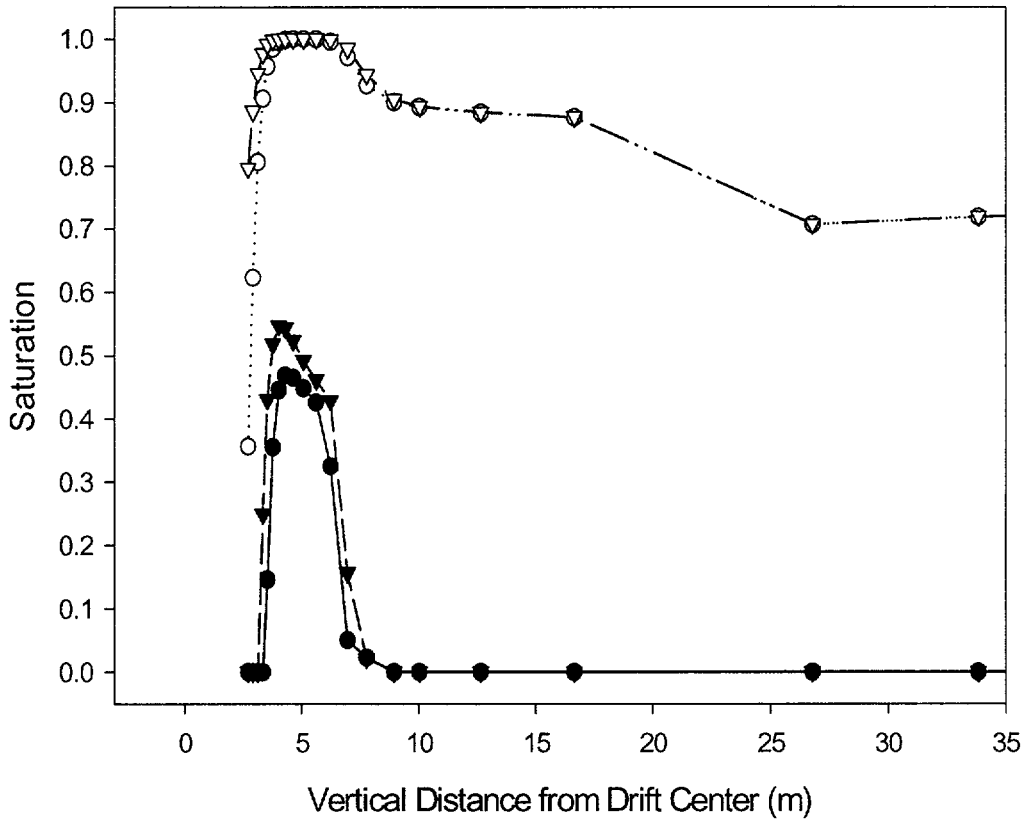

Figure 3-19. Comparison of matrix saturation with no mass loss (open triangle), fracture saturation with no mass loss (closed triangle), matrix saturation with 80 mL/hr mass loss (open circle), and fracture saturation with 80 mL/hr mass loss(closed circle) for a 10^{-2} reduction in fracture permeability, and an infiltration rate of 0.036 mm/yr

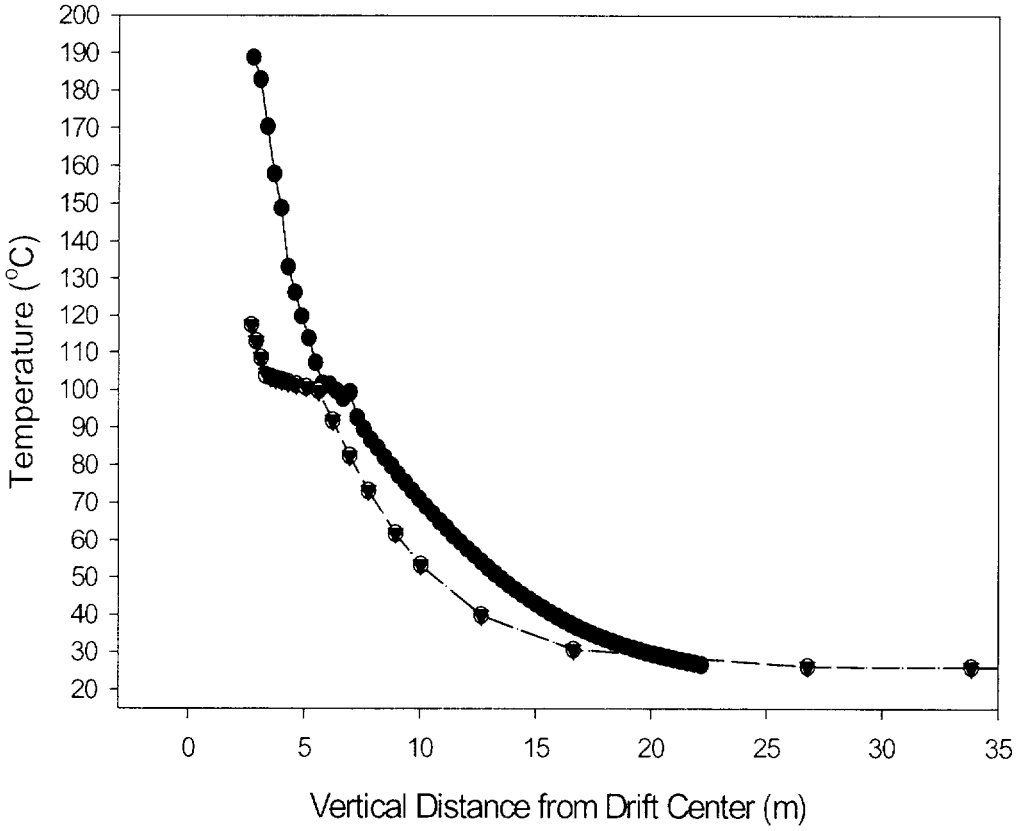

Figure 3-20a. Comparison of measured temperatures (solid circle) versus simulated temperatures in the matrix (closed triangle) and fracture (open circle) for vertical Borehole 158 for a 10^{-2} reduction in fracture permeability, a one-third increase in thermal conductivity, and an infiltration rate of 0.036 mm/yr

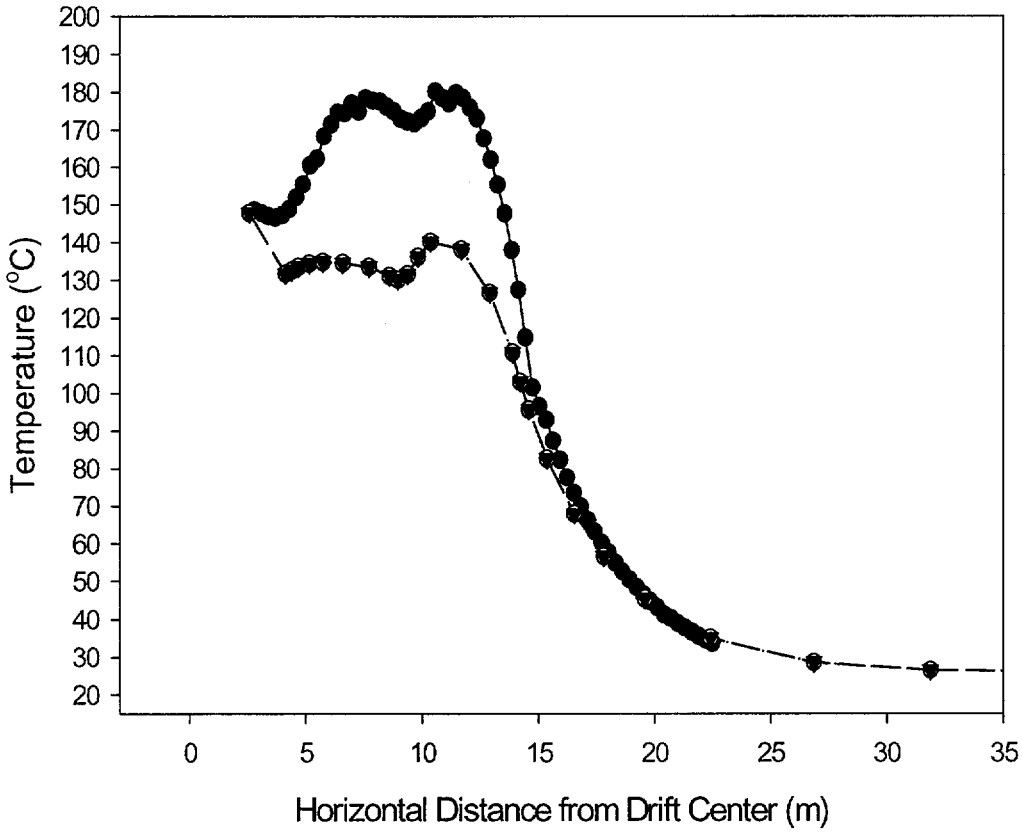

Figure 3-20b. Comparison of measured temperatures (solid circle) versus simulated temperatures in the matrix (closed triangle) and fracture (open circle) for horizontal Borehole 160 for a 10^{-2} reduction in fracture permeability, a one-third increase in thermal conductivity, and an infiltration rate of 0.036 mm/yr

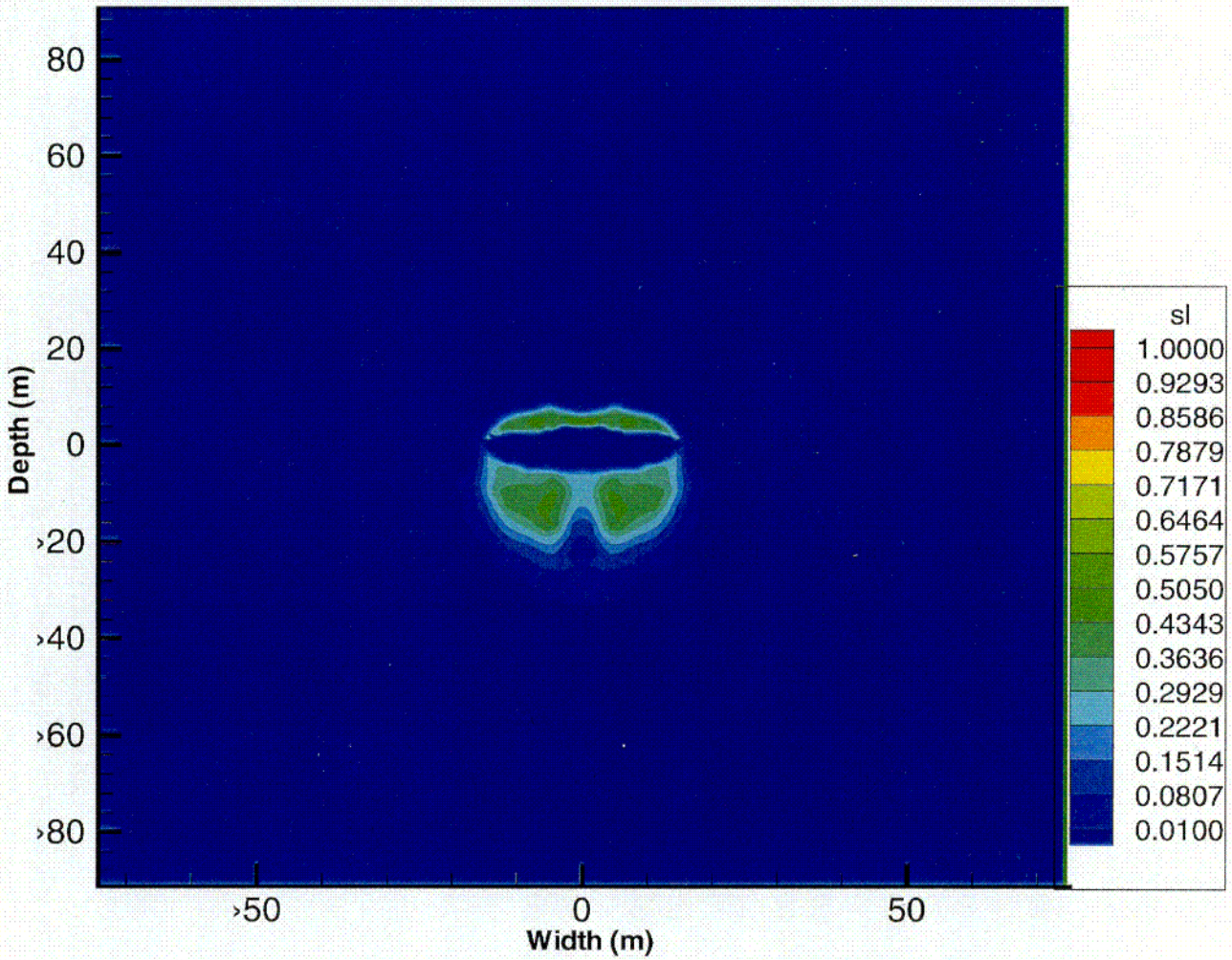

Figure 3-21a. Contour plot of simulated matrix temperature for a 10^{-2} reduction in fracture permeability, a 1/3 increase in thermal conductivity, and an infiltration rate of 0.036 mm/yr

C25

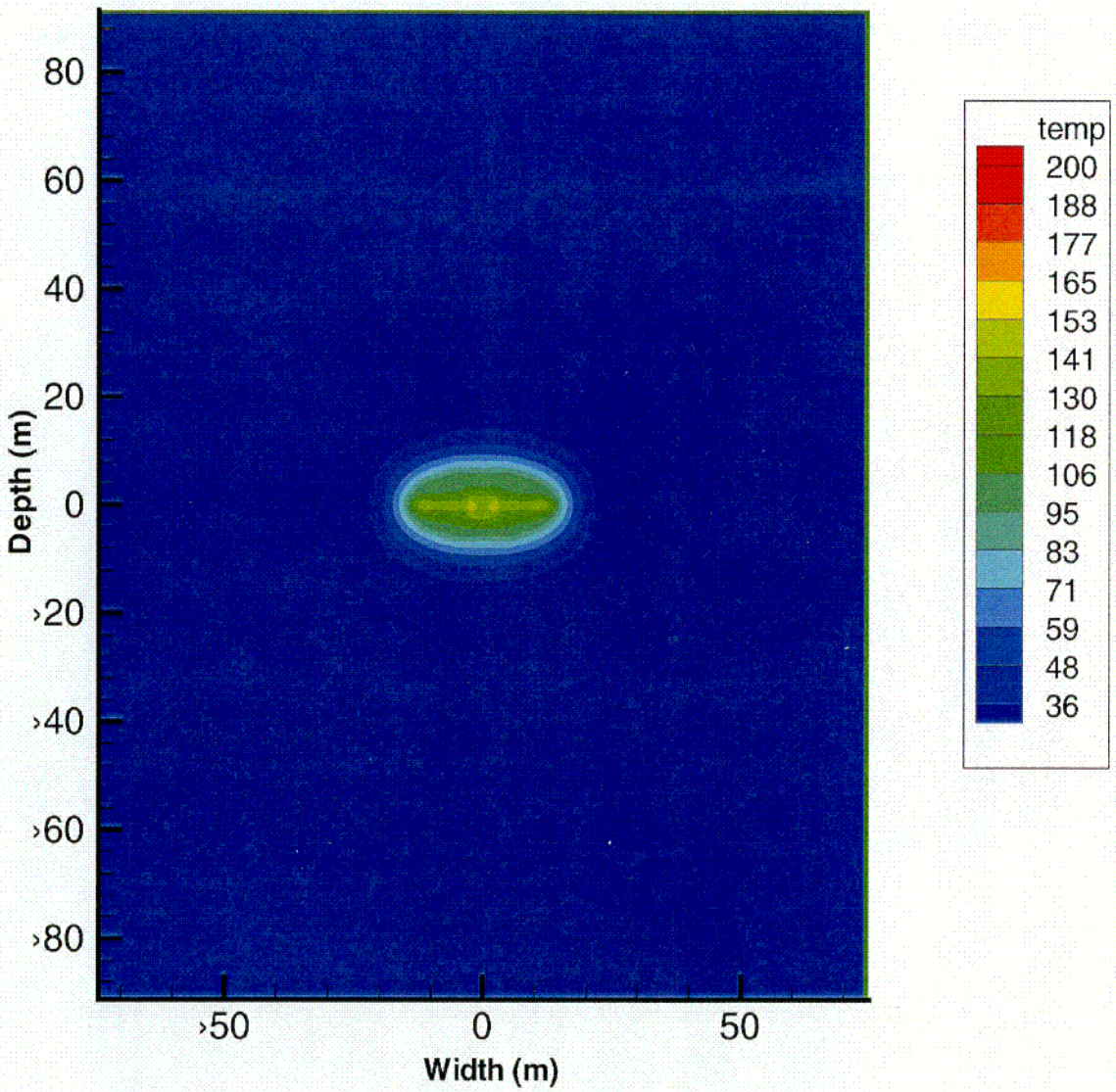

Figure 3-21b. Contour plot of simulated fracture temperature for a 10^{-2} reduction in fracture permeability, a 1/3 increase in thermal conductivity, and an infiltration rate of 0.036 mm/yr

C26

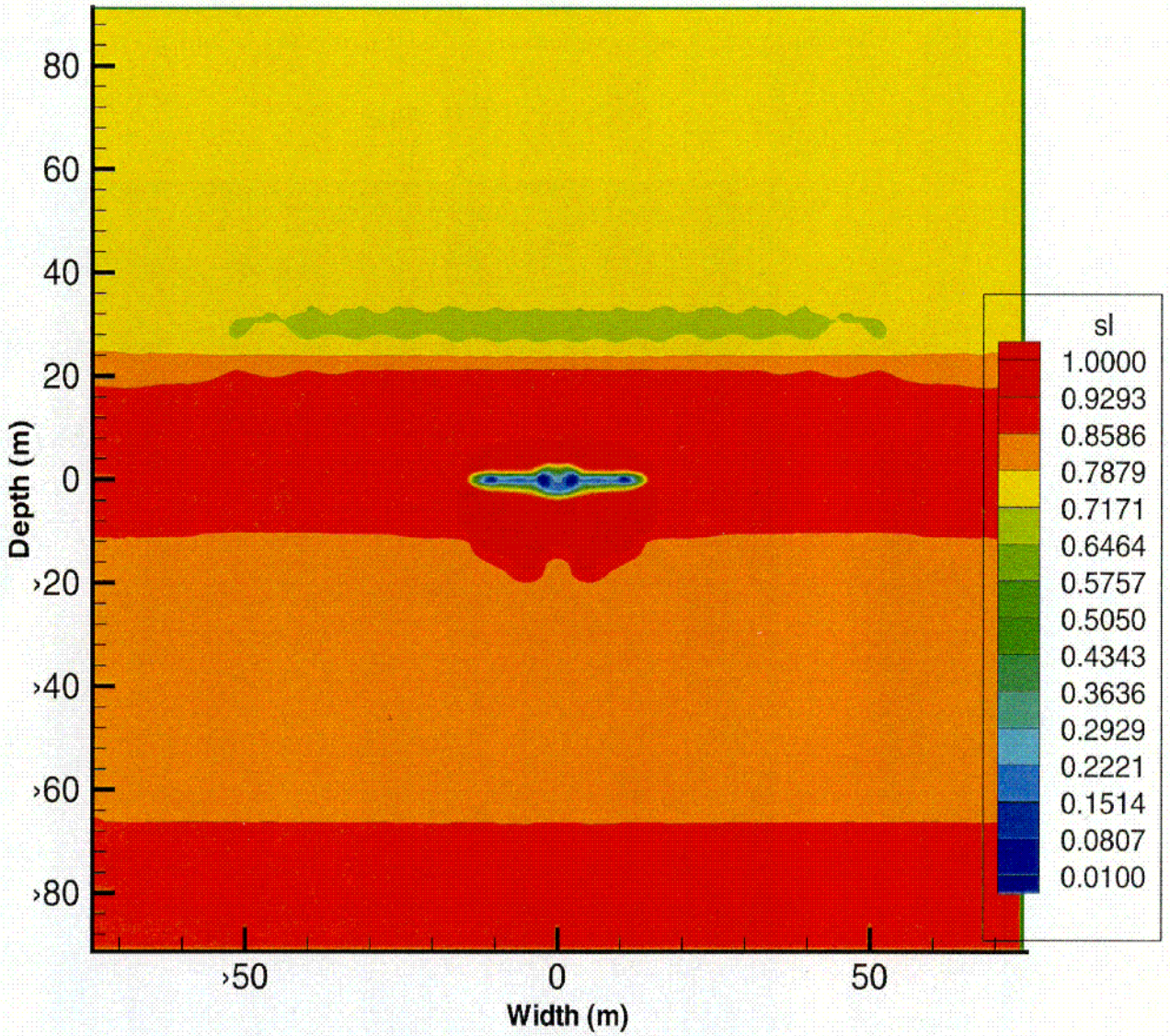

Figure 3-21c. Contour plot of simulated matrix saturation for a 10^{-2} reduction in fracture permeability, a 1/3 increase in thermal conductivity, and an infiltration rate of 0.036 mm/yr

C27

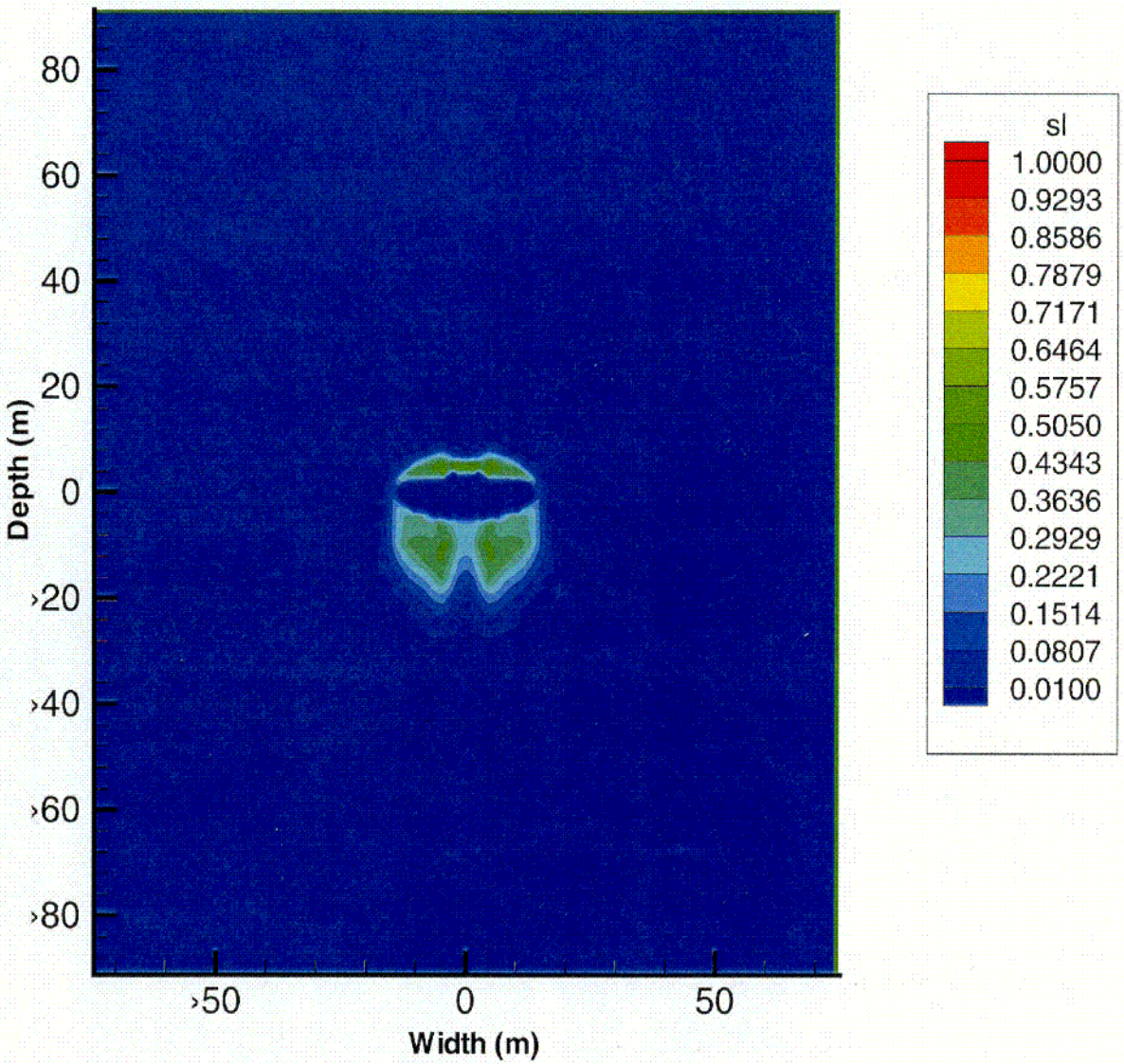

Figure 3-21d. Contour plot of simulated fracture saturation for a 10^{-2} reduction in fracture permeability, a 1/3 increase in thermal conductivity, and an infiltration rate of 0.036 mm/yr

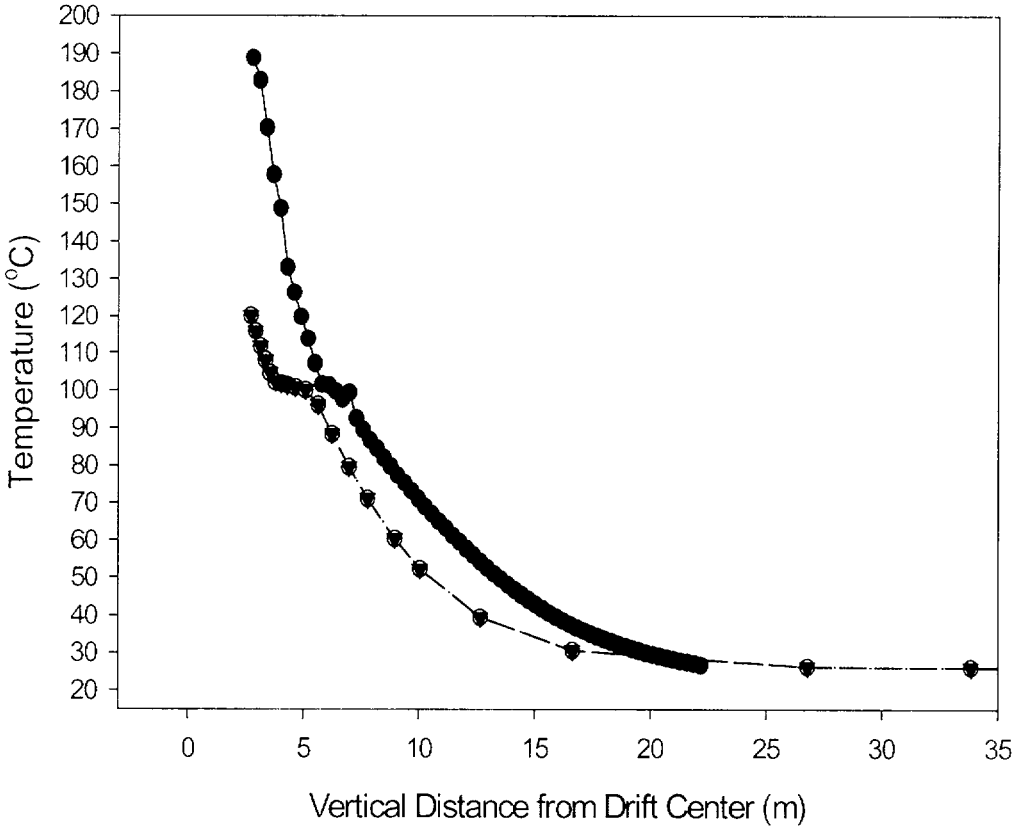

Figure 3-22a. Comparison of measured temperatures (solid circle) versus simulated temperatures in the matrix (closed triangle) and fracture (open circle) for vertical Borehole 158 for a 10^{-2} reduction in fracture permeability, an infiltration rate of 0.036 mm/yr, a one-third increase in thermal conductivity, and a mass loss rate of 80 mL/hr through the thermal bulkhead

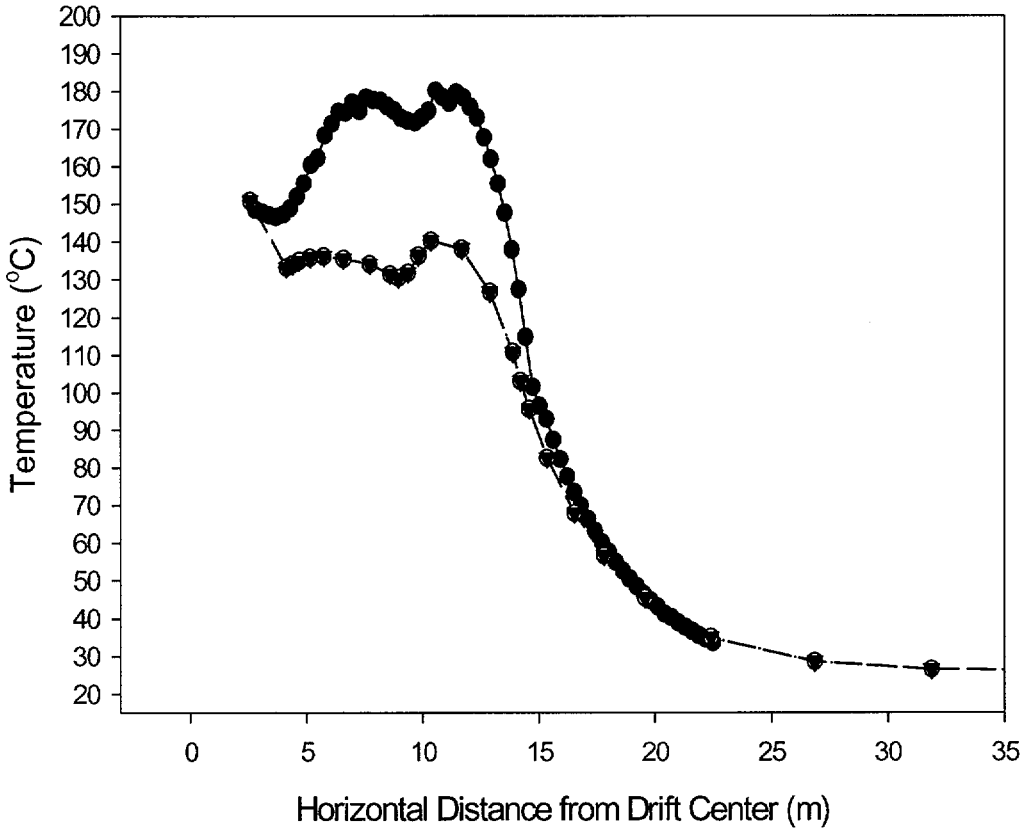

Figure 3-22b. Comparison of measured temperatures (solid circle) versus simulated temperatures in the matrix (closed triangle) and fracture (open circle) for horizontal Borehole 160 for a 10^{-2} reduction in fracture permeability, an infiltration rate of 0.036 mm/yr, a one-third increase in thermal conductivity, and a mass loss rate of 80 mL/hr through the thermal bulkhead

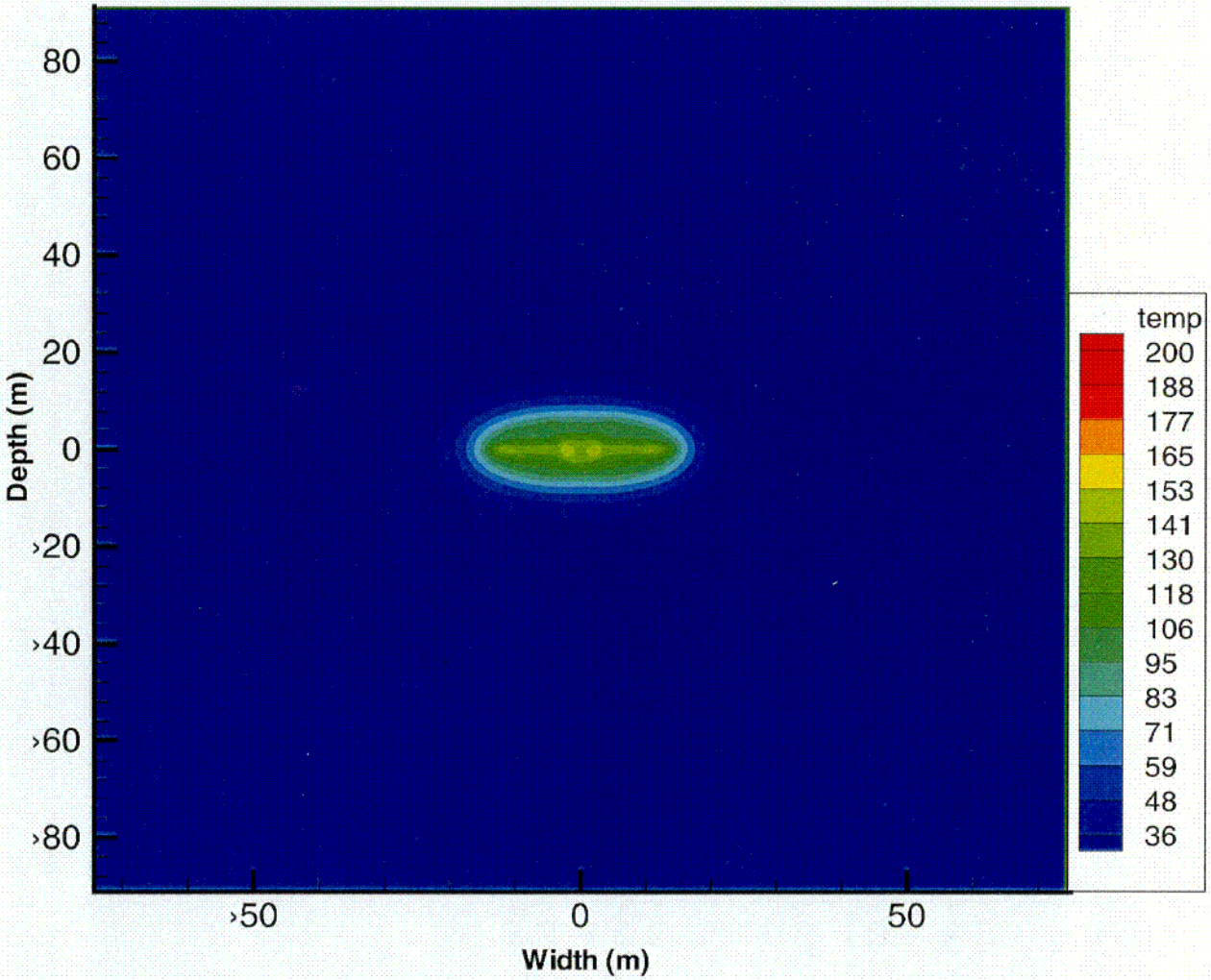

Figure 3-23a. Contour plot of simulated matrix temperature for a 10^{-2} reduction in fracture permeability, an infiltration rate of 0.036 mm/yr, a 1/3 increase in thermal conductivity, and a mass loss rate of 80 mL/hr through the thermal bulkhead

C29

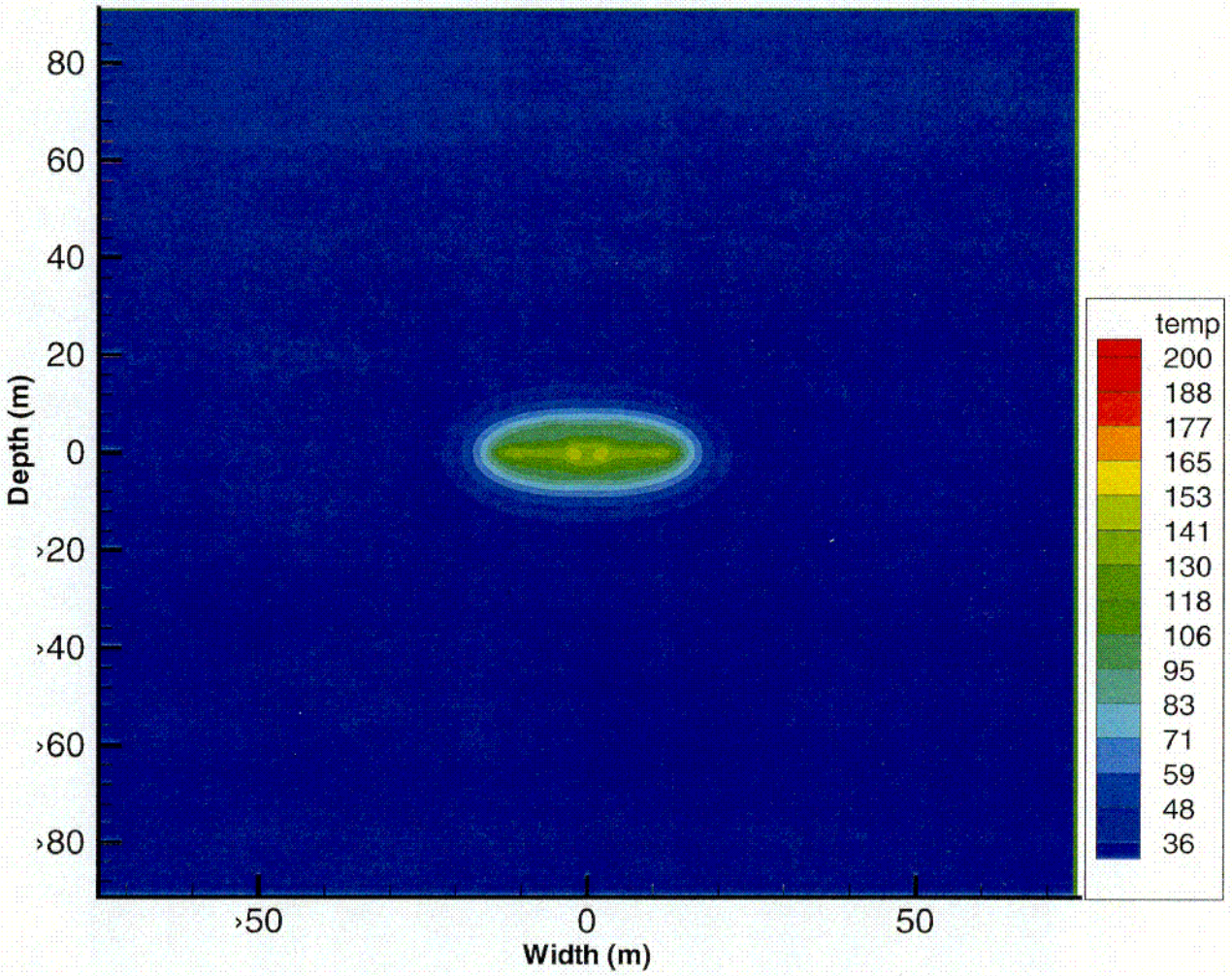

Figure 3-23b. Contour plot of simulated fracture temperature for a 10^{-2} reduction in fracture permeability, an infiltration rate of 0.036 mm/yr, a 1/3 increase in thermal conductivity, and a mass loss rate of 80 mL/hr through the thermal bulkhead

C30

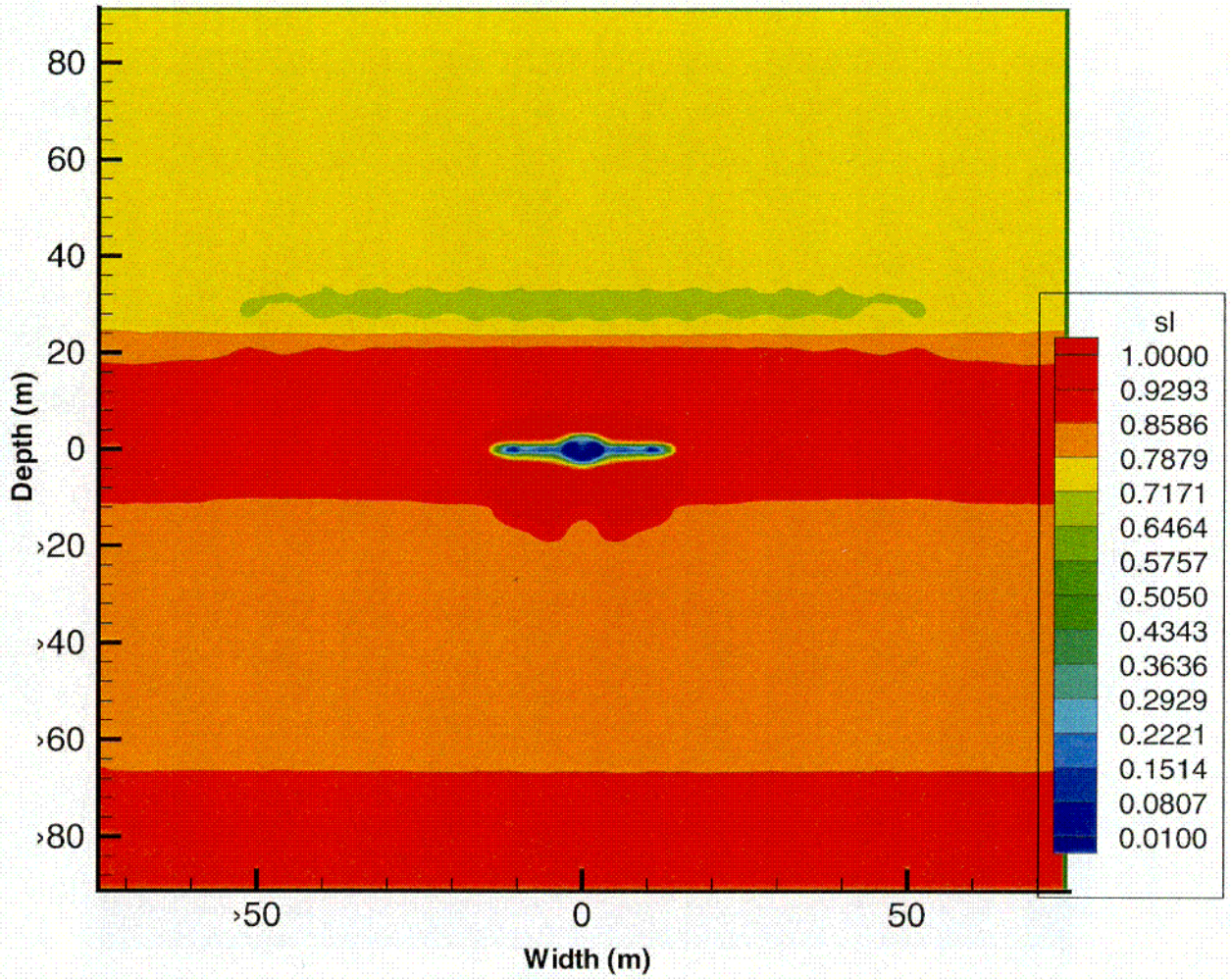

Figure 3-23c. Contour plot of simulated matrix saturation for a 10^{-2} reduction in fracture permeability, an infiltration rate of 0.036 mm/yr, a 1/3 increase in thermal conductivity, and a mass loss rate of 80 mL/hr through the thermal bulkhead

C31

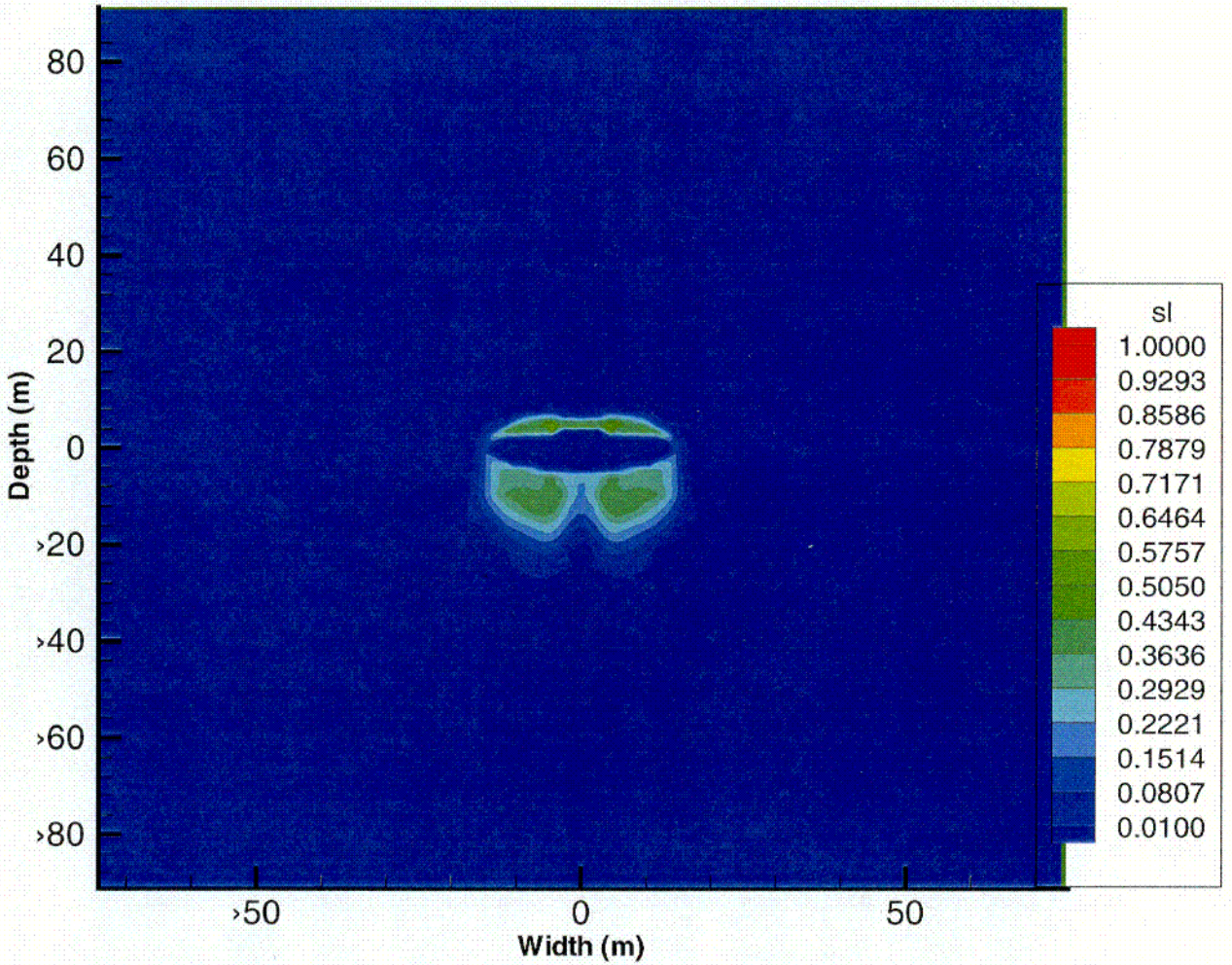

Figure 3-23d. Contour plot of simulated fracture saturation for a 10^{-2} reduction in fracture permeability, an infiltration rate of 0.036 mm/yr, a 1/3 increase in thermal conductivity, and a mass loss rate of 80 mL/hr through the thermal bulkhead

C32

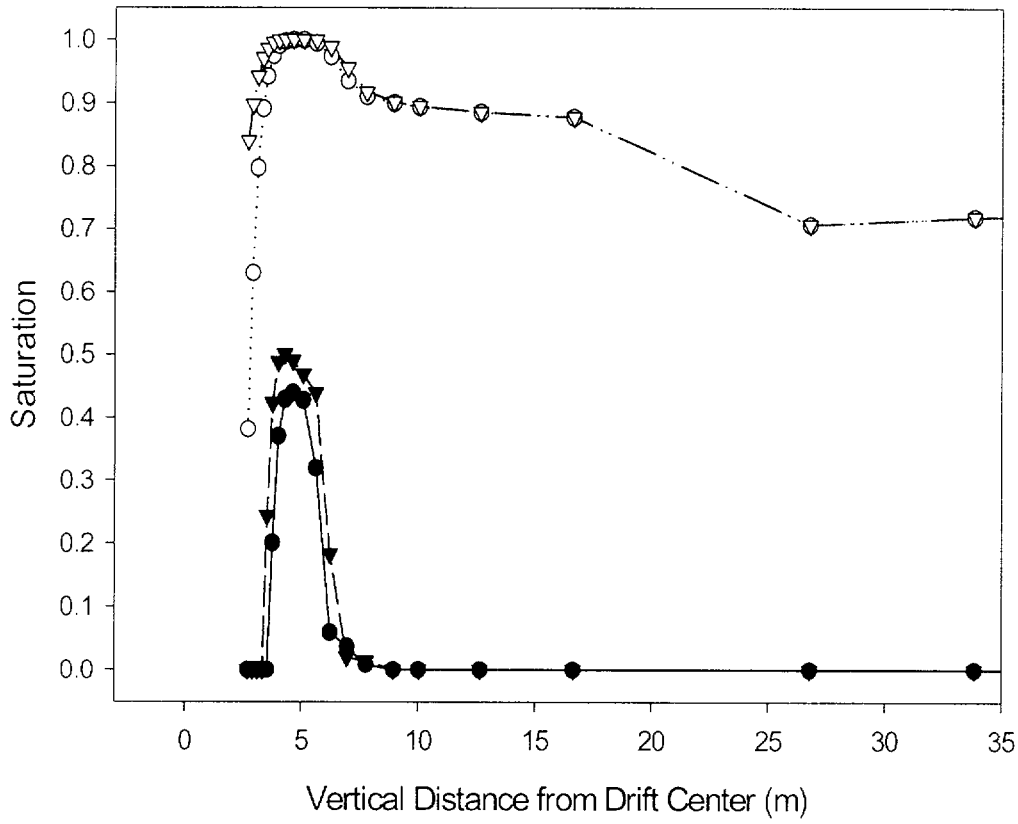

Figure 3-24. Comparison of matrix saturation and no mass loss (open triangle), fracture saturation with no mass loss (closed triangle), matrix saturation with 80ml/hr mass loss (open circle), and fracture saturation with 80 mL/hr (closed circle) for a 10^{-2} reduction in fracture permeability, and infiltration rate of 0.036 mm/yr, and a one-third increase in thermal conductivity

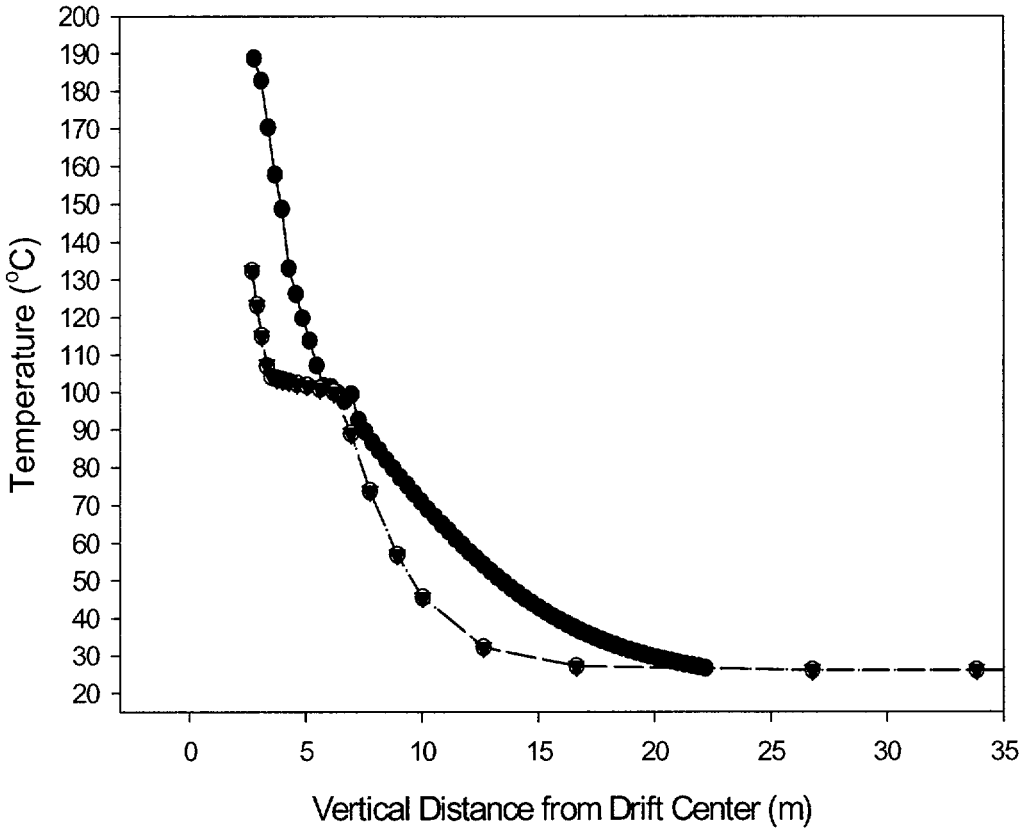

Figure 3-25a. Comparison of measured temperatures (solid circle) versus simulated temperatures in the matrix (closed triangle) and fracture (open circle) for vertical Borehole 158 for a 10^{-2} reduction in fracture permeability, an infiltration rate of 0.036 mm/yr, a one-third decrease in thermal conductivity, and a mass loss rate of 80 mL/hr through the thermal bulkhead

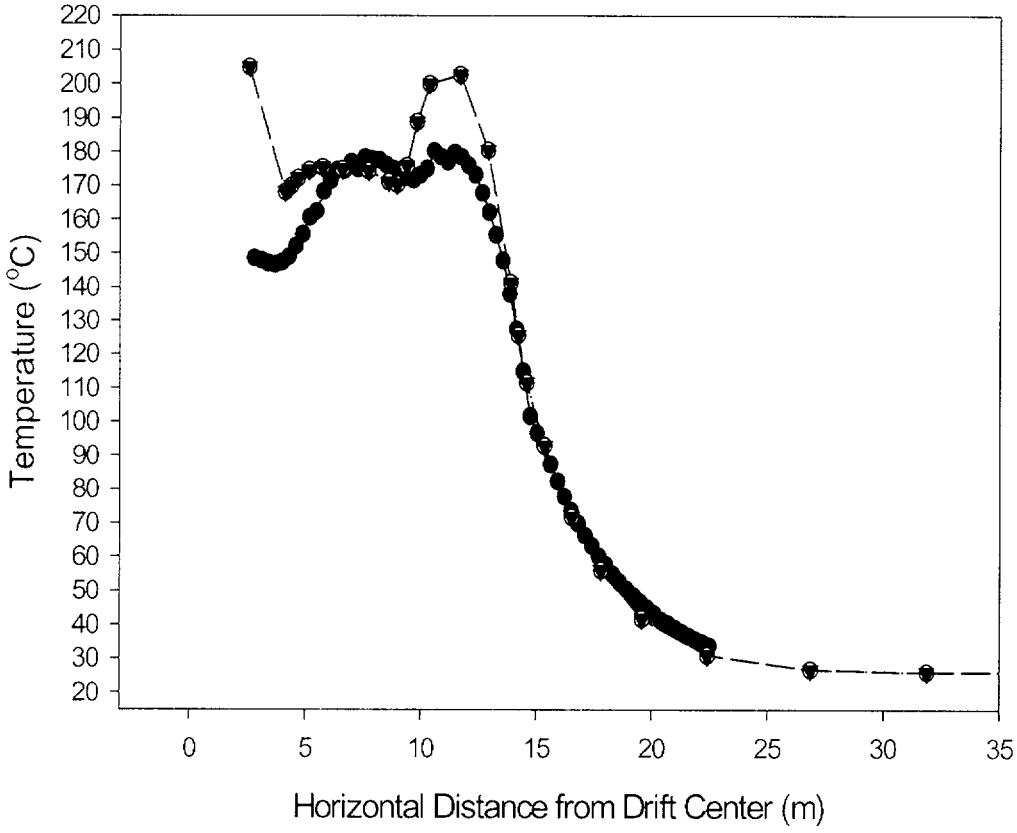

Figure 3-25b. Comparison of measured temperatures (solid circle) versus simulated temperatures in the matrix (closed triangle) and fracture (open circle) for horizontal Borehole 160 for a 10^{-2} reduction in fracture permeability, an infiltration rate of 0.036 mm/yr, a one-third decrease in thermal conductivity, and a mass loss rate of 80 mL/hr through the thermal bulkhead

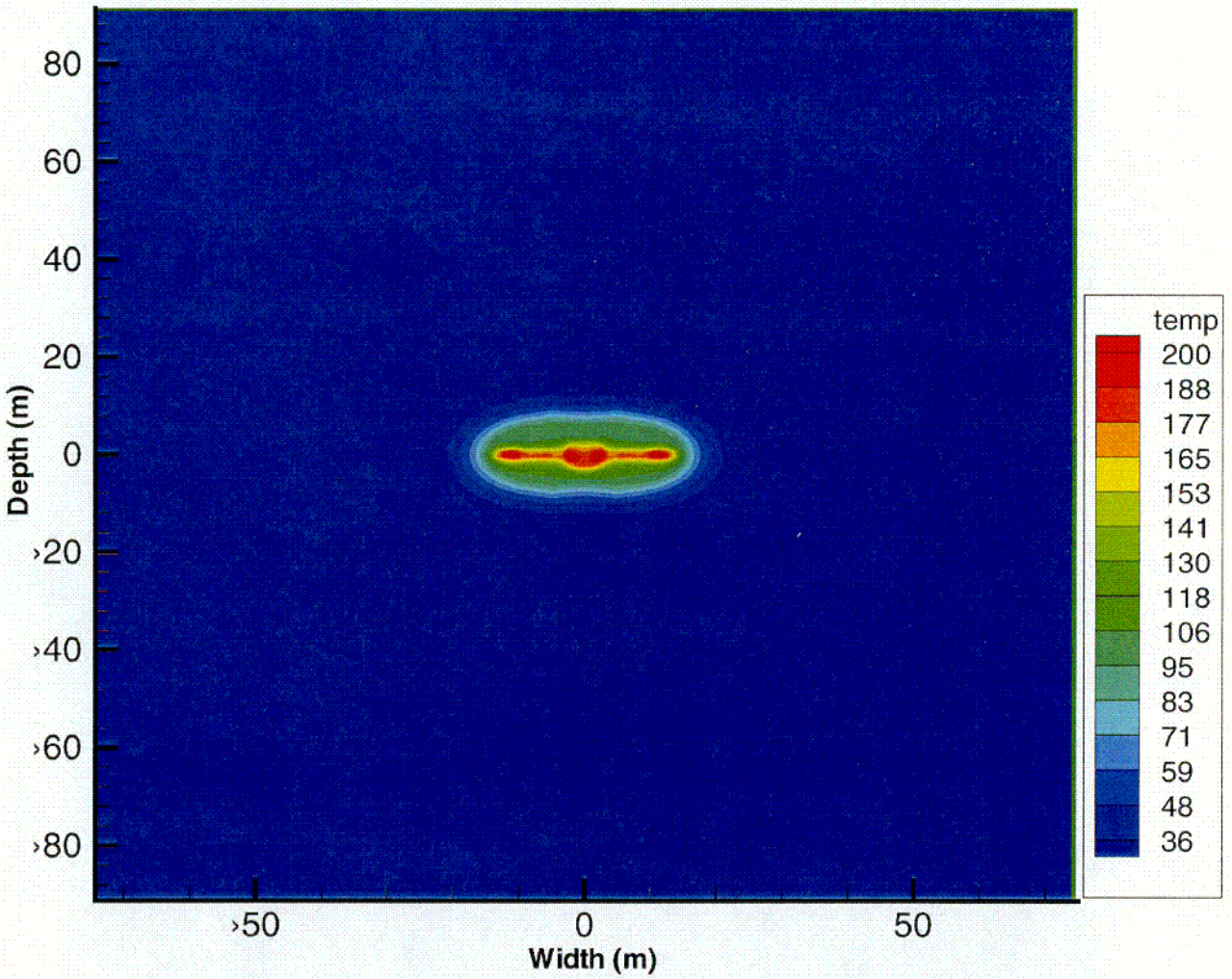

Figure 3-26a. Contour plot of simulated matrix temperature for a 10^{-2} reduction in fracture permeability, an infiltration rate of 0.036 mm/yr, a 1/3 decrease in thermal conductivity, and a mass loss rate of 80 mL/hr through the thermal bulkhead

C33

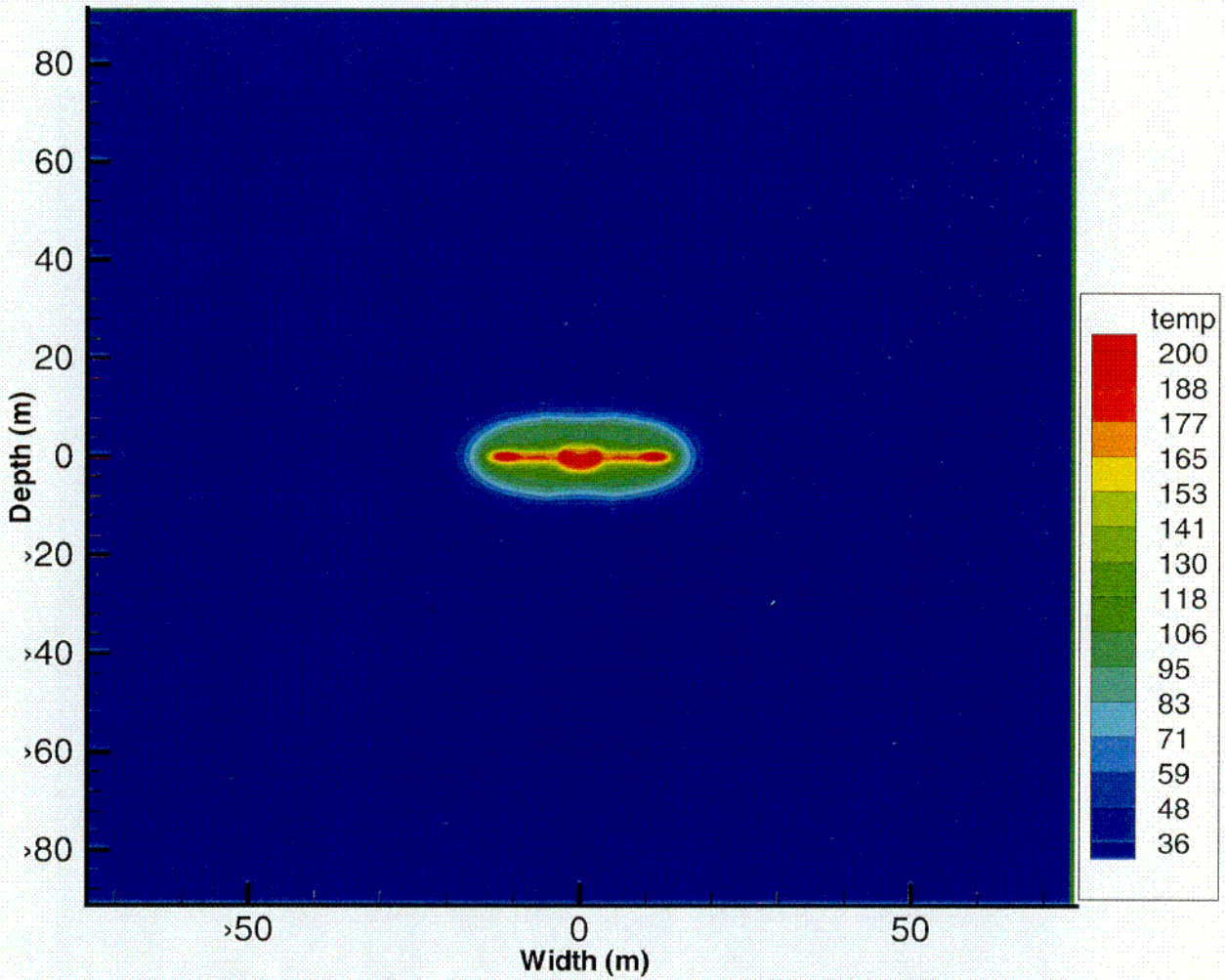

Figure 3-26b. Contour plot of simulated fracture temperature for a 10^{-2} reduction in fracture permeability, an infiltration rate of 0.036 mm/yr, a 1/3 decrease in thermal conductivity, and a mass loss rate of 80 mL/hr through the thermal bulkhead

C34

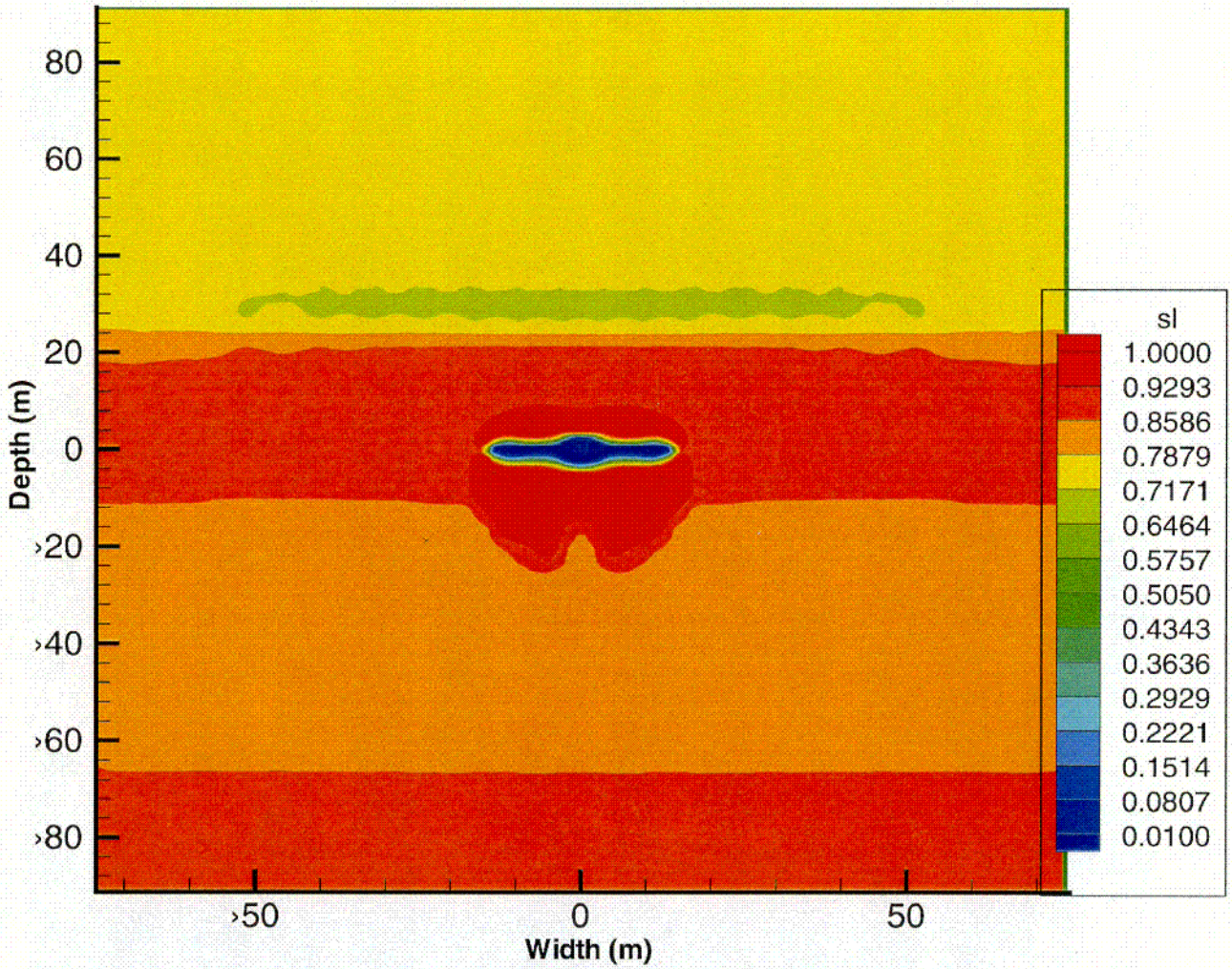

Figure 3-26c. Contour plot of simulated matrix saturation for a 10^{-2} reduction in fracture permeability, an infiltration rate of 0.036 mm/yr, a 1/3 decrease in thermal conductivity, and a mass loss rate of 80 mL/hr through the thermal bulkhead

C35

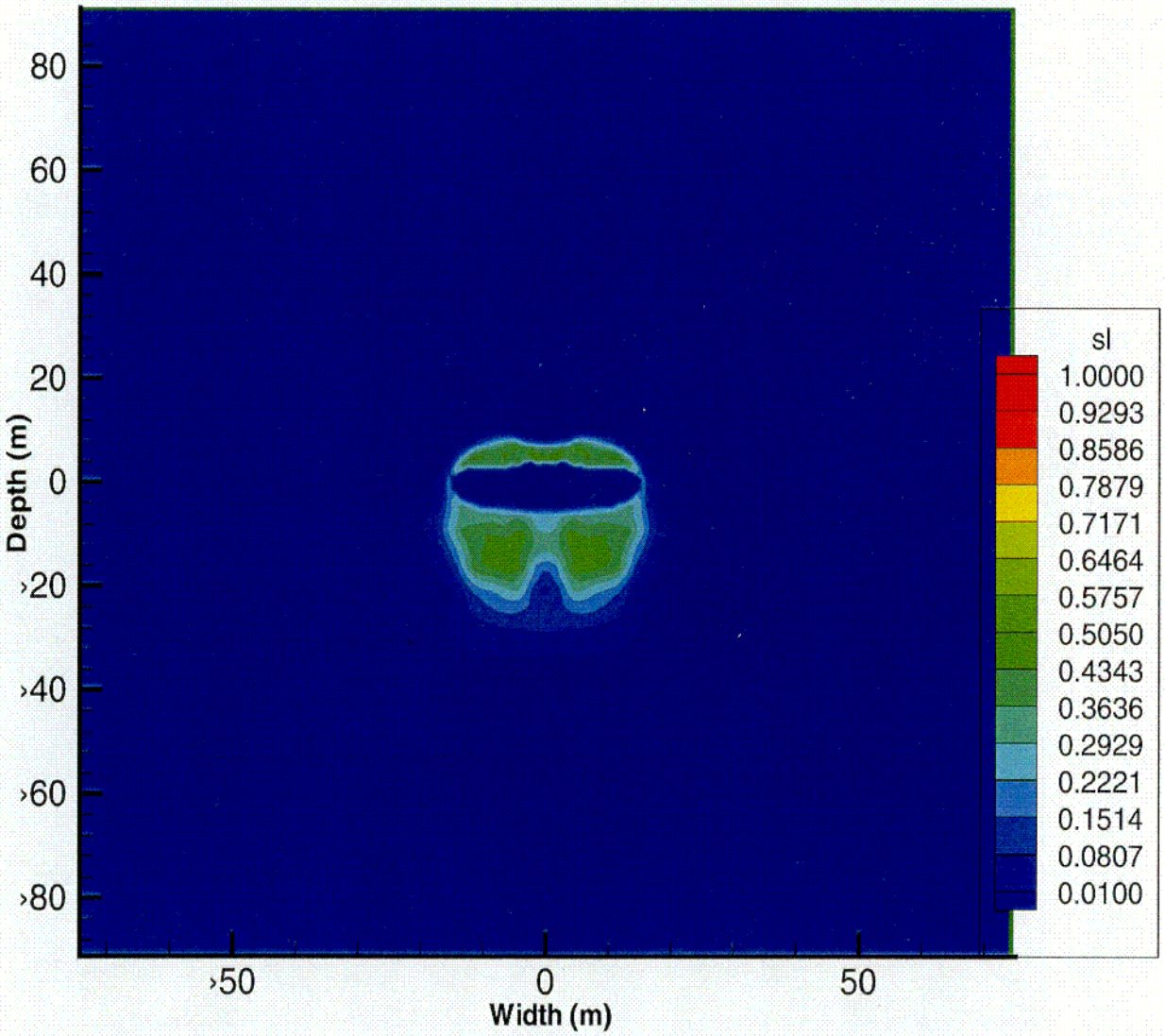

Figure 3-26d. Contour plot of simulated fracture saturation for a 10^{-2} reduction in fracture permeability, an infiltration rate of 0.036 mm/yr, a 1/3 decrease in thermal conductivity, and a mass loss rate of 80 mL/hr through the thermal bulkhead

Rock saturation at the DST has been indirectly measured using several geophysical techniques including ERT, GPR, and borehole neutron probe measurement. The scale of the volume of measurement varies with technique—ERT measures the largest area (a 2D slice), and neutron probe measures the smallest (a sphere of about 0.25-m radius). GPR measurements (figure 2.5-1 in TRW Environmental Safety Systems, Inc., 1999b) do not provide conclusive evidence of the presence of asymmetrical wetting/drying in the DST. Plots of neutron probe measurements versus time for selected boreholes [i.e., Boreholes 50, 67, and 68 presented in figures 2.6-2, 2.5-3, and 2.6-5 of TRW Environmental Safety Systems, Inc. (1999b)] illustrate changes in saturation over time. These plots effectively illustrate that the media below the outer ends of the outer wing heaters have dried out significantly since the onset of heating.

Tomographs of changes in saturation detected by ERT measurements [figures 2.4-6 through 2.4-9 in TRW Environmental Safety Systems, Inc. (1999b)] are ambiguous regarding vertical asymmetry in drying/wetting. Inferring relatively small changes in saturation in the heated block using ERT is especially challenging because of thermally induced changes in rock and water electrical conductivity. When comparing the area above the heaters with the area below, however, an argument may be made that some drying above and wetting below the heated drift is detected in one interpretation method [Model 2, as described by Blair et al. (1998)] of ERT data taken from the vertically oriented plane located along the heated drift axis. In particular, ERT results based on inversions using Model 2 after 511, 582, and 611 days of heating suggested wetting below the heated drift and drying above, whereas an interpretation of ERT data based on Model 1 inversion (Blair et al., 1998) shows less vertical asymmetry in wetting/drying. Asymmetrical wetting/drying cannot be discerned solely from ERT results in a plane perpendicular to the heated drift and intersecting the drift near the middle because the region below the outer edge of the wing heaters is outside the tomograph. An argument may be made that the wetting above the end of the outer edge of the outer wing heater can be discerned using ERT, and drying below the outer edge of the wing can be discerned with neutron probe measurements. Counter to this argument, however, is the ambiguity associated with the location of dryout/wetting zones relative to heater placement. Unless better control on the precise location of dryout/wetting locations can be established, the ERT and neutron probe data may not be effective, either individually or in concert, to address the question of TH asymmetry above and below the heater horizon.

Data and information collected from the DST suggest that the TH regime at the test site is unthrottled, buoyant, advective rock dryout, however, neither the data nor this assessment are conclusive. The modeling results presented in this section also indicate that the TH regime is unthrottled, buoyant, advective rock dryout. Collecting additional DST data and adding evaluations of existing and future data should reduce uncertainty in the nature of the DST TH regime.

3.4.4 Comparison of Drift-Scale Heater Test Modeling by the Center for Nuclear Waste Regulatory Analyses with U.S. Department of Energy Modeling Results

Results from CNWRA DST model predictions are compared in this section with similar results from two pretest modeling analyses (Buscheck et al., 1997; Birkholzer and Tsang, 1997; and Birkholzer and Tsang, 2000). Inspection of CNWRA predictions, particularly regarding vertical symmetry in saturation and temperature profiles from simulations of the DST, suggests the TH regime is unthrottled, buoyant, advective rock dryout. Buscheck et al. (1997) evaluated vertical asymmetry in moisture redistribution, using an equivalent continuum formulation, for infiltration rates of 0.36, 3.6, and 6.2 mm/yr. These analyses by Buscheck et al. (1997) presumably used air permeability from the pneumatic testing done by Tsang and Cook (1997) and summarized in TRW Environmental Safety Systems, Inc. (1997b). Tsang and Cook (1997) measured air permeabilities in the range of 1–100 mD. From the results of Buscheck and Nitao (1996)

(section 2.1), unthrottled, nonbuoyant, advective rock dryout is to be expected with bulk permeabilities in this range. Buscheck et al. (1997) did not see significant vertical asymmetry in predictions of temperature for any of the three infiltration rates they investigated. Some slight vertical asymmetry in their saturation plots may be because of the Tptpll-Tptpmn contact. These early pretest models (Buscheck et al., 1997) thus predicted unthrottled, nonbuoyant, advective rock dryout.

Birkholzer and Tsang (1997) pretest analyses used matrix permeabilities of about 0.01 to 0.1 mD and fracture permeabilities in the range of about 1 D. Depending on the particular matrix/fracture model selected, the bulk permeability, k_b, would likely be greater than 1 mD, which would characterize the TH regime as unthrottled, nonbuoyant, advective rock dryout. If the bulk permeability should exceed 5 D, however, an unthrottled, buoyant advective rock dryout would be expected. Predictions of the DST for an infiltration at 0.36 mm/yr by Birkholzer and Tsang (1997) indicated vertical asymmetry in the saturation. A zone of elevated matrix saturation, located approximately 10–25 m below the heated drift in their model, may have been an artifact of different hydrological properties of the three model layers. In particular, the proximity of the transition from the Tptpul to the Tptpmn unit, approximately 12 m above the top of the heated drift, may have prevented the development of a zone of higher saturation in the region above the drift similar to the one that formed below the drift. Regardless of this possibility, vertical asymmetry in temperature and saturation could be inferred from the Birkholzer and Tsang (1997) pretest analyses. Thus, these pretest analyses suggest the formation of an unthrottled, buoyant, advective rock dryout TH regime at the DST.

Birkholzer and Tsang (2000) had approximately 400 days worth of data from the DST to refine their models although not all data for the entire 400-day period were available. Also, not all data reduction and interpretation of data collected for the 400-day period had been completed at the time of their modeling studies. Simulations by Birkholzer and Tsang using the DKM formulation clearly predicted vertical asymmetry after 1 yr of heating for both the fracture continuum [figure 13d in Birkholzer and Tsang (2000)] and matrix continuum [figure 15c in Birkholzer and Tsang (2000)]. Although CNWRA model results are in qualitative agreement with those of Birkholzer and Tsang (2000), there are, nonetheless, significant differences in the general shape of the zone exhibiting elevated saturation and in the magnitudes of simulated saturation. Significant differences are predicted using various conceptual models, such as the ECM, DKM, and the Active Fracture Model. Unfortunately, techniques for measuring fracture saturation, particularly on the bulk field scale are not available. Therefore, given uncertainties in both models and data, the DST may not be sufficient to discern which model more appropriately represents the TH of the repository site. Discriminating between these various conceptual models will most likely depend on the success of techniques to measure bulk saturation—a combination of fracture and matrix saturation.

4 SUMMARY AND CONCLUSIONS

4.1 SUMMARY OF OBJECTIVES FOR THE CURRENT DRIFT-SCALE HEATER TEST THERMAL-HYDROLOGICAL ANALYSES

The status of the DOE objectives of the DST are considered as follows:

1. *Do results from the DST permit identification of the dominant mode(s) of heat flow and the dominant TH flow regime?* Although not entirely conclusive, early results from the DST suggest that the TH regime is unthrottled, buoyant, advective rock dryout, however, this assessment is dependent on property value assignments. This assessment could be considered preliminary pending additional data and modeling analyses. This preliminary evaluation is also subject to review when the complete effects of heat and mass loss through the thermal bulkhead are more fully evaluated.

2. *Is it possible to determine if a sufficiently large network of fractures has been incorporated by the DST to assess important decay-heat-driven processes such as boiling, vapor diffusion, buoyant gas-phase convection, and nonequilibrium, liquid-phase fracture flow?* Test results are just beginning to reveal interesting large-scale TH fracture flow behavior. Continuing test results are needed to better understand moisture redistribution as condensate flow in fractures and vapor transport. Observation of the DST during its cool-down phase will be important in evaluating large-scale condensate return flows in fractures and dryout zone rewetting. Current data collected from the DST and related analyses are inadequate to assess whether a sufficiently large network of fractures are incorporated by the DST.

3. *Is the DST sufficient*

    a. *To allow for potential condensate buildup above the boiling zone?* Preliminary analyses of the effects of mass loss on development of reflux zones in models suggest that losses through the thermal bulkhead may significantly reduce condensation buildup above the boiling zone. These models illustrate the need for bounding estimates of mass loss through the thermal bulkhead. However, collection of condensate above the boiling zone in hydrology holes shows condensate buildup is occurring in the DST.

    b. *To assess whether or not spatial variability in the gas- and liquid-phase pathways could focus enough condensate drainage to cause water to drip onto WPs?* If sufficient mass is lost from the DST, it may have the effect of reducing the potential for condensate return flow to enter the drift. Further modeling analyses may suggest ideas for conducting the cool-down phase of the DST to maximize the possibility of return flow entering the drift.

    c. *To prevent edge-cooling effects from dominating TH behavior?* The current 2D modeling analysis did not address edge effects. Future planned three-dimensional (3D) models will address this question. Continued observation of TH processes perpendicular to the heater drift may provide sufficient data to determine the edge effects of the wing heater/heater drift design.

    d. *To allow evaluation of the significance of buoyant, gas-phase convection on moisture movement and heat flow?* Moisture movement and heat flow observed in the DST in the

presence of mass loss through the thermal bulkhead may be somewhat different than those that would occur in the presence of a completely sealed bulkhead. Analyses of the effects of mass loss on the DST suggest that formation of a condensation zone above the heater drift may be affected by mass loss through the thermal bulkhead.

4.2 MODELING OF THE DRIFT-SCALE HEATER TEST

Horizontal asymmetry in the modeling results of the DST for saturations and temperatures indicates the TH regime is the unthrottled, buoyant, advective rock dryout type identified and defined during the pretest analyses of Buscheck and Nitao (1996). The importance to repository performance of identifying the TH regime regards transport of vapor, buildup of condensate above emplacement drifts, possible fracture-matrix nonequilibrium condensate drainage, and, ultimately, the potential for water to enter emplacement drifts and contact WPs. Sensitivity of DST modeling results to potential losses from the heated drift through the thermal bulkhead were simulated by mass sink terms uniformly distributed in the grid elements surrounding the drift wall boundary.

Temperature and saturation predictions are compared with measured temperatures taken along Borehole 158 (placed into the heater drift crown) and Borehole 160 (placed horizontally above the wing heaters). Temperature predictions for the model with basecase properties did not compare well with measurements taken after 1 yr of heating. A 10^{-2} reduction in fracture permeability and a one-third decrease in thermal conductivity compared to the basecase property values significantly reduced the differences between simulated and measured temperatures, although the differences remained significant. Conclusions drawn from the modeling results remain tentative until these differences are resolved. Nonetheless, the modeling results are informative and relative importance among model properties, boundary conditions, and heat and mass input can be evaluated.

These preliminary results suggest that removal of mass as small as 80 mL/hr from the model system at the drift wall boundary can reduce condensate buildup and refluxing above the heated drift. This 80 mL/hr mass removal rate is small even compared to an estimated mass removal rate of 200 mL/hr,[1] which has not been demonstrated to be conservative. The importance to repository performance is that reduced condensate buildup and refluxing above the heated drift increase uncertainty in evaluating results from the DST and reduce the potential for condensate return flow back to the heated drift. Recall that one of the primary objectives of the DST is to maximize the potential for observing possible refluxing into drifts and/or condensate drainage into drifts following the above boiling period. These preliminary results indicate the need to monitor, or otherwise bound, mass and energy losses through the thermal bulkhead and to evaluate the consequences to DST observations and conclusions regarding repository performance drawn from DST data.

4.3 THE FOCUS OF FUTURE DRIFT-SCALE HEATER TEST MODELING EFFORTS

Additional activities are planned that would help clarify possible effects of the thermal bulkhead on TH processes in the DST and reduce uncertainty in the DST model results. These activities include using additional DST data as they are made available to evaluate the TH modeling ability to represent the TH

[1]TRW Environmental Safety Systems, Inc., Interoffice correspondence memo dated October 21, 1999.

processes. More work needs to be done to evaluate the effect of the upper boundary condition and the resulting effect on ambient saturation. In addition, a clearer understanding of the heat and mass transfer mechanisms active above the heater drift is needed to explain differences between predicted and observed temperatures. Evaluation of the effect of changes in the matrix/fracture interaction term, A^*_{mod}, on ambient saturation and transient TH processes will be completed as part of this activity. Additional analysis is required to evaluate the full effect of changes in thermal conductivity. A 3D model will be required to evaluate edge effects. The set analyses reported in this study will be extended beyond the first year of the heating phase of the DST. Modifications to MULTIFLO to allow mass removal in the vapor phase will be considered. Implementation of this modeling mechanism would allow for evaluation of greater mass removal through the thermal bulkhead.

Furthermore, modeling analyses can be used to evaluate alternative cool-down strategies. For example, an alternative cool-down scenario in which the heat load from the canister heaters is reduced, while the wing heater loads are maintained, may increase the possibility of saturation buildup at the drift crown and, perhaps, focus condensate drainage into the heated drift. Such analyses may lead to more thorough performance assessments of potential water flow into emplacement drifts, both during and following the thermal period.

5 REFERENCES

Birkholzer, J.T., and Y.W. Tsang. *Pretest Analysis of the Thermal-Hydrological Conditions of the ESF Drift-Scale Test.* Earth Sciences Division Level 4 Milestone Report SP9322M4. Berkeley, CA: Lawrence Berkeley National Laboratory. 1997.

Birkholzer, J.T., and Y.W. Tsang. *Modeling the Thermal-Hydrologic Processes in a Large-Scale Underground Heater Test in Partially Saturated Fractured Tuff.* Accepted for publication. *Water Resources Research.* 2000.

Brechtel, C.E., G. Lin, E. Martin, and D.S. Kessel. *Geochemical Characterization of the North Ramp of the Exploratory Studies Area.* SAND95–0488. Albuquerque, NM: Sandia National Laboratories. 1995.

Blair, S., T. Buscheck, L. DeLoach, W. Lin, and A. Ramirez. *Single Heater Test Final Report.* UCRL–ID–131491. Livermore, CA: Lawrence Livermore National Laboratory. 1998.

Buscheck, T.A., and J.J. Nitao. *Thermal-hydrological Analysis of Large-Scale Thermal Tests in the Exploratory Studies Facility at Yucca Mountain.* UCRL–ID–121791. Livermore, CA: Lawrence Livermore National Laboratory. 1996.

Buscheck, T.A., R.J. Schaffer, and J.J. Nitao. *Pretest Thermal-hydrological Analysis of the Drift-scale Thermal Test at Yucca Mountain.* Livermore, CA: Lawrence Livermore National Laboratory. 1997.

Lichtner, P.C. and M.S. Seth. *MULTIFLO Users Manual: Multicomponent-Multiphase Reactive Transport Model.* San Antonio, TX: Center for Nuclear Waste Regulatory Analyses. 1997.

Lichtner, P.C., M.S. Seth, and S. Painter. *MULTIFLO User's Manual MULTIFLO Version 1.2—Two-Phase Nonisothermal Coupled Thermal-Hydrologic-Chemical Flow Simulator.* Revision 2. Change 1. San Antonio, TX: Center for Nuclear Waste Regulatory Analyses. 2000.

Mualem, Y. A new model for predicting hydraulic conductivity of unsaturated porous media. *Water Resources Research* 12: 513–522. 1976.

Somerton, W.H., A.H. El-Shaarani, and S.M. Mobarak. High temperature behavior of rocks associated with geothermal type reservoirs. *Society of Petroleum Engineers—44th Annual California Regional Meeting.* San Francisco, CA: Society of Petroleum Engineers. Paper SPE–4897. 1974

TRW Environmental Safety Systems, Inc. *Drift-Scale Test Design and Forecast Results.* B00000000–01717–4600–00007. Revision 00. Las Vegas, NV: TRW Environmental Safety Systems, Inc. 1997a.

TRW Environmental Safety Systems, Inc. *Ambient Characterization of the Drift-Scale Test Block.* BADD00000–01717–5705–00001. Revision 01. Las Vegas, NV: TRW Environmental Safety Systems, Inc. 1997b.

TRW Environmental Safety Systems, Inc. *Total System Performance Assessment-Viability Assessment Analyses—Technical Basis Document.* B00000000–01717–4301–00001. Revision 01. Las Vegas, NV: TRW Environmental Safety Systems, Inc. 1998a.

TRW Environmental Safety Systems, Inc. *Drift-Scale Test As-Built Report.* BAB00000–01717–5700–0003. Revision 01. Las Vegas, NV: TRW Environmental Safety Systems, Inc. 1998b.

TRW Environmental Safety Systems, Inc. *Thermal Test Progress Report #1.* Las Vegas, NV: TRW Environmental Safety Systems, Inc., 1998c.

TRW Environmental Safety Systems, Inc. *Thermal Test Progress Report #2.* Las Vegas, NV: TRW Environmental Safety Systems, Inc. 1998d.

TRW Environmental Safety Systems, Inc. *Thermal Test Progress Report #3.* Las Vegas, NV: TRW Environmental Safety Systems, Inc. 1999a.

TRW Environmental Safety Systems, Inc. *Thermal Test Progress Report #4,* Las Vegas, NV: TRW Environmental Safety Systems, Inc. 1999b.

TRW Environmental Safety Systems, Inc. *Thermal Tests Thermal-Hydrological Analyses/Model Report,* Las Vegas, NV: TRW Environmental Safety Systems, Inc. 2000.

Tsang, Y.W., and P. Cook. *Ambient Characterization of the ESF Drift-scale Test Area by Field Air Permeability Measurements.* Yucca Mountain Site Project Milestone Report SP9512M4. DTN: LB9706000123142.001. Berkeley, CA: Lawrence Berkeley National Laboratory. 1997.

U.S. Department of Energy. *Site Characterization Plan: Yucca Mountain Site, Nevada Research and Development Area, Nevada.* DOE/RW–0199. Washington, DC: U.S. Department of Energy. 1988.

U.S. Nuclear Regulatory Commission. *Issue Resolution Status Report (Key Technical Issue: Evolution of the Near-Field Environment, Revision 2).* Washington, DC: U.S. Nuclear Regulatory Commission. 1999.

van Genuchten, M. Th. A closed-form equation for predicting the hydraulic conductivity of unsaturated soils. *Soil Science Society of American Journal* 44: 892–898. 1980.